I give permission for public access to my thesis and for any copying to be done at the direction of the archives librarian and/or the College librarian.

Catherine Braine	May 2011

PINK1 RNAI AND *PARKIN* EXPRESSION IN *DROSOPHILA MELANOGASTER*

By

Catherine E. Braine

A Paper Presented to the

Faculty of Mount Holyoke College in

Partial Fulfillment of the Requirements for

The Degree of Bachelors of Arts with

Honor

Department of Biological Sciences

South Hadley, MA 01075

May 2011

This paper was prepared

under the direction of

Professor Craig Woodard

for eight credits

To $C_8H_{10}N_4O_2$,

an invigorating companion on all those late nights.

I couldn't have done it without you.

ACKNOWLDEGEMENTS

First and foremost, I would like to thank Professor Craig Woodard for his unending support and guidance over the past three years. As a freshman, I approached him to inquire about doing independent research in his lab; he signed me up *before* I had taken his class. His commitment to his students goes above and beyond any reasonable expectation. His optimism, guidance, and dedication have led me to challenge myself in new ways and to direct my research interests. In addition to being an exemplary advisor, I would like to thank him for being someone with whom I can discuss both science and science fiction (oftentimes within the same conversation).

I am indebted to Marian Rice, one of the two 'Microscopy Goddesses' of the Biology Department. Without her help and support, a vast portion of this thesis would still be in its abstract stages. Her expertise, insight, and dedication have been invaluable throughout this process.

Professor Rachel Fink has been an inspirational role model throughout my years at Mount Holyoke. She is a wonderful mentor in so many ways, and incredibly, remains accessible to her students on both an academic and personal basis. I would also like to thank Professor Will Millard for offering his expertise as part of my thesis committee and for having a sly sense of humor that kept me attentive and amused in 8:35am classes. Additionally, I would like to thank the Mount Holyoke College Department of Biological Sciences for funding my project.

I would have been unable to do this without the love and support of my family and friends. Although I may have inadvertently become the go-to person when stray fruit flies are witnessed in kitchens (it's getting old, guys), I truly appreciate their ability to endure my temporary bouts of insanity. Finally, I would like to thank my fellow lab-mates; only they know the look of the uninitiated as you proclaim that you are, "going to lab to collect virgins".

TABLE OF CONTENTS

LIST OF FIGURES

LIST OF TABLES

ABSTRACT

Sporadic Inclusion Body Myositis (s-IBM) is a degenerative muscle disorder. Symptoms include muscle weakness and loss of motor control. Abnormal accumulation of human Amyloid Precursor Protein (hAPP) and its proteolytic fragments (Aß) are found in the protein aggregates characteristic of s-IBM pathology. The aggregates impair the function of the Ubiquitin Proteasome System (UPS), a cellular mechanism that degrades unwanted protein. Over-expression of *Parkin*, which encodes a UPS subunit, combats the detrimental effects of Aß accumulation. *Parkin* over-expression also ameliorates mitochondrial defects of knocked-out *Pink1*.

Transgenic *Drosophila melanogaster* were used to investigate interactions between *Pink1*, *Parkin* and *hAPP*. The first part of this project found that expression of human Parkin reverses the negative behavioral effects of expressing, from a transgene, hAPP in fly musculature. The second part of this study used *Pink1 RNAi* flies to determine the effect *Pink1* RNA interference has on endogenous *Parkin* expression in skeletal musculature. qPCR techniques revealed no differential expression of endogenous *Parkin* between wild-type and *Pink1 RNAi* flies of various ages. Complementarily, Transmission Electron Microscopy on indirect flight muscle revealed the absence of hypothesized mitochondrial abnormalities in all flies but one; however, other morphological differences were found. The focus of this project was to ascertain potential therapeutic effects of Parkin.

INTRODUCTION

Degenerative muscle disorders (also known as degenerative myopathies or muscular dystrophies) are diseases with pathologies that incorporate degradation of muscle tissue. Clinical manifestations of myopathies, usually to some degree, include muscle weakness, muscle atrophy, and verifiable histological changes. The main focus of this project is the muscular dystrophy Sporadic Inclusion Body Myositis.

Sporadic Inclusion Body Myositis

General Pathology and Clinical Symptoms:

Sporadic Inclusion Body Myositis (s-IBM) is an idiopathic muscle disorder that leads to muscle tissue inflammation and muscle atrophy. It is the most commonly diagnosed muscle disorder in adults, and the progression of symptoms is gradual, progressive, pervasive, and perpetuative. Tissue atrophy, resulting from three main contributing factors, is distinguished by muscle

weakness and loss of motor control in individuals afflicted with s-IBM. This myasthenia affects both proximal and distal muscles, and the causative degeneration is easily viewed as a wasting of muscles in the arms and legs. The most extensively affected muscle groups are those of the knees, hips, and fingers. In later stages, the degeneration of oral, pharyngeal, and esophageal muscles may lead to difficulty swallowing (Moslemi & Oldfors, 1997). Myositic degeneration also affects respiratory muscles, leading to multiple respiratory problems that include dyspnea (shortness of breath) and in rare cases, respiratory failure (Tiexiera, 2004). s-IBM is diagnosed via muscle biopsy. There is no cure and symptoms are only assuaged by palliative treatment.

Muscle tissue samples taken from s-IBM patients reveal extensive cellular inflammation, vacuolar degeneration of myocytes, and multi-protein aggregates of Amyloid-ß and tau proteins (Askanas, 2009). Presence of aggregates accompanies the vacuolar degeneration of myofibrils, suggesting the involvement of these aggregates in degeneration. Extensive mononuclear cell inflammation is generally seen in histochemical analysis of s-IBM muscle tissue biopsies. The etiology and exact pathogenesis of s-IBM is still unknown, but the combination of inflammation, vacuolization, and protein aggregation make s-IBM a disease with both immunological and proteopathic components (Askanas, 2007).

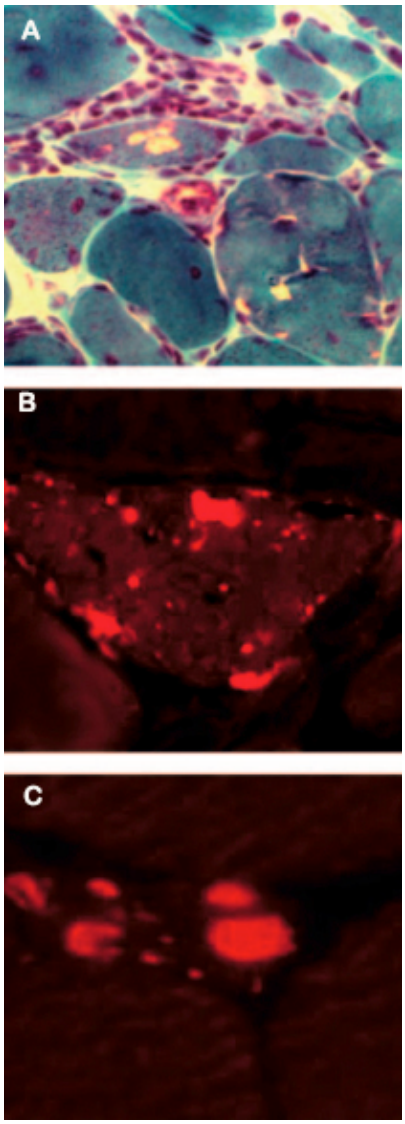

Figure 1: **Protein aggregation and vacuolization in s-IBM muscle fibers.** A. Vacuolization and mononuclear cell inflammation in a cross section of myofibrils. B. Amyloid accumulations in muscle fibers. C. s-IBM muscle tissue stained for amyloid- ß (Askanas, 2007)

s-IBM Immunopathogenesis:

s-IBM pathogenesis has an immunological component. Biopsies of s-IBM muscle tissue reveal the presence of MHC-I/CD8 complexes (Dalakas, 2004). The ubiquitous, if abnormal, expression of MHC-I on these myofibers allows for them to act as antigen presenting cells (Dalakas, 2006). The myofibers expressing the surface MHC-I activate $CD8^+$ T-cells to cytotoxic T-cells (CTLs). Antigen activation induces clonal expansion of the $CD8^+$ cells within the muscle tissue, resulting in an MHC-I directed cytotoxicity carried out by a repertoire of CTLs (Dalakas, 2004). These autoinvasive CTLs release perforin granules, the major $CD8^+$ T-cell effector, at the immunological synapse to lyse the MHC-I presenting myocytes (Goebels, 1996). The $CD8^+$ T-cell invasion and expansion is seen predominantly in non-vacuolated muscle fibers.

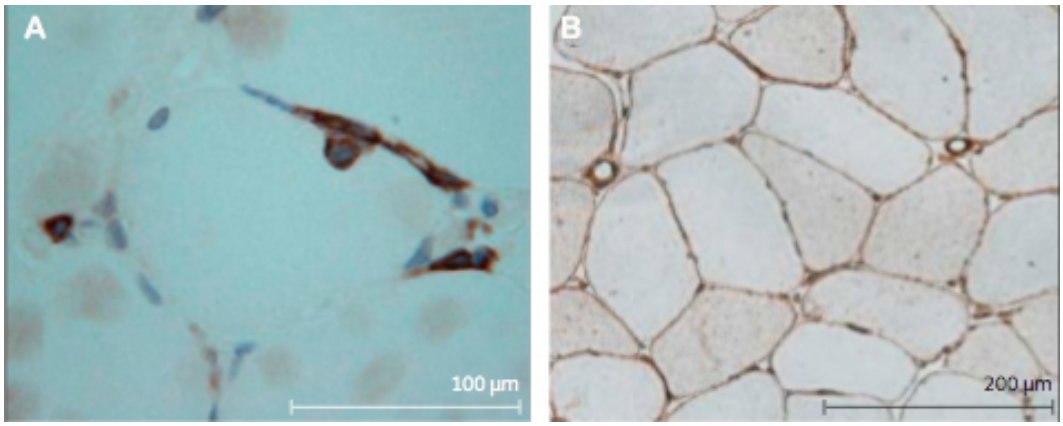

Figure 2. **CD8+ T-cell infiltration and MHC-I expression in s-IBM muscle tissue.**
A. Immunohistochemical staining of invading of $CD8^+$ cells into healthy muscle tissue. B. MHC-I expression in healthy muscle tissue shown via immunohistochemical techniques. (Needham, 2007).

T-cell targeted myofibers express co-stimulatory receptors. Complementary to MHC-I expression, myofibers targeted by $CD8^+$ T-cells synthesize and release chemokines and cytokines that attract additional $CD8^+$ cells and upregulate endothelial adhesion molecules for T-cell homing. (Lundberg, 2000). There is also an upregulation of $CD8^+$ co-stimulatory molecules on the myofibers. BB-1, a member of the B7 family of ligands, is upregulated on T-cell targeted myofibers, and CD-28 and CTLA-4 upregulation occurs on the invading CD8+ cells. BB-1 and CTLA-4 interaction is co-stimulatory to the CD8 T-cell receptor and MHC-I interaction. s-IBM myofibers also over-express ICOS ligand, another member of the B7 family. Interaction of ICOS ligand and its cognate receptor on $CD8^+$ cells also acts as a secondary co-stimulatory signal (Schmidt, 2004). ICOS interaction has been correlated to areas of CD8 T-cell invasion and the presence of ICOS to the ensuing release of perforin at the immunological synapse (Schmidt, 2004). Both these types of co-stimulation seem to direct and facilitate CD8 T-cell activation in s-IBM pathogenesis (Murata & Dalakas, 1999). The upregulation of certain chemokines and cytokines such as IL-1, IL-2, IL-5, IL-10, IFNγ, and TNFß also occurs (Dalakas 2006; Raju, 2003).

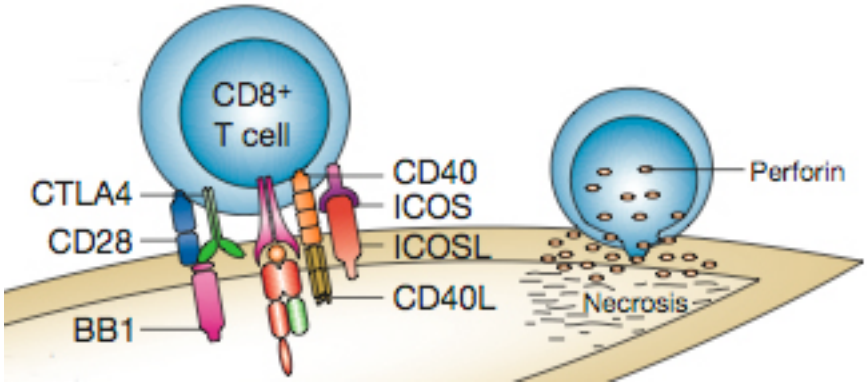

Figure 3: **Costimulation of CD8$^+$ T-cells for perforin release.**
Interactions of between CTLA4, CD28, CD40 and ICOS on CD8$^+$ T-cells and BB-1, CD40L and ICOS ligand on the surface of s-IBM affected myocytes lead to perforin granule release and myocyte necrosis (Dalakas, 2006).

CD8$^+$ T-cells undergo clonal expansion in s-IBM muscle tissue, but there is little variability in the T-cell receptors (TCRs) that are expressed. This limitation is notable in complement determining region 3 (CDR3) of the TCR. Variability in CDR3, one of the three variable domains of the TCR, allows for variability in antigen binding. Here, the limited number of TCRs implies uniformity of the peptide presented by MHC-I (Amemiya and Dalakas, 2000). In addition to this limitation, certain MHC haplotypes have been positively correlated to s-IBM. Higher rates of human leukocyte antigen (HLA) haplotype B8-DR3-DR52-DQ2 (the 8.1 ancestral haplotype), the HLA DR$\beta_1$0301 and DQ$\beta_1$0201 alleles, and the HLA-B8 allele are seen in individuals who develop s-IBM (Price, 2004; Dalakas, 2006; Raju, 2005). This immunogenetic association can be observed in familial inheritance patterns of the disease.

Autoimmune disorders and viral infections are associated with s-IBM onset. Patients with s-IBM commonly have an autoimmune disorder such as rheurmatoid arthritis, myasthenia gravis, or multiple sclerosis. Viruses, such as Epstein-Barr and influenza, have also been correlated to s-IBM. There is a strikingly high association between HIV and HTLV-1 infection and s-IBM, but there does not appear to exist an exacerbation of the immunological s-IBM phenotype in HIV/HTLA-1 patients (Raju, 2005).

The antigen presented by the MHC-I is currently unknown. T-cell activation is seen in biopsies of non-vacuolated muscle tissue only, despite ubiquitous MHC-I expression. It appears that without expression of the co-stimulatory ligand, T-cell activation, clonal expansion, and aggression are unseen. (Dalakas, 2004).

s-IBM Muscle Vacuolization, the Immune Response, and Autophagy:

The vacuolization and atrophy of muscle tissue is not found in areas with inclusion bodies, nor are s-IBM aggregates found within the vacuoles (Askanas & Engel, 2007). There may not be concurrency of vacuolization and s-IBM protein aggregation; however aggregation may be responsible for initiating a defensive autophagic response which induces the characteristic s-IBM vacuolarization (Arkansas & Engel 2007; 2008). Autophagy is a process by which the cell selectively degrades its own components, primarily via lysosomal activity.

As with autophagic activity in neurodegenerative conditions, such as Alzheimer's disease (AD), Aß deposition promotes autophagy in s-IBM muscle tissue. GFP-Atg8/LC3, a complex strongly expressed in human myocyte autophagosomes, is labeled via fluorescent microscopy techniques in order to track autophagosome activity (Lünemann et al., 2007). These autophagosomes join with lysosomes within the cell to degrade unwanted cellular components. In s-IBM human skeletal muscle biopsies, with and without vacuoles, APP and its proteolytic fragments are co-localized with the autophagosomes. This indicates that muscle cells target APP/Aß for autophagosomal degeneration. The Aß degeneration may be part of a cellular survival mechanism. Autophagosomes fuse with MHC II loading compartments, and in this way may contribute to the immune response of s-IBM. Although MHCII is not expressed ubiquitously on s-IBM muscle fibers, as MHCI is, muscle fibers which express MHCII are found to be surrounded by effector T-cells. These infiltrating T-cells may mediate the pro-inflammatory response of s-IBM via chemokine production (Lünemann et al., 2007).

The action of the autophagosomes has been implicated in the formation of the vacuoles found in s-IBM skeletal musculature. As with other skeletal muscle dystrophies, the vacuoles of s-IBM are rimmed. The rimmed vacuoles are an indication of autophagy, a process by which the cell degrades its own components via lysosomal activity (Takeuchi et al., 1985). There is an upregulation of lysosome associated proteins in vacuolized muscle tissue of s-IBM.

Histochemical and PCR tests demonstrate increased presence and expression of two lysosomal proteins, M6PR and clathrin, in vacuolized s-IBM tissue. The upregulation of these two proteins further suggests the connections between vacuolization and autophagy (Kumamoto et al., 2004).

The Basics of s-IBM Proteopathology and its Pathological Relationships:

Non-immunological factors are involved in s-IMB pathology. The vacuolization and tissue atrophy present in s-IBM patients is only partially attributable to aggravation of an immune response resulting in the influx of mononuclear cells to muscle tissue. As consistently mentioned, the pathogenesis of sIBM has a heavy proteopathic component. It is the proteopathic components that make a unique link between s-IBM pathogenesis and AD.

Accumulation of disruptive protein aggregates are found in the muscle biopsies of those with s-IBM. The intra-myofibril aggregation of select proteins is correlated to the characteristic vacuolization. These aggregations can be seen with different types of histochemical staining. The protein accumulations are present in all muscle tissue, despite the degree of vacuolization seen. Light microscopy techniques reveal the presence of these inclusion bodies (Arkansas & Engel, 1998).

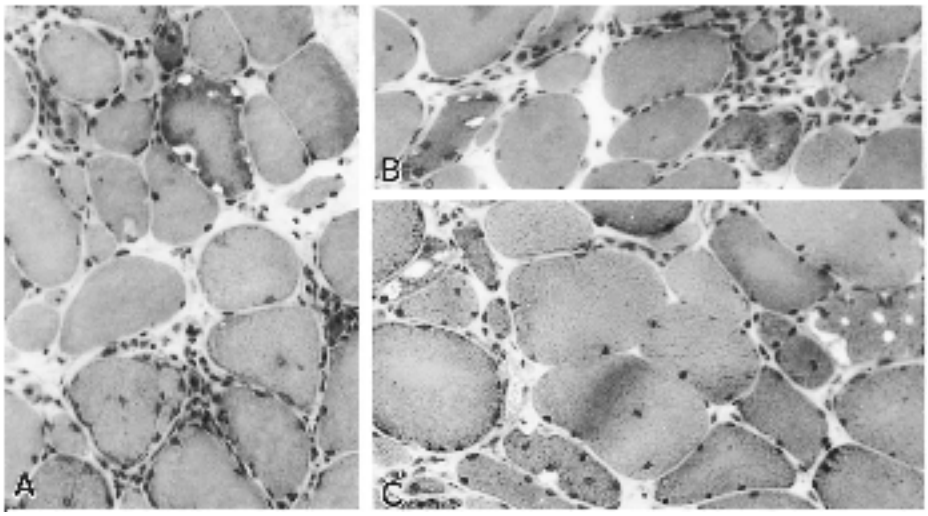

Figure 4: **Stained Aß protein aggregations in s-IBM muscle biopsies.**
Their presence is observed in both vacuolated (A and B) and non-vacuolated (C) muscle tissue (Arkansas & Engel, 1998).

Amyloid-ß Precursor Protein (APP) and ubiquitin were the first proteins to be identified in these accumulations. Aß, first identified in plaques of the nerve cells of Alzheimer's patients, was discovered in the muscles of s-IBM patients. Their deep internalization within the muscle fibers suggested their intracellular origin and prompted further study of the proteopathological component of s-IBM (Askanas 1992). Now, it is known that APP, its proteolytic fragments, Amyloid ß (Aß), Presenelin 1, and phosphorylated tau (p-Tau), are amongst the long list of proteins found in these intra myofibril accumulations (Askanas et al., 2005). As with Alzheimer's disease, it is the miscleavage of APP by secretases that leads to the toxic protein aggregation.

APP, in its proper form, is a 4k-Da transmembrane cell-surface glycoprotein (Hussein 2000; Haass & Selkoe, 2007). As a transmembrane protein,

it possesses both hydrophobic and hydrophilic domains. The hydrophobic domain bisects the hydrophobic plasma lipid bilayer. A mutation found in this hydrophobic region, called the Aß domain, is responsible for the proteolytic cleavage of APP to insoluble Aß fragments. In AD, the actions of a secretase, beta-site APP cleaving enzyme 1 (BACE1), are responsible for the generation of Aβ in neurons (Luo et al., 2001). The generated Aß fragments, which range from 39 to 42 amino acids in length, self-aggregate to compensate for their hydrophobic nature. In turn, insoluble plaques are formed within the cytoplasm (Askanas et al., 1998). These plaques are toxic to the cell and contribute to cell death.

While the presence of Aβ creates a solid connection between the pathologies of s-IBM and AD, another protein immunolocalized to the inclusion bodies, makes a solid connection between s-IBM and Parkinson's Disease (PD) (Askanas et al. 2000). A missense mutation of the *α-synuclein* gene creates a version of the α-synuclein protein with a hydrophobic region that facilitates unwanted agglomeration in neurons (Askanas et al. 2000; Polymeropoulos et al., 1997). These agglomerations are both the etiological and diagnostic factor of PD. α-synuclein is found co-localized with Aβ fibrils in 60% of vacuolized muscle tissue from biopsies of s-IBM patients (Askanas et al. 2000). This same co-localization is also observed in the brains of AD patients, once again correlating Aβ deposition with α-synuclein presence (Askanas et al. 2000; Lippa etal., 1998; Bennet et al., 2005).

APP and its Upregulation in s-IBM:

Increased expression of APP protein and its proteolytic fragments act as upstream mediators of s-IBM pathogenesis (Arkasas & Engel, 2008). The upstream nature of APP's control of s-IBM pathogenesis is solidified by its pattern of expression, correlated to manifestation of s-IBM phenotype. mRNA encoding for APP has been found to be upregulated in s-IBM myofibrils prior to the onset of abnormalities (Askanas & Engel, 1998; Fratta et al. 2005). Overexpression of APP in normal cultured human myocytes resulted in vacuolization and the characteristic amyloid inclusion bodies. This correlation between upregulation of APP in normal muscles and induction of s-IBM abnormalities has been further substantiated in vivo.

An s-IBM model was generated in transgenic mice. These mice overexpress the 99 amino acids of the carboxy terminus of APP (with an amino acid substitution to eradicate unwanted secretase cleavage at the Aß site) in skeletal muscles (Jin et al., 1998). Characteristics of s-IBM myopathy became apparent in these muscles after 24 months of age—highlighting age-dependent indicia as sarcoplasmic vacuolization, mononuclear cell infiltration, and myofibril degeneration. These fibers stained positive for Aß, indicating that there existed an endogenous means of cleavage for Aß production. Aß production was present and most extensively in the quadriceps. The same protein, inserted as a transgene and activated in the neurons of the same mice, did not result in any abnormality. This

suggests that the APP cleavage prevented in neurons by the manipulated amino acid substitution was insufficient in muscle tissue (Jin et al., 1998).

Aß presence in s-IBM:

Deposition of APP and its proteolytic fragments, resulting from APP cleavage, form a major component of the inclusion bodies. Not only is intact APP present in the protein aggregations, but inclusion bodies include both subclasses of Aß. The Aß peptides are either 40 or 42 amino acid residues in length, hence their respective nomenclatorial designations of Amyloid-ß-40 (Aß40) and Amyloid-ß-42 (Aß42). Aß deposits are found as paired helical fragments within the myocyte cytoplasm. The use of Congo red fluorescent techniques shows that Aß accumulations are primarily found in the ß-pleated sheet aggregation/accumulation pattern (Askanas et al., 2009). The ß-pleated sheet conformation is an abnormal aggregation and Aß accumulation results from a miscleaving of APP by a restriction enzyme, ß secretase (Askanas et al., 2001). Depending on the mutation present in the APP sequence, two subclasses of Aß proteolytic fragments can be generated. Both forms of Aß are present in inclusion bodies.

In plasma samples taken from s-IBM patients, Aβ42 is the form of Aβ that is more commonly produced (Abdo et al., 2009). Aβ42 is co-localized with p-tau in s-IBM plaques; these two proteins form what researchers have referred to as ‘squiggly’ paired helical fragments (Askanas et al., 2011). The preferential

accumulation of these 6-10nm loosely packed Aβ42 fibrils results in even further problems for the cell (Askanas et al., 2009). Aβ42 is more hydrophobic than Aβ40, and therefore oligomerized faster within the aqueous cytoplasm. This increased rate of oligomarization increases Aβ42 cytotoxicity (Askanas et al, 2009; 2008).

The distinct connection between Aβ plaque development in muscles and the development of s-IBM like symptoms was solidified via experiments with mice which overexpressed human APP (hAPP). Selective APP expression in the skeletal muscles of mice produced an s-IBM phenotype characterized by both histological and behavioral changes with time.

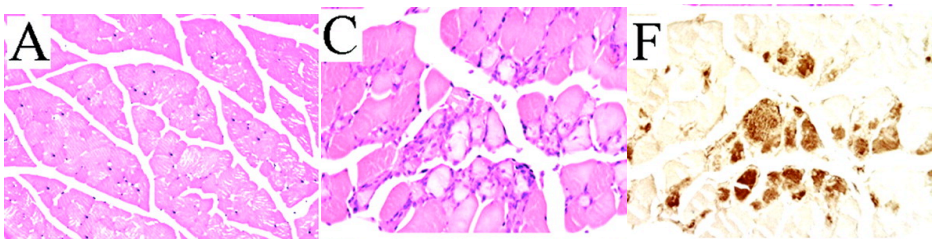

Figure 5: **s-IBM like degradation of mice skeletal muscles due to hAPP transgene insertion.**
A. Non-transgenic tissue shows normal skeletal muscle morphology. C. Tissue in which hAPP is expressed via a transgene exhibits variation in myofibril size the presence of mononuclear cells. F. This section, the same tissue in panel C, exhibits globular Aβ aggregates via immunohistochemical techniques (Sugarman et al., 2002).

Aβ Generation:

Generation of Aß plaques in s-IBM is similar to the generation of the same plaques in Alzheimer's Disease. As mentioned briefly before, the generation of

Aβ occurs via abnormal interactions between APP and its processing machinery (Askanas et al., 2009). Three different secretases, α, β, and γ are responsible for the cleavage of APP into oligomerizable forms (Nunan & Small, 2000). The actions of these three secretases act to increase total Aβ production.

Two types of ß secretases are involved in generation of Aß40 and Aß42. These transmembrane ß secretases belong to the protein family of type I transmembrane aspartyl proteases. The two types of ß secretase implicated in Aß40 and Aß42 production are, BACE1 (Asp2) and BACE2 (Asp1). BACE1 and BACE2 both possess an N-terminal catalytic domain, a 17 amino acid long transmembrane domain, and a short cytoplasmic tail (Nunan & Small, 2000). BACE1 is a 501 amino acid long protein found localized to endosomes and trans-Golgi vesicles (Vassar et al., 2009). Expression of BACE1 is seen throughout the body, in all tissues but the pancreas, but the highest concentrations are found in neurons of the brain (Vassar et al. 1999; 2009). BACE1 is capable of cleaving APP at two residues, Asp1 and Glu11, within the Aß domain.

BACE2, also known as Asp1, is very similar in sequence and function to BACE1 (Vassar et al. 2009). Both enzymes have similar substrate specificity and share a conserved active site capable of the endoproteolytic cleavage that frees APP from its anchored site within the cytoplasm (Askanas et al., 2001; Hussain et al., 2000). Unlike BACE1, BACE2 is not ubiquitously expressed within the human body, but is found co-localized with APP in the brain (Hussain et al., 2000). Its presence in the brain is comparably low to BACE1, indicating the

BACE1 is the predominant β-secretase of APP in vivo (Vassar et al., 2009). Although both aspartyl proteases are capable of cleaving the transmembrane APP, the cleavage site of BACE2 differs from that of BACE1. The BACE2 cleavage site, at residues Phe-19 and Phe-20, are still within Aβ domain (Farzan et al., 2000). BACE2 is demonstrated to be more efficient at Aß site cleavage than BACE1 (Cai et al., 2001). The ectodomain shedding of APP by ß-secretases either releases a soluble product, sAPPβ, into the extracellular space, or generates a 99 residue membrane tethered C99 fragment (Nunan & Small, 2000; Dries & Yu, 2008). BACE1 and BACE2 are co-localized with Aβ in s-IBM myocytes, suggesting its role in localized Aß generation and deposition (Vattemi et al., 2001; Askanas et al., 2011).

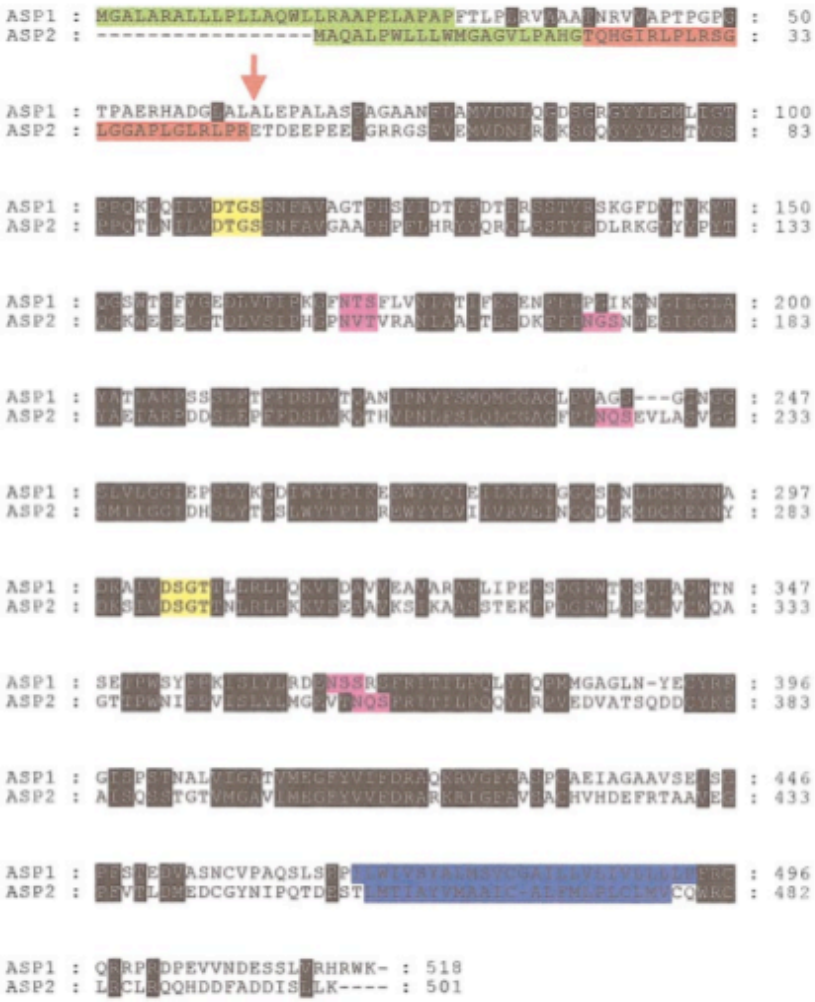

Figure 6. **Aligned Sequences of BACE1 (Asp2) and BACE2 (Asp1).** The amino acids highlighted in black are conserved between the two sequences The conserved active site is highlighted in yellow (Hussain et al., 2000).

ß secretases are not alone in their ability to initiate the initial cleavage of APP. One of the main routes of APP processing occurs via the actions of α-secretase. α-secretase cleaves the 16th residue of the C-terminus side of the Aβ sequence. This cleavage generates a membrane bound 83 amino acid residue, commonly referred to as C83, and a soluable, secreted APPα (Nunan & Small

2000; Hare 2010). An upregulation of α-secretase processing of APP has been induced in kidney cells via expression of a transfected human muscarinic acetylcholine receptor. Agonism of these receptors via a synthesized carbamylcholine has been shown to increase the production of non-neurotoxic APPα and C83 (Nitsch 1992). Neither C83 nor APPα continues on the Aβ production pathway, nor do they result in the presence of any egregious toxic species.

Further processing of C99 makes creates the toxic Aβ species. Additional enzymatic processing of the membrane bound C99 fragments continues to be processed by the γ-secretase complex. Amyloidgenic Aβ species occurs as a result of a γ-secretase mitigated unique proteolytic event in which a hydrophobic transmembrane domain is cleaved at positions 40 and 42 (Nunan & Small, 2000; Sisodia & St. George-Hylop, 2002).

Presenelin 1 (PS1) and Presenelin 2 (PS2) have been implicated as members of the γ-secretase complex in AD Aβ processing (Sisodia & St. George–Hylop, 2002). Mutations in human *ps1* gene found on chromosome 21, which encodes for the 467 amino acid PS1 transmembrane protein, have been positively correlated to development of inherited forms of AD and to the accumulation of Aβ42 in these forms (Hardy et al., 1997). Knock-out of *ps1* and *ps2* in mice leads to a reduction of Aβ40 and Aβ42 species. The Presenilin dependent activity of the γ-secretase complex implicates PS1 and PS2 as members of the γ-secretase complex. Within the γ-secretase complex, PS1 and PS2 are hypthothesized to act

as aspartyl proteases, however their active sites contain a novel GxGD motif; this motif implies a new mechanism of aspartyl protease activity (Haass & Steiner, 2002). Mutations to two aspartate residues of PS1 block γ-secretase cleavage of hAPP; it is possible that these two residues create an active site and function as proteases (Wolfe et al., 1999). PS1 and PS2 may be responsible for the activity of γ-secretase, but other members of the complex are also vital. Nicastrin, is a 130kDa membrane protein that stabilizes PS, however, co-expression of PS and Nicastrin do not initiate γ-secretase activity.

PS1 has been immunolocalized to the abnormal and degraded muscle fibers of individuals with s-IBM, correlating this location with the suggested function (Askanas 1998; 2003; 2011). Mutations of human *PS1* and *PS2* genes, on chromosomes 1 and 14 respectively, are positively correlated to development of early onset AD (Hardy et al., 1997).

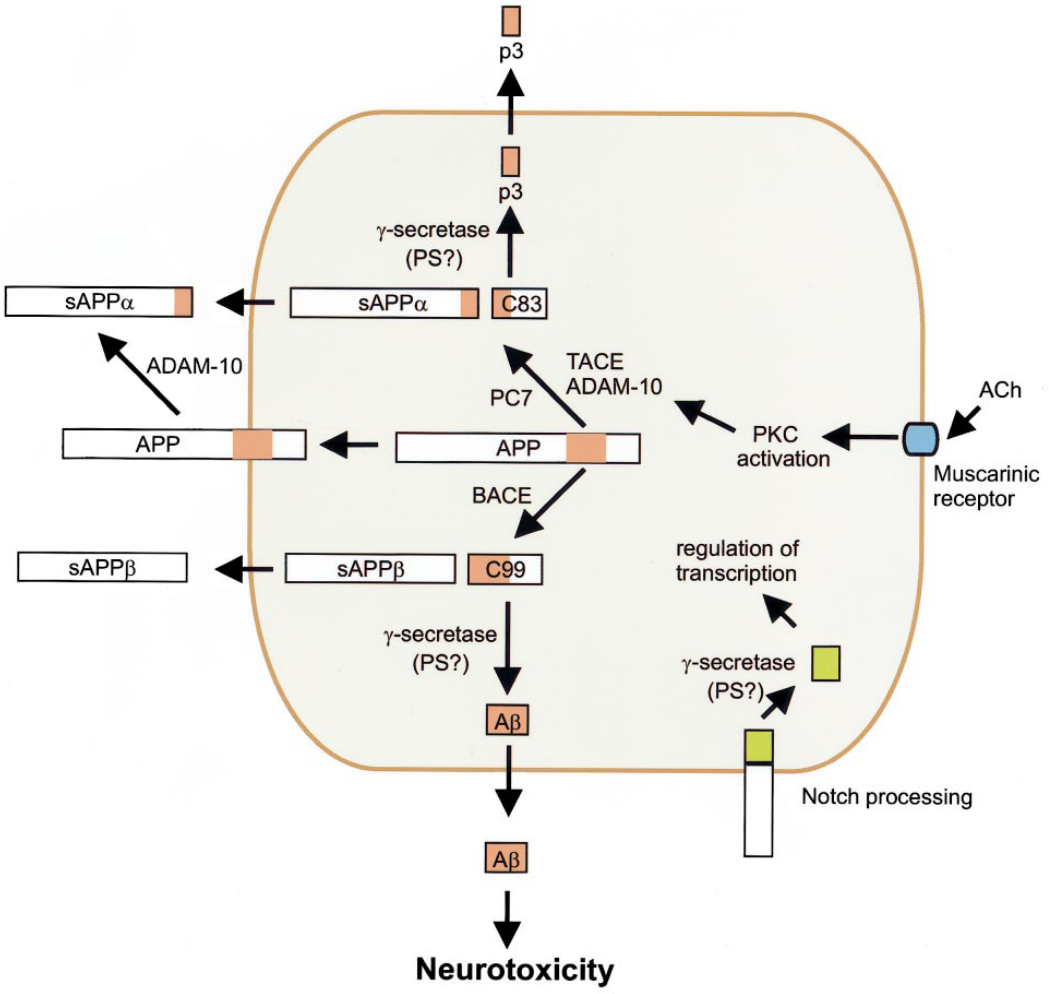

Figure 7. **The Aβ Casade diagrammed within a nerve.**
The processing of APP by BACE and α-secretases is followed by the cleavage of proteolytic products, C83 and C99, respectively. The actions of the γ-secretase complex, hypothesized to occur via the actions of presenelins (PS) further processes C99 to neurotoxic Aβ. This same processing occurs in the myocytes of those afflicted with s-IBM (Nunan & Small, 2000).

Aβ and mitochondria:

The buildup of Aβ in both AD and s-IBM affects the cells in a variety of ways. In s-IBM, oxidative stress, mitochondrial abnormalities, and proteasomal

dysfunctions are three interrelated processes that contribute to the tissue degradation.

Mitochondrial abnormalities, such as cytochrome c-oxidase deficient muscle fibers, are seen in s-IBM muscle. This phenomenon is attributable to deletion and mutation of mtDNA; an effect that is exacerbated with mitochondria regeneration (Moslemi & Oldfors, 1997). The deletion seen in s-IBM mitochondria is referred to as the "common deletion" and is related to senescence (Moslemi & Oldfors, 1997; Pesce et al., 2001). Immunohistochemical stains show age related increases in COX activity that are seen in natural aging patterns (Pesce et al. 2001; Chiveri et al., 2006). Use of a viral vector to transfer the APP gene into normal myocytes induced age-dependent mitochondrial abnormalities. These abnormalities included enlarged cristae, shedding of the mitochondrial outer membrane, inclusions, and vacuolization (Askanas, 1996).

Aβ Accumulation and Parkin:

Parkin is a protein that acts as the E3 ubiquitin ligase of the UPS. Mutations of this protein are directly associated with the development of familial Parkinson's Disease. Parkin has been studied primarily within the nervous system. Mutation of *Parkin* are associated with the development of autosomal recessive juvenile Parkinson's Disease (Kitada et al. 1998).

In the absence of Parkin in *Drosophila*, oxidative stress and diminished respiratory capacity are seen (Greene, 2003; Whitworth et al., 2005). There occurs degeneration of indirect flight muscle via apoptosis. Analysis of *Parkin Drosophila* mutants shows increased apoptosis of indirect flight muscle myocytes. Myofibril degradation is an assumed repercussion of the mitochondrial degradation which is also observed in these mutants (Pesah 2005). The myofibril degradation is seen as a secondary effect to the mitochondrial degradation; the high energy needs of the myocyte are not being met by the damaged mitochondria (Pesah, 2005). This same energy dependent destruction due to loss of Parkin function in *Drosophila* has been shown to halt sperm activity, leading to male infertility. This occurs due to the necessity of mitochondria for flagellar movement of the sperm and the impediment to mitochondrial morphogenesis due to the *Parkin* knock-out (Riparbelli & Callaini, 2006).

Exposure to Paraquat, a generator of radical oxygen species, is demonstrated to increase the deleterious changes to the muscle tissue (Pesah, 2005). This implicates *Drosophila Parkin* as a protector against oxidative stress. *Parkin* expression has also been seen to ameliorate ceramide induced neuron death; its presence on the outer membrane of mitochondria acted to maintain mitochondrial integrity with exposure (Darios, 2003).

The aggregations of Aβ are one of the main causes of oxidative stress within the s-IBM myocyte (Askanas, 2011). Parkin's roles as the E3 component of the Ubiquitin Proteasome System, a means of degradation of unwanted

intracellular protein, would act to reduce oxidative stress via the degradation of inclusion bodies (Lim & Tan, 2007). Parkin reduces oxidative stress resulting from protein accumulation via its activity as the E3 component of the UPS complex. Parkin suppresses unfolded protein induced stress via upregulation of the destruction of ubiquitin-targeted proteins within the cell (Imai, 2000; Rosen, 2006). In mouse neuron cultures in which Aβ processing had been initiated via transgenic manipulation, *Parkin* overexpression was able to decrease Aβ deposition via UPS upregulation (Rosen, 2010).

Parkinson's Disease

General Neuropathology and Clinical Symptoms:

Parkinson's Disease (PD) was first identified as the "shaking palsy" in 1817. PD is a neurodegenerative disease, which affects the neurons of the central nervous system. PD pathology is distinguished by the progressive and incurable degeneration of dopaminergic (DA) neurons, primarily in the substantia nigra and ventral tegmental area. DA is a catecholamine neurotransmitter and is involved in the regulation of voluntary movement. The loss of DA producing neurons logically manifests itself in a number of motor behavioral impairments. These impairments include bradykinesia, tremor at rest, rigidity, freezing, postural instability and postural deformities, to name a few. Non-motor features may also manifest themselves. Autonomic dysfunction and cognitive and neurobehavioral abnormalities, mostly associated with later stages of the disease, complement the

motor dysfunction (Jankovic 2008). The full or partial presentation of any of these symptoms can be characterized as 'parkinsonism'. The true cause of parkinsonism can only be determined post-mortem, via examination of the brain and assaying for the presence of characteristic Lewy bodies (Hughes et al. 1992; Braak et al. 2003).

The presence and proliferation of Lewy bodies is the hallmark characteristic of PD. Lewy bodies are specific inclusion bodies of agglomerated proteins which collect in the neurons of those with PD. The presence of Lewy bodies in the Parkinsonian brain, and the subsequent neurodegeneration beheld, occurs in a systematic manner (Braak, 2003). There is a progression of Lewy body development and neural lesioning beginning in the olfactory structures and progressing on a path to the neocortex, passing through structures of the intermediate reticular zone, the medulla oblongta, midbrain, and mesocortex (Braak, 2003). The presence of Lewy bodies is positively correlated to progression of clinical symptoms. PD neuronal death is caused by the contributing factors of oxidative stress, mitochondrial dysfunction, inflammation, and excitotoxicity (Olanow, 2007).

Lewy Bodies, α-synuclein, and their connection to s-IBM:

Along with nerve cell loss in the substantia nigra, the presence of Lewy bodies (and Lewy neurites) in PD are definitive characteristics of the disease. The main component of these filamentous aggregations is α-synuclein (Spillantini et

al. 1998). Accumulation of α-synuclein, a pre-synaptic protein, into Lewy bodies in familial PD has been linked to a genetic defect at the 4q21-23 position (Polymeropoulos et al. 1997). This area is home to the human α-synuclein gene. A G to A point substitution at position 209 in the *α-synuclein* sequence results in an Ala to Thr substitution at amino acid position 53 (A53T) in the transcribed protein. This mutation disrupts the α-helical and β-pleated sheet conformation of the protein, exposing hydrophobic residues to the aqueous cytoplasm (Polymeropoulos et al. 1997). A second point mutation, resulting in an Ala to Proline switch at position 30 is also positively correlated to the development of α-synuclein accumulation (Krüger, 1998). Mutant α-synuclein over-expression in *Drosophila* has been shown to lead to PD-like phenotypes, such as degeneration of dopaminergic (DA) neurons and deficits in motor ability (assayed using climbing assays). The DA neuron destruction is targeted, despite the presence of α-synuclein in all neurons (Feany & Bender, 2000)

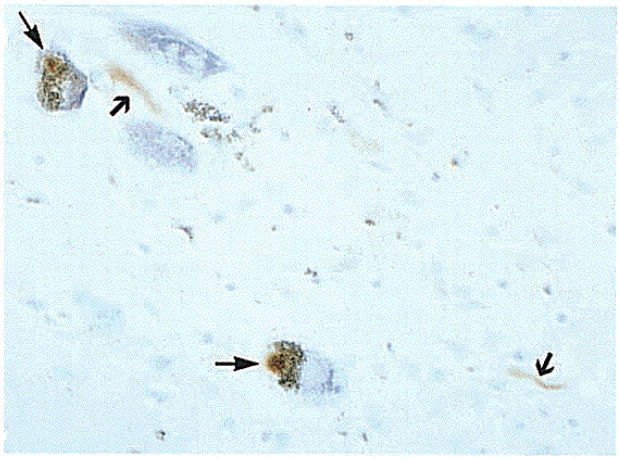

Figure 8. **Lewy bodies stained for α-synuclein.**
Pigmented nerve cells of the substantia nigra with Lewy bodies immunohistochemically stained for the presence of α-synuclein. (Spillantini, 1997).

Although the mutant α-synuclein sequence is present in all somatic cells, accumulation of α-synuclein selectively apoptoses DA neurons of Parkinson's patients. Agglomeration of α-synuclein has been seen to be upregulated in the presence of oxidants. Overexpression of α-synuclein in DA neurons increases their susceptibility to mitochondrial dependent apoptosis resulting from the release of cytochrome c. Reactive oxygen species result from the hydrolysis of hydrogen peroxide to hydroxide radicals during DA synthesis (Junn & Mouradian, 2002).

The accumulation of α-synuclein, its neurotoxic effects, and its ability to lower a cell's defenses to oxidative stress, may not only lead to a true explanation of its true role in Lewy body formation, but the role it's presence plays in the inclusion bodies of s-IBM.

PARK Family of Genes:

The inheritance of familial Parkinson's Disease is correlated to mutations of 11 genes referred to as the PARK family (Nagatsu & Sawada, 2006). PARK1 and PARK2, which encode for *α-synuclein* and *Parkin* respectively, have been discussed previously in this paper. Mutations of a third gene, PARK6, or *Pink1*, encodes for a protein whose mutations are associated with early onset PD (Nagatsu & Sawada, 2006). Five different known mutations, which include point mutations, deletions, and exon mutations, of *Pink1* have been correlated to development of early onset PD (Klein et al., 2005; Samaranch, 2010).

Pink1 has been mapped to the p arm of human chromosome one, where it inhabits as 12.5 cM region. The gene encodes for the Pink1 protein, PTEN-induced putative kinase 1, which is ubiquitously expressed in humans (Valente 2004). Pink1 is a serine/threonine kinase that demonstrates a high degree of homology with proteins of the Ca2+/calmodulin family (Valente, 2004). Pink1 possesses autophosphorylative ability and has been localized to the inner membrane of the mitochondria in mammals (Silvestri, 2005).

Although manipulation and knock out of *Pink1* implicates its role in maintaining mitochondria integrity, its precise function is unknown. *Drosophila Pink1* mutants are rescued by the upregulation of mitochondrial fission/fusion machinery. The insertion of an additional *Drp1* and *Opa 1*, two directors of mitochondrial fission and fusion, are seen to ameliorate the micro and macroscopic manifestations of *Pink1* mutation in IFM myocytes and DA neurons.

Expression of these proteins restores abnormal wing-posture characteristic of *Pink1* knock-out, normal IFM ultrastructure, and DA neuron integrity (Yang 2008; Poole 2008).

Ubiquitous inhibition of *dPink1* (*Drosophila Pink1*) was seen to result in flies with parkinsonian like symptoms. These *dPink1 RNAi* flies exhibited walking difficulties, wing abnormalities, a 70% decrease in ATP levels, and selective disruption of IFM muscle ultrastructure (Yang et al. 2006). Both ubiquitous and muscle specific knock-out of *dPink1* led to the presentation of IFM with irregular and reduced distribution of mitochondria. The mitochondria within these myocytes, via transmission electron microscopy techniques, appeared less electron dense than their wild-type counterparts, were swollen, and showed membrane disintegration (particularly of the cristae) (Yang 2006). These adverse phenotypic effects could be rectified via the expression of *hParkin* by a transgene. The same inactivation of *dPink1* in dopaminergic neurons leads to an age-dependent decline in DA synthesis. Once again, *hParkin* over expression ameliorated these effects. No adverse effects to the myocytes or neurons were visible with the overexpression of *hParkin* alone (Yang 2006).

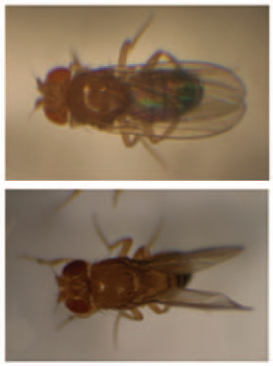

Figure 9. **Wing posture in *dPink1 RNAi* flies compared to a control.** Control flies in the top panel display normal straightwing posture, while the *dPink1 RNAi* flies demonstrate abnormal wing posture. This abnormality appeared as wings which were held-up or drooped. (Yang 2006)

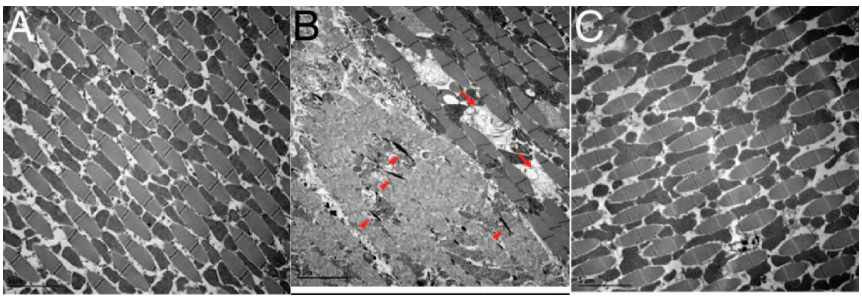

Figure 10. **Restoration of normal muscle ultrastructure via *hParkin* overexpression.**
A. TEM preparation of control *Drosophila* IFM tissue displays normal myofibril and mitochondrial integrity. B. Vacuolarization and disintegration of cristae is apparent in *dPink1 RNAi* tissue. C. Restoration of normal morphology in *dPink1 RNAi* tissue with *hParkin* overexpression (Yang, 2006).

Pink1 has also been shown to interact with Parkin and another PARK family protein, DJ-1, to restore mitochondrial damages inflicted by α-synuclein (Kamp et al. 2010). Additionally, knock out of *Pink1* in mouse fibroblasts is seen to results in mitochondrial dysfunction via respiratory chain defects (Amo 2010).

Loss of *Pink1* and loss of *Parkin* result in similar phenotypic effects, and double mutants show exacerbated deleterious phenotypes, indicating that the two proteins work on a shared biochemical pathway. The ability of *Parkin* expression to ameliorate *Pink1* deficiency indicates that *Parkin* acts downstream of *Pink1* on this pathway, although it is a possibility that they may act upon the same product (Clark et al., 2006). This pathway is also linked to the occurrence of mitophagy in PD (Deas et al., 2011).

Laboratory use of *Drosophila melanogaster* as a model organism:

Genetic laboratory use of *Drosophila melanogaster* has a long and illustrious history. Thomas Hunt Morgan, a distinguished evolutionary biologist and geneticist, is credited with the creation of the first fruit fly lab at Columbia University in 1908. In his laboratory, Morgan crossbred mutated flies in order to explore the chromosomal basis of Mendelian inheritance patterns. Today, that same spirit is witnessed in *Drosophila* 'Fly Rooms', where advanced laboratory techniques are able to create models of various inherited human diseases in *Drosophila*.

Drosophila is a popular model organism for several significant reasons. The *Drosophila* life-cycle is short; large numbers of progeny may be amassed and contained without much work. The short generational time makes it a powerful tool in genetics laboratories, where crosses between genotypes yield large F_1 generations in a timely fashion. The genome of *Drosophila melanogaster* was

among the first genomes to be sequenced. Many *Drosophila* homologues to human proteins exist and many biochemical pathways remain conserved between the species (Schneider 2000).

In 1982, Spradling and Rubin pioneered the process of transgenic manipulation of *Drosophila* (Spradling & Rubin, 1982). Recombinant DNA using a P-element vector (a family of transposons in *Drosophila melanogaster*) can be successfully transposed into *Drosophila* chromosomes (Spradling & Rubin, 1982). This technique has since been streamlined and popularized as a method of manipulating protein expression in *Drosophila*, particularly via the insertion of human transgenes. The UAS/Gal4 system takes advantage of these techniques (Duffy, 2002). Integrases, such as the φC31 integrase isolated from *E. coli*, permits researchers to achieve site-specific integration of a desired transgene (Groth et al., 2004).

In conjunction with the availability and efficiency of laboratory techniques, many conserved biological pathways make *Drosophila melanogaster* an excellent animal upon which to create disease models (Driscoll & Gerstbrein, 2003).

Drosophila melanogaster **as a model for s-IBM:**

APP is a protein that is highly conserved across species. It is the high conservation of this protein which allows for the creation of relevant animal

models. The sequence of the protein may be highly conserved across species; however the Aβ domain is unique to human APP (hAPP).

A 6.5kB transcript that encodes for a *Drosophila* APP-like protein is produced from the *Appl* gene, cytogenically mapped to position 1B9-1B10 (Rosen, 1989; *Fly Base* 2011). This protein, known as amyloid protein precursor-like (APPL), is homologous to hAPP. Drosophila *Appl* mRNA is transcribed and translated to 145kDa peptide, a precursor protein form to the 130kDa secreted form of APPL. N-linked glycosylation occurs in to both APPL and hAPP, presumably by the machinery of the Golgi apparatus. The presence of APPL is localized to neurons during development, suggesting a function within the nervous system (Luo, 1990). The expression of *Appl* is not vital to fly survival, however the cleaved 130kDa form is the one that is active within the cell (Chan & Bonini, 2000). The human APP locus is has been mapped to the long arm of chromosome 21 (Goate et al., 1991).

The Aβ region (also known as the βA4 region) of hAPP is not found on APPL orthologue, nor is a β-secretase homologue present in *Drosophila*. (Fossgreen et al., 1998). Nevertheless, *Drosophila* have both α- and γ-secretase homologues; this includes a *Drosophila* Presenelin and Nicatrasin (Fossgreen et al., 1998; Fortini et al., 1999; Bilen & Bonini, 2005; Driscoll & Gerstbrein, 2003).

Drosophila have a conserved *Parkin* homologue at the 78C2 to 78C2 position of their third chromosome (*FlyBase*, *2011)*. The homologous *dParkin*

gene was identified via BLAST search (Fortini et al., 2000; Horowitz et al., 2001). A conserved *Drosophila Pink1* (*dPink1*) homologue has been mapped to the 6C6-6C6 position of the *Drosophila* X chromosome. There is a single *Pink1* homologue of *Drosophila* melanogaster. As in humans, both *Parkin* and *Pink1* *Drosophila* homologues are expressed ubiquitously throughout the animal (Clark et al., 2006).

Project Components, Goals and Hypotheses:

This project contains two distinct parts, both of which are connected by one factor, *Parkin.* This first study focuses on the possible ameliorative effects human *Parkin* (*hParkin*) expression may have on human APP (*hAPP*) overexpression in *Drosophila* skeletal muscles. Previous experiments in our laboratory have shown that flies which express *hAPP* in their skeletal muscles display decreased motor capability. This decreased motor capability presumably results from activation of the Aβ cascade and the subsequent accumulation of *hAPP* and its proteolytic fragments within *Drosophila* myocytes. No endogenous machinery has yet been identified with the ability to cleave *hAPP* in *Drosophila* skeletal muscle, but it is presumed that the Aβ cascade is initiated. If this cascade is, in fact, occurring within the myocytes, *hParkin* over-expression would be beneficial; any Aβ accumulation potentially hampering the UPS machinery would be reversed by upregulation of the UPS via the presence of its *Parkin* subunit. In this way, this experiment is the generation of a partial model of s-IBM

pathogenesis. For this experiment, behavioral climbing assays will be used as a measure of muscle activity; muscle activity is correlated to the effects of *hAPP* and *hParkin* expression. The previously demonstrated ameliorative effects of *hParkin* over-expression in situations of unwanted protein aggregation would be mimicked here.

The second set of experiments was designed with reference to the outcome of the first part of this project, which preceded it. The amelioration of the degenerative effects of muscle specific *hAPP* expression, via *hParkin* co-expression, and presumably via UPS up-regulation, has great potential for therapeutic use. Rather than conducting further exploration of the ubiquitin ligating function of Parkin's role as the E3 component of the UPS, the interrelatedness of the mitochondrial function of Parkin and Pink1 was explored. As mentioned earlier, *Parkin* acts downstream of *Pink1*, forming a pathway of mitochondrial maintenance. In this experiment, RNA interference is used as a means of fashioning flies in which *Pink1* has been knocked out of the skeletal muscles. It is hypothesized that proper *Pink1* expression is integral to proper *Parkin* expression. Due to this down-stream regulation, lower levels of endogenous *Parkin* are hypothesized to be found in the *Pink1* knock-out flies, as compared to wild-type controls. Additionally, this research should corroborate previous research which demonstrates the muscle and activity degeneration which proceeds *Pink1* knock-out in *Drosophila.*

Both of these experiment sets are in concurrence with the goal of the Woodard Laboratory, to identify proteins with potential to intervene in the pathogenesis of diseases such as s-IBM and PD.

MATERIALS AND METHODS

hAPP and *hParkin*

Drosophila melanogaster stocks and crosses:

The *Drosophila* husbandry techniques employed to engineer the transgenic flies for this experiment were similar to those used in the first half of this study. As with the generation of *Pink1RNAi* flies, the desired genotypes were generated using the UAS-Gal4 system (Duffy 2002). Here, four initial genotypes were crossed in order to obtain *Drosophila* lines that express the desired human proteins in the skeletal muscles. The initial genotypes are as follows:

1. w^{1118}
2. *UAS-hAPP; Dmef-Gal4*
   Cyo-TM6
3. *UAS-hParkin*
4. *Dmef-Gal4*

Progeny of each initial genotypes was amassed in plastic vials in a 25°C at 50% humidity. Virgins were collected and the following crosses performed:

1. $\frac{+}{+};\frac{\text{Dmef}-\text{Gal4}}{\text{Dmef}-\text{Gal4}} \times \frac{\text{UAS-hParkin}}{\text{UAS-hParkin}};\frac{+}{+} \rightarrow \frac{\text{UAS}-\text{hParkin}}{+};\frac{\text{Dmef}-\text{Gal4}}{+}$

   Two variations of this cross were generated. The first contained females that were *Dmef-Gal4/+*, while the second contained females that were *UAS-hParkin/UAS-hParkin*. The variation of this cross was performed to confirm that no variation in climbing ability occurred due to the sex of the parental gene carrier. This cross yielded flies, which expressed human Parkin alone (*hParkin*).

2. $\frac{\text{UAS-hAPP;Dmef-Gal4}}{\text{Cyo-TM6}};\frac{\text{UAS-hParkin}}{\text{UAS-hParkin}};\frac{+}{+} \rightarrow \frac{\text{UAS}-\text{hAPP}}{\text{UAS}-\text{hParkin}};\frac{\text{Dmef}-\text{Gal4}}{+}$

   Two variations of this cross were performed as well, in which the sex of the parental carriers of the genotype was the variant. This also was performed to confirm that there existed no disparity between the crosses due to the sex of the parental gene carrier. This cross produced flies that expressed both hAPP and Parkin (*hAPP+hParkin*).

3. $\frac{\text{UAS-hAPP ; Dmef-Gal4}}{\text{Cyo-TM6}}$ x $\frac{\text{UAS-hAPP ; Dmef-Gal4}}{\text{Cyo-TM6}} \rightarrow \frac{\text{UAS-hAPP ; Dmef-Gal4}}{\text{Cyo-TM6}}$

   This cross yielded flies that would express hAPP alone (*hAPP*).

Using the promoter of the *Dmef* gene, muscle specific expression of these human proteins was achieved. *Dmef*, or Myocyte enhancer factor 2, is a protein encoding gene that codes for a transcription factor vital to skeletal muscle differentiation (*FlyBase* 2011). Here, the *Dmef* promoter drives muscle-specific

expression of *Gal4* (Lovato et al., 2005). This same tactic was used in the generation of *Pink1 RNAi* flies. Both the *Cyo* and *TM6B* balancers acted as phenotypic markers of the desired genes.

Behavioral Climbing Assays

Our lab utilizes the climbing ability of *Drosophila* as a measure of muscle capability. In climbing assays, climbing ability is assessed by determining the flies' ability to scale a vertical surface within a set period of time.

hAPP and *hParkin* Climbing Assays:

The w^{1118}, *hAPP, hParkin,* and *hAPP+hParkin* flies were stored in the 25ºC incubator and transferred multiple times in order to amass enough progeny to set up the climbing assays. To set up climbing assays, newly eclosed flies of comparable ages were collected in groups of 30 and stored in glass vials. Age comparable members of each genotype were collected. 24 hours prior to each collection, stock vials were emptied to ensure comparable ages between animals within each sample. The collected flies were transferred to new glass vials every six days in order to prevent cross-generational contamination. Climbing assays were performed on each vial every seven days for four consecutive weeks.

The collection of newly eclosed flies in glass vials created a condition in which the effects of activity dependence on muscles could be assayed. Glass vials

provided a slippery surface, promoting greater muscle activity in order for the fly to maintain purchase on the substrate. By rearing flies in this way, we created a mechanically stressful condition, in which not only age-dependent climbing ability, but muscle activity-dependent climbing ability could be tested.

To perform the climbing assay, flies were transferred to a 50 mL glass graduated cylinder. They were given a one-minute recovery period following this transfer. After, the cylinder was tapped to force the flies to the bottom. The innate negative geotropism of *Drosophila* compels the flies to instinctually scale the sides of the cylinder (Gargano et al., 2005). The number of flies unable to cross the 30 mL line in 15 seconds was recorded. The process was repeated in the glass cylinder, three times per vial of flies. A second round of climbing assays used the same procedure, but a plastic graduated cylinder was substituted. Flies were given a five-minute recovery period between these two types of assays in addition to their one-minute rest period between individual trials. The climbing assays performed on the glass medium were considered the stressed group; activity-dependent muscle capability could be measured against the control of the climbing assays performed on the plastic medium.

Pink1 RNAi and *Parkin*

Drosophila melanogaster stocks and crosses:

The stock genotypes for this experiment were generated to take advantage of the *UAS-Gal4* system. The Gal4 protein acts as a transcriptional activator of sequences under the control of *GAL10* and *GAL1*, two sequences that compose the Upstream Activation Sequence (UAS) (Duffy 2002). Gal4 activation of the UAS prompts the transcription of the adjacent gene. If *Gal4* remains unexpressed, even in the presence of the UAS, the transcription of the downstream gene does not occur (Duffy 2002). Manipulation of the activation/deactivation of the UAS made it possible to obtain the desired genotypes for this experiment.

1. w^{1118}
2. *w; UAS-Pink1-RNAi*
3. *w;* $\frac{\textit{Dmef Gal-4}}{\textit{TM6B}}$

w^{1118} flies act as a wild-type control in this study. In order to generate a stock in which *Pink1* expression is knocked down, *w; UAS- Pink1-RNAi* and *Dmef-Gal4* virgins were collected and the following cross was performed:

$$\underset{+}{\underline{\textit{w; UAS-Pink1 RNAi}}} \; x \; \underset{\textit{TM6B, Hu Tb}}{\underline{\textit{Dmef Gal-4}}} \rightarrow \textit{w;} \; \underset{+}{\underline{\textit{UAS-Pink1 RNAi}}} \; ; \; \underset{+}{\underline{\textit{Dmef-Gal4}}}$$

In this cross, *Dmef* once again is a muscle specific promoter of *Gal4,* which then activates the UAS for *Pink1RNAi* expression. The introduced double stranded Pink1 transcript activates the RNase III family endoribonuclease Dicer—an

enzyme that cleaves the double strand into small interfering RNAs (siRNA). siRNAs are integrated into the RNA induced silencing complex (RISC) where they activate argonaute, a component endonuclease. The argonaute protein then cleaves any complement of the bound siRNA, effectively knocking out *Pink1* (Mello & Conte 2004).

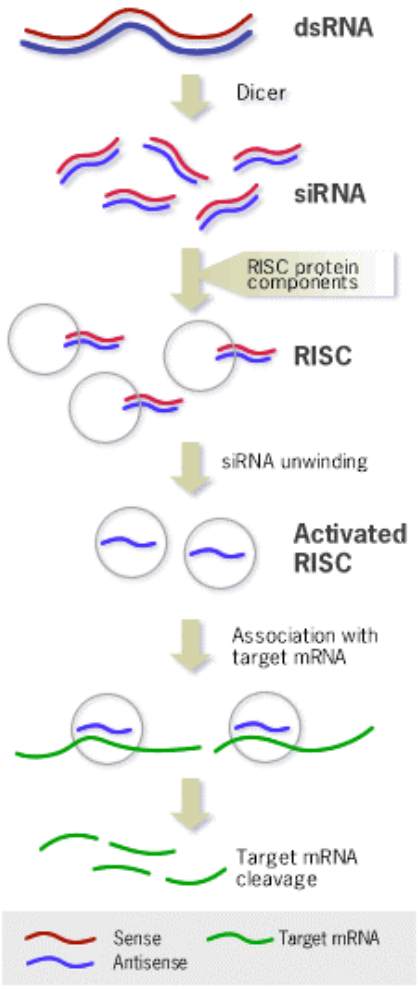

Figure 11. **RNA interference mechanism.** The process of RNA interference begins with the activation of the dimeric endoribonuclease Dicer by the presence of a dsRNA transcript. Dicer cleaves the dsRNA into 20-25 nucleotide long fragments with 3 base pair overhangs at the cleavage sites. These dsRNA fragments, called siRNAs, are integrated into the nuclease RISC. The protein R2D2 that transfers the siRNAs from Dicer to RISC facilitates this integration. Upon integration into the RISC complex, one strand (the guide strand) of the siRNA associates with the argonaute protein of RISC. This association between the guide strand and the argonaute protein creates a nucleation site for the target mRNA substrate to be cleaved. (Hannon 2002) (Liu 2003) (Ambion).

Crosses between male *Dmef Gal-4* and female *w; UAS-Pink1-RNAi* and crosses between female *Dmef Gal-4* and male *w; UAS-Pink1-RNAi* were performed in order to obtain *w; UAS-Pink1-RNAi ; Dmef-Gal4* (*Pink1 RNAi*) progeny. Once pupation of progeny from the original cross was witnessed, the vials were emptied to ensure that none of the flies of the parental genotype remained. Crosses were stored in the 25°C incubator and were transferred multiple times to accumulate sufficient progeny for the aging process. For each vial, it was necessary that the flies were of approximately the same age. To ensure this, the stock bottles were emptied and newly eclosed flies were collected into plastic vials within 24 hours. No male:female ratio was observed during these collections. All vials were stored in the 25°C incubator until use. Vials were changed once per week to control against unwanted proliferation, which would result in cross-generational contamination. Both w^{1118} and *Pink1 RNAi* flies were collected and aged for either one, two, three, or four weeks.

Polymerase Chain Reaction (PCR) Analysis:

RNA Isolation:

For each week, 8 samples of 8 flies each were collected. Flies were anaesthetized with CO_2 and placed in 1.5 mL chilled microfuge tubes. 1 mL of TriZol (guanidium thiocyanate-phenol-chloroform) reagent (Invitrogen) was added per sample (Chomczynski et al. 2006). Flies were smashed and vortexed to release RNA into the solution. The TriZol suspension was transferred to 2 mL Phase Lock Heavy Gel tubes (5Prime) which had been pre-spun at 1500 rpm for 30 seconds at room temperature. After transfer, each sample remained in the Phase Lock Tubes for 5 minutes at room temperature. 200 μL of chloroform was added to each microfuge tube. With addition, each sample was shaken vigorously by hand for 15 seconds. Samples were then centrifuged at 12000 rpm for 10 minutes at 2-8ºC. After centrifugation the aqueous layer was transferred to a fresh 1.5 mL microfuge tube to which .5 mL of Isopropyl Alcohol was added. Tubes were mixed by inversion and remained at room temperature for 10 minutes thereafter. Samples were once again centrifuged at 12000 rpm for 10 minutes at 2-8ºC to create a pellet. The supernatant was decanted to leave behind the RNA pellet. 1 mL of a 3:1 solution of ethanol:nuclease free water was added to each pellet. With this addition, samples were centrifuged for 5 minutes at 7500 rpm at 2-8ºC. The supernatant was decanted one last time and the pellet was left to dry at room temperature for approximately 10 minutes. Depending on the size of the

pellet, the RNA was re-suspended in 10-20 µL of nuclease free water. Samples were incubated at 55-65ºC for 10 minutes to facilitate re-suspension. RNA concentration was determined via spectrometer; the quality gauged using the concentration and 260/280 values. To increase the efficacy of the DNase treatment, all RNA sample concentrations were normalized to 1000ng/µL.

DNase Treatment:

To eliminate extraneous genomic DNA from the isolated RNA, all samples were DNase treated using the Ambion DNA-free DNase treatment kit. 10x DNase buffer and rDNase-I were added to each sample in a volumetric ratio of 1:10 reagent to isolated RNA. Samples were mixed manually and incubated at 37º C for 30 minutes. Following this, DNase inactivation reagent was added to each sample in a ratio of 2:10 reagent to isolated RNA. Samples were incubated at room temperature for 2 minutes, mixing frequently. Samples were then centrifuged at 10,000 rpm for 90 seconds or longer (until a white pellet appeared).

The supernatant was transferred to a fresh 1.5 mL RNase-free microfuge tube, where this procedure was carried out a second time. In this second iteration, 10X DNase buffer was added in a 3:20 ratio of reagent to isolated RNA. RNA concentration was again quantified by spectrometer and analyzed using the nucleic acid concentration and OD260/280 values.

cDNA Synthesis:

cDNA polymerization was performed using SuperScript® Double-Stranded cDNA Synthesis Kit (Invitrogen). A master mix of 2 µL dNTP (10mM), 2 µL Oligo (dT), and 16 µL nuclease free water per sample was made and aliquoted in 8 µL amounts to 2 µL samples of isolated RNA. At this point, duplicates of each sample were made in order to have samples on which reverse transcription had and had not been performed; these samples were called RT and No RT respectively. No RT samples would serve as a negative control to the RT samples and be used to assay the presence of extraneous genomic DNA.

After addition of the master mix, samples were incubated at 65ºC for 5 minutes and then placed on ice for at least 1 minute. A reaction mixture of 2 µL 10 RT buffer, 4 µL 25 mM $MgCl_2$, 2 µL DTT, and 1 µL RNaseOUT™ was added to each sample. This mixture was made for n+1 samples and 9 µL was aliquoted to each sample. Samples were incubated at 42ºC for 2 minutes. Following incubation, 1 µL of SuperScript™ II RT was added to each RT samples and 1 µL of nuclease free water to each No RT sample. All samples were incubated at 42ºC for 50 minutes.

To terminate the reaction, samples were incubated at 70ºC for 15 minutes. 1 µL of RNase H was aliquoted to each sample and samples were then incubated at 37ºC for 20 minutes. If not used immediately, polymerized cDNA samples were stored at -20ºC until use.

PCR Primer Design:

Primers specific to endogenous Dmel/park-RC *Drosophila Parkin*, were designed using *PrimerQuest* and *FlyBase* and synthesized by Integrated DNA Technologies (IDT). The amplicon of this primer is 94 bp in length. The primer sequences are as follows.

Parkin Primers:

Forward: 5'-TTGAAGTCGCGTAGAATTCCCGGT- 3'

Reverse: 5' -AGAAGAATTCAGCGAAGGGCGGAT- 3'

To act as a control, primers for *Actin 5C* were also used on cDNA samples. These primers were designed using *NCBI Primer-Blast* and *FlyBase* by Kathryn Gorski and synthesized by Integrated DNA Technologies (IDT). The sequences of the *Actin 5C* primers are as follows.

Actin 5C Primers:

Forward Primer: 5'- TCTACGAGGGTTATGCCCTT -3'

Reverse Primer: 5' -GCACAGCTTCTCCTTGATGT- 3'

The *Actin 5C* primers produce an amplicon 158 base pairs in length. All primers were diluted to a concentration of 10μM prior to use in reverse transcription polymerase chain reaction.

Reverse Transcription Polymerase Chain Reaction (PCR):

Using the primers detailed above, PCR reactions were set up with the desired cDNA samples. The reaction mixture detailed in Table 1 was set up for each reaction; the cDNA and primers varied with the desired target amplification. A master mix of the reaction mixture that excluded *Taq* Polymerase, primers, and cDNA was made for n+2 samples. 44 µL of this master mix was transferred to .5mL PCR tubes where the remaining components were added separately. All reactions were run on a Techne Techgene Thermocycler. The temperature profile used is outlined in Table 2.

Table 1: **Reaction mixture used in RT-PCR**

Reagent	**Amount Added**
10X PCR Buffer	5µL
50mM $MgCl_2$	3µL
10mM dNTPs	1µL
10µL of 10µM forward primer	2µL
10µL of 10µM reverse primer	2µL
Nuclease free water	34.6µL
Taq Polymerase	.4µL
Total volume:	50µL

Table 2: **Thermocycler Temperature Profile for each PCR reaction**

Stage	**Temperature**	**Time (per cycle)**	**Cycle Count**
Separation	94°C	30 seconds	35 cycles
Annealing	61°C	30 seconds	35 cycles
Extension	72°C	30 seconds	35 cycles
Final Extension	72°C	5 minutes	1 cycle
Final Hold	4°C	-	-

Gel Electrophoresis:

PCR products were run on 1.6% agarose gels. 2.4 g of agarose was added to 150 mL of 1X TAE buffer. The beaker was placed in a microwave on high for three minutes (or until the agarose dissolved and the mixture became clear). The beaker was removed promptly upon vigorous bubbling and the contents stirred. After heating, 10 µL of 10mg/mL Ethidium Bromide (EtBr) was incorporated into the agarose mixture. The mixture was poured into a gel mold and left to polymerize for at least one hour.

Prior to the addition of samples, the gel comb was removed and the gel submerged in 1X TAE buffer (20 mL of 50X TAE: 242g Tris Base; 57.1mL glacial aceitic acid; 100mL .5M EDTA (ph 8.0); in 980mL of dH_2O). 2 µL of 6X SDS loading dye (400µL 80% glycerol; 1µL .5M EDTA, 80µL 25mg/mL BPB; 80µL 25mg/µL XC) was added to 50 µL of PCR product. Samples were vortexed and 25 µL of this mixture was pipetted into the appropriate loading wells. In order to determine cDNA size, one loading well always contained a DNA ladder (2 µl New England Biolabs 100bp DNA Ladder, 2 µl SDS loading dye, and 16 µl nuclease free water). Products were run at 150V for approximately 1 hour. Gels were imaged using a Luminescent Image Analyzer LAS 3000 (Fuji Film). Products of the *Parkin* primer set were visible as bands of 94bp.

Samples analyzed via gel electrophoresis were stored at -20ºC until their use in real-time polymerase chain reactions.

Quantitative Polymerase Chain Reaction:

Real time polymerase chain reaction, also known as quantitative real time polymerase chain reaction (qPCR), is a molecular biology laboratory technique used to amplify and quantify target sequences of DNA. The presence of PCR product is measured with each PCR reaction cycle. A fluorescent probe is used to measure the presence of amplified DNA. SYBR Green the most commonly used flourophore in qPCR reactions, was used in this experiment. It binds to double-stranded DNA and fluoresces with excitation. Fluorescence, measured during the extension phase of each qPCR reaction cycle, is indicative of the amount of PCR product produced. Template cDNA in PCR is single-stranded; the source of any double-stranded DNA is solely attributable to the qPCR reaction.

The qPCR thermocycler graphs the fluorescence versus cycle number on a logarithmic scale in order to keep track of amplification. From these graphs, the amplification of targeted DNA sequences can be seen to enter three distinct phases: exponential, linear, and plateau. The exponential phase of amplicon production is seen as a linear line on a logarithmic scale. During the exponential phase of amplification, the thermocycler determines a threshold value for which the degree of fluorescence compensates for any background noise (Yuan 2006). The cycle number in which this threshold is reached is the cycle threshold value (C_t) and it is used to determine both the efficiency of the reaction and the concentration of PCR product. The C_t value is relative to the amount of PCR

product produced in the reaction, and is therefore relative to the amount of template present in the reaction (Yuan 2006).

qPCR reactions were performed and monitored by Life Technologies Applied Biosystem's 7300 Real-Time PCR system. This technique was used in this experiment in order to quantify the amount of *Parkin* relative to a housekeeping gene, *Actin 5C*.

Primer Optimization:

In qPCR, primers are optimized using a cDNA standard. Primer optimization allows the amplification efficiency of the reaction to be calculated (Yuan 2006). In this experiment, both *Parkin* primers and *Actin 5C* primers were optimized using a 250ng/µL sample of one-week old w^{1118} RT cDNA. Combinations of 100nM, 300nM, and 500nM concentrations of forward and reverse primer were tested. Each standard curve reaction was set up using the schema in Table 3. The thermocycler profile was adjusted as per the values listed in Table 4.

Table 3: **Reaction mixture for each Primer Optimization qPCR reaction**

Reagent	**Amount Per Reaction**
cDNA template (250ng/µL)	2.5 µL
Forward primer (100nM, 300nM, or 500nM)	2.5 µL
Reverse primer (100nM, 300nM, or 500nM)	2.5 µL
Nuclease free water	5 µL
2X Perfecta SYBR Green Supermix with ROX	12.5 µL

Table 4: **Thermocycler profile for the Primer Optimization qPCR reactions**

Stage	Cycles	Temperature	Time
1: *Taq* activation	1	92°C	2 minutes
2: Separation, Annealing, Extension	40	95°C	15 seconds
		61°C	30 seconds
		72°C	30 seconds
3: Dissociation	1	95°C	15 seconds
		60°C	1 minute
		95°C	15 seconds
		60°C	1 minute

The optimal primer concentration combination was determined by the sample with the lowest C_t. Optimal primer concentrations are as follows: *Parkin* primers was optimized at 100nM forward primer with 300nM reverse primer concentrations, while optimal *Actin 5C* Primer concentrations were 300nM reverse primer with 500nM forward primer.

Standard Curves:

Standard curves of *Parkin* primer and *Actin 5C* primer were set up on each experimental qPCR plate. The optimized primer concentrations were used in each standard curve reaction. Standard curve reactions are used to determine the efficiency of the optimized primer concentrations against a cDNA dilution series. A two-fold serial dilution starting with a 160ng/µL suspension of w^{1118} RT cDNA was made for each standard curve. The cDNA concentrations, created via serial dilution of cDNA samples in nuclease free water, ranged from 160ng/µL to 10ng/µL. Duplicate reaction wells of each cDNA concentration were set up in

each standard curce. cDNA was added in 2.5µL aliquots to each reaction well, creating a final cDNA concentration series of 400ng, 200ng, 100ng, 50ng, and 25ng. Standard curves using both optimized *Parkin* and optimized *Actin 5C* primers were set up and run using the outlined reagents and thermocycler profile in Tables 3 and 4.

The C_t values of the standard curve reaction were used to generate a linear standard curve. The slope of the trend line of C_t values versus the log of the cDNA concentration is used to calculate primer efficiency. Efficiency is calculated via the following equation:

$$\text{Primer efficiency} = 10^{(-1/\text{slope})}$$

Optimal primer efficiency is 2, although some choose to calculate this value as a percent.

Experimental qPCR:

Experimental reactions using 10ng/µL RT cDNA isolated from each *Drosophila* genotype collected at the 1, 2, 3, and 4 week markers were set up with the optimized *Parkin* and *Actin 5C* primer concentrations. Each of these reactions was run in duplicate. The corresponding No RT cDNA for each sample was also run in order to act as a negative control. Duplicates of No Template qPCR reactions for each primer, in which no cDNA was added to the reaction well, were also set up on each plate to function as a control for amplification. Once again, the pipetting schema and thermocycler profile for each reaction is iterated in

Tables 3 and 4.

qPCR Calculations for Relative Amplification:

The Pfaffl method of qPCR analysis was utilized to quantify amplification of the *Parkin* sequence (Pfaffl, 2001). The C_t values of each duplicate reaction were averaged. The difference in average C_t values between amplification of the target gene and the endogeneous control in both the w^{1118} and *Pink1RNAi* flies was calculated for each time point. The following equations were utilized:

$$\Delta Ct_{target} = \text{control} - \text{target}$$
$$\Delta Ct_{reference} = \text{control} - \text{target}$$

In these equations ΔCt_{target} is the difference in average amplification of control sequence (*Actin 5C*) and the target sequence (*Parkin*) in *Pink1RNAi Drosophila* cDNA samples. The $\Delta Ct_{reference}$ is the same calculation in w^{1118} animals. These values are used with the efficiency values of each primer to quantify the ratio of expression of the target gene to the reference gene. The following equation is utilized:

$$\text{ratio} = \frac{(E_{target})^{\Delta Ct\ target}}{(E_{ref})^{\Delta Ct\ reference}}$$

This equation compares the *Parkin* primer efficiency (E_{target}) raised to the ΔCt_{target} to the *Actin 5C* primer efficiency (E_{ref}) raised to the $\Delta Ct_{reference.}$ This calculation was performed for cDNA of samples collected at each week.

Transmission Electron Microscopy

To complement the PCR analysis of the two transgenic *Drosophila* lines, morphologic analysis of thoracic skeletal musculature was also completed. This analysis was done using transmission electron microscopy. As with PCR, w^{1118} and *Pink-1RNAi* flies were collected and aged at 25°C to one, two, three, and four weeks. Previous trial runs had determined that a sodium cacadylate buffer (as opposed to a sodium phosphate buffer) was ideal for *Drosophila* tissue. Flies were dissected using a freeze-fracture protocol, embedded in resin, stained, and viewed using a transmission electron microscope.

Dissection:

In order to preserve the organelle integrity of the collected myocytes, a freeze fracture method was employed. Freeze fracture dissection procedures have been previously employed, with high rates of success, on *Drosophila* muscle tissues (Allikian, 2006). Flies were anaesthetized for five minutes with CO_2 and kept on ice until dissection. Flies were then placed dorsal side up on a glass slide in a thin layer of Optimal Cutting Temperature (OCT) compound. The fly was not submerged in the compound, but rather stabilized in position. The entire slide was submerged in liquid nitrogen until the transparent OCT became opaque (approximately 7-10 seconds). This cryofixation not only prevents sample degradation, but ensures the formation of only vitreous ice - avoiding any damaging ice crystals. After submersion, flies were transferred to a large dish

with a thin layer of liquid nitrogen; here, they were bisected. Continued submersion during this process was imperative to maintain the temperature and prevent air exposure. To bisect the thorax, a hammer was used to apply light force to a razor above the desired cutting site. The bisection occurred along the longitudinal axis of the fly, but the increased brittleness of the specimens due to the cold facilitated further specimen fracture. The fractured specimens were transferred to primary fixative and stored at 4°C overnight. The primary fixative of 2.5% glutaraldehyde in 0.1 M sodium cacadylate buffer, pH 7.4, was made fresh for each fixation and kept at room temperature until use.

Post Fixation and Dehydration:

On the second day, samples were removed from primary fixative and washed 6 times (10 minutes each wash) in fresh 0.1 M solution sodium cacadylate buffer. After washing, samples were post-fixed in 2% osmium tetroxide solution (4% OsO_4 and .2M sodium cacadylate, pH 7.4 in a 1:1 ratio) for 1 hour at room temperature. Flies were then stained in 1% uranyl acetate solution or 30 minutes in semi-darkness. Prior to the addition of 1% uranyl acetate, flies were washed with dH_20 in order to avoid any unwanted precipitation. After staining, flies were washed with dH20 and then dehydrated in a 30, 50, 70, 80, 90, and 100% graded ethanol series.

Infiltration:

Propylene oxide was a used as a transitional solvent between the ethanol series and infiltration with Embed 812 medium-hardness resin. Samples were washed once in a 1:1 solution of 100% ethanol and propylene oxide and then twice in 100% propylene oxide. The samples were infiltrated at room temperature on a rotator by a series of propylene oxide to resin solutions (ratios of 2:1, 1:1, 1:2 and 1:0). Flies remained in the 2:1 and 1:1 solutions for 1 hour each, the 1:2 solution for 75 minutes, and 100% resin for 3 to 5 hours. Following infiltration with pure resin, flies were transferred to fresh resin for overnight infiltration.

Embedding, Polymerization, Sectioning, Staining and Viewing:

The following day, samples were transferred to fresh resin for polymerization. These samples were placed in a 50°C vacuum oven for 30-60 minutes and then transferred to a 70°C oven for overnight polymerization. After polymerization, small blocks of resin containing samples were cut, trimmed, and sectioned. Thick sections, 0.5µM in width, were stained with .5% toluidine blue in order to visualize tissue composition. Thin sections, 65 nm in width, were collected for staining. Sections were post-stained with 2% uranyl acetate and stained with Reynolds's Lead Citrate. Samples were viewed with a Phillips CM-100 TEM. Micrographs were scanned to a computer and figures were prepared using Adobe PhotoShop.

Pink1 RNAi and w^{1118} Climbing Assays:

The climbing assays for the *Pink1 RNAi* and w^{1118} flies were set up in the same manner as the climbing assays for the *hAPP*, *hParkin*, and *hAPP+hParkin* flies. Age comparable members of each genotype were collected in groups of 30 and maintained to prevent cross-generational contamination. Unlike the previous climbing trials, flies were collected only into plastic vials. These climbing assays were performed in the same manner as the *hAPP*, *hParkin*, and *hAPP+hParkin*, however all trials were performed in a plastic graduated cylinder only. The continuous use of plastic substrates ensured that age-dependence remained the only independent variable.

RESULTS

hAPP and *hParkin* Climbing Assays:

The climbing ability of w^{1118}, *Parkin*, *hAPP*, and *hAPP+hParkin* flies, was tested every week for four weeks after fly eclosion. The flies' ability to ascend the side of a glass or plastic graduated cylinder was noted and the average climbing ability for each genotype for each week was calculated. These tests serve as a correlational measure of climbing ability to genotype, and the plastic and glass mediums would serve to analyze the dependence of muscle stress on climbing ability. The negative geotropism of *Drosophila* serves to correlate muscle ability and integrity to climbing ability. To briefly reiterate, w^{1118} flies serve as a control; protein expression in their musculature remains unmanipulated. As with w^{1118}, there is no expected molecular impingement to climbing ability in *hParkin* flies. hParkin should not accumulate within the myocytes. Detrimental effects to climbing ability are assumed of the *hAPP* genotype. These same effects are predicted to be present to a lesser extent in the *hAPP+Parkin* flies, considering Parkin's involvement in degradation of hAPP fragments. Apart from

any transgenic protein express, decreased climbing ability due to natural senescence is anticipated in all genotypes. The effects of senescence should increase over the four-week period.

The data confirms the age-dependence of climbing ability; a gradual decrease in climbing capacity is seen across genotypes. Each genotype begins with an average rate of climbing success of approximately 90%. From the initial uniformity in week 1, w^{1118}, *hAPP+hParkin*, and *hParkin* flies show the same general diminution in climbing ability, but the trend for *hAPP* divaricates sharply to show a pattern of greatly reduced climbing capacity over the four-week span. There appears to be no immediate affects of climbing substrate on climbing capacity. Due to the lack of significance for this variable, the climbing data for both glass and plastic was combined.

w^{1118} flies begin with an average climbing success rate of 94.2%, a figure that gradually decreases to 73.5% in week 4. The h*Parkin* and the *hAPP+hParkin*, flies demonstrate a similar trend in their decrease in climbing ability. *hAPP+hParkin* flies begin with 93.2% successful climb rate and deteriorate to 67.1% success while h*Parkin* flies begin with 92.8% and end with 74.9%. It is notable that h*Parkin* continues to both have a higher rate of successful climbs than *hAPP+hParkin* and be closer to the w^{1118} results than *hAPP+hParkin*. *hAPP* has the most drastic decrease in climbing ability over time; the final average percent of successful climbs at four weeks is 50.8%.

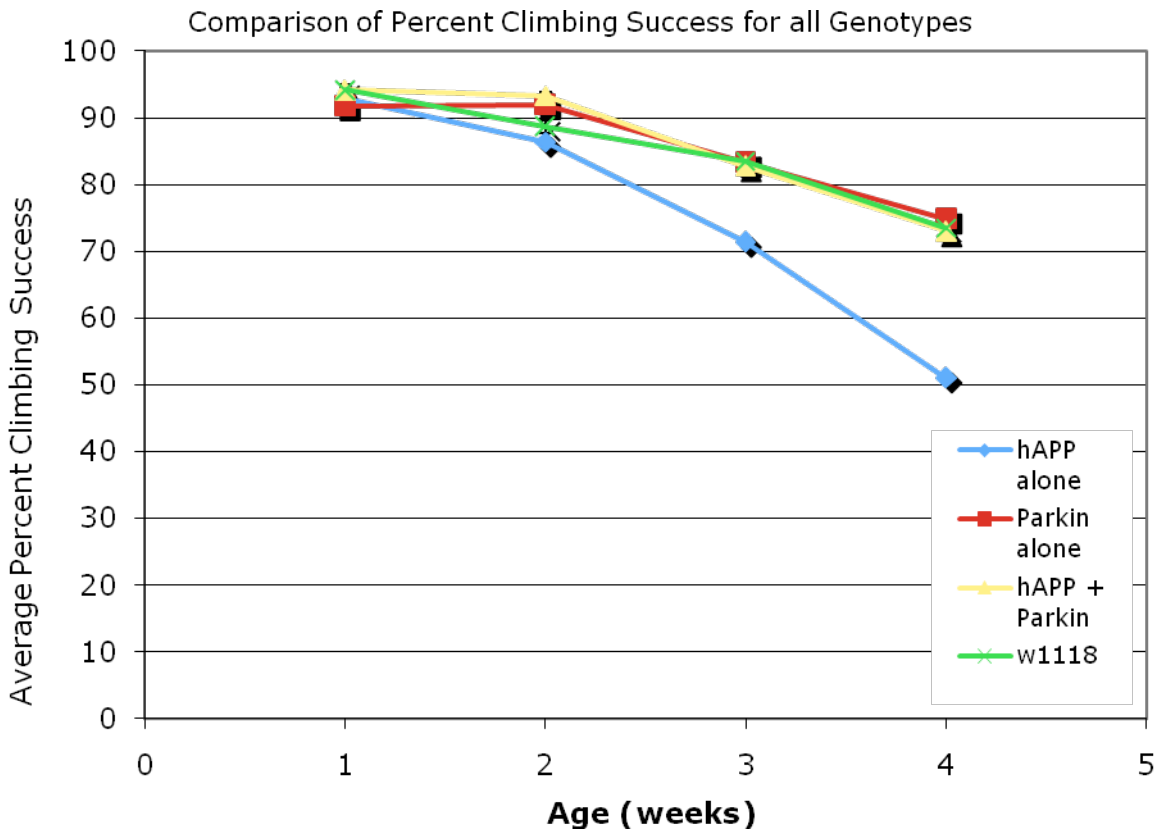

Figure 12. **A comparative analysis of the climbing success of *hAPP*, *hParkin*, *hAPP+hParkin*, and w^{1118} over the four week period.** Consistent with the hypothesis of this investigation, *hAPP* flies experienced the most dramatic decrease in climbing ability, the expression of *Parkin* acted to rescue the effects of *hAPP* expression, and w^{1118} and *Parkin* flies experienced no dramatic decrease in climbing ability.

RT-PCR Analysis of *Parkin* Expression in *Pink-1RNAi* and w^{1118}:

The electrophoretic results of the RT-PCR products were used as qualitative means of comparison of *Parkin* expression between genotypes and with age. RT-PCR was performed as a control of proper cDNA synthesis and PCR primer function. Proper banding patterns, corresponding to the expected base pair length of each primer amplicon, were verified via electrophoresis.

Additionally, the lack of bands in the No RT control lanes and the presence of bands in the RT lanes were also verified. Of the multiple cDNA samples tested, few No RT cDNA samples produced a complete lack of PCR product. Samples analyzed using this qualitative method were then run in a qPCR reaction in order to quantify the presence of *Parkin* relative to *Actin 5C*. Below, in Figure 14, is an example of a gel in which the samples used show the proper No RT/RT banding pattern which would conscript the cDNA samples to qPCR analysis. The corresponding gel loading schema can be viewed in Table 5.

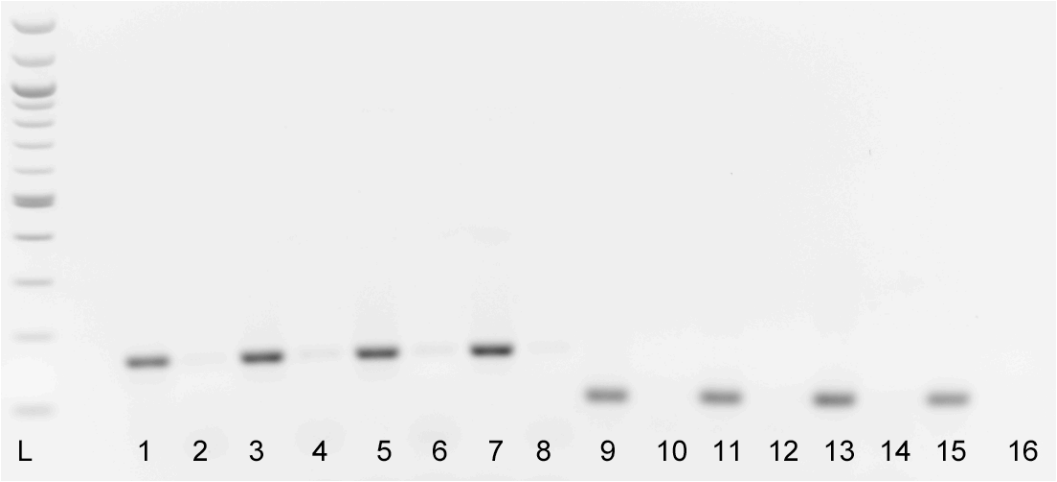

Figure 13. **4% Agarose gel of PCR products of one-week and two-week aged w^{1118} and *Pink1 RNAi* flies.** This gel serves as an example of the expected band pattern differenced expected between RT and No RT samples. This gel was run at 150V for approximately 80 minutes. The identities of the labeled lanes may be cross-referenced with Table 5.

Table 5: **Gel loading schema for the gel displayed as *Figure 14*.**

Lane	Sample	Lane	Sample
L	100 BP Ladder	9	One-week old *Pink1 RNAi* RT Primer: *Parkin*
1	One-week old *Pink1 RNAi* RT Primer: *Actin 5C*	10	One-week old *Pink1 RNAi* No RT Primer: *Parkin*
2	One-week old *Pink1 RNAi* No RT Primer: *Actin 5C*	11	One-week old w^{1118} RT Primer: *Parkin*
3	One-week old w^{1118} RT Primer: *Actin 5C*	12	One-week old w^{1118} No RT Primer: *Parkin*
4	One-week old w^{1118} No RT Primer: *Actin 5C*	13	Two-week old *Pink1 RNAi* RT Primer: *Parkin*
5	Two-week old *Pink1 RNAi* RT Primer: *Actin 5C*	14	Two-week old *Pink1 RNAi* No RT Primer: *Parkin*
6	Two-week old *Pink1 RNAi* No RT Primer: *Actin 5C*	15	Two-week old w^{1118} RT Primer: *Parkin*
7	Two-week old w^{1118} RT Primer: *Actin 5C*	17	Two-week old w^{1118} No RT Primer: *Parkin*
8	Two-week old w^{1118} No RT Primer: *Actin 5C*	-	-

qPCR Analysis of *Parkin* Expression in *Pink1 RNAi* and w^{1118}:

Primer Efficiencies:

Primer efficiencies were calculated using the C_t values collected from each standard curve. The 7300 BioAnalyzer software used the C_t values for reactions using cDNA concentrations of 160ng/µL, 80ng/µL, 40ng/µL, 20ng/µL, and 10ng/µL to calculate the slope of the standard curve. The slope of the standard curve was used to calculate the efficiency of each primer. Since standard curves were set up on each experimental qPCR plate run, efficiency values differ with the plate. The efficiency values of each primer for each plate can be viewed in Table 6 and Table 7.

Table 6: **Primer Efficiency values for qPCR Experimental Plate 1**

Primer	Efficiency
Parkin	2.06
Actin 5C	2.64

Table 7: **Primer Efficiency values for qPCR Experimental Plate 2**

Primer	Efficiency
Parkin	1.99
Actin 5C	2.23

These efficiency values were used in calculating the ratio of *Parkin* amplification between w^{1118} and *Pink-1RNAi* flies.

Relative Expression of *Parkin* in *Pink-1RNAi* and w^{1118}:

There existed no significant difference in *Parkin* expression between w^{1118} and *Pink1 RNAi* flies at any age. The Pfaffl method was used to quantify the relative expression of *Parkin* in all flies to the expression of a house-keeping gene, *Actin 5C* (please see Methods and Materials for sample calculations). All relative expression values are out of one; a ratio value of one would communicate that both the target gene and the house-keeping gene had been equally expressed. Expression of the house-keeping gene is expected to remain constant with time; therefore, the degree of change in the ratio of expression becomes statistically valid for as a measure of target gene expression.

Despite a rise in *Parkin* expression during week 2, there exists no continuous decrease of endogenous *Parkin.* The relative expression ratio of *Parkin* to *Actin 5C* between genotypes was .82 in the first week of life, 2.07 in the

second week of life, .94 in the third week of life, and .92 in the fourth week of life. This trend is viewable in Figure 15.

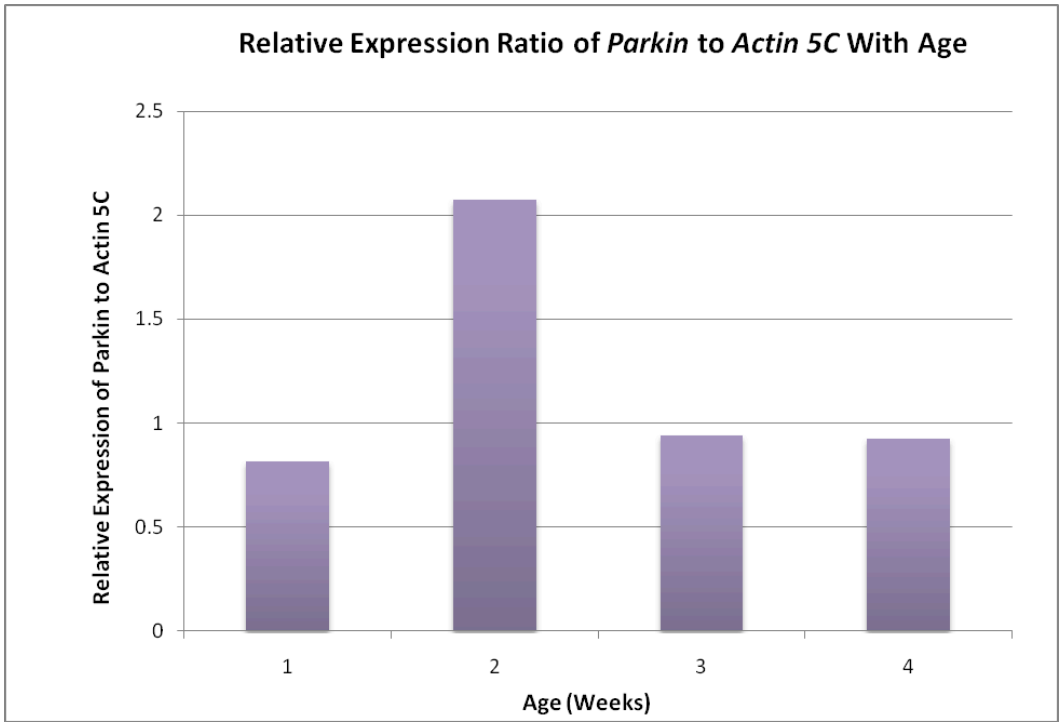

Figure 14: **The relative expression ratio of *Parkin* to *Actin 5C* expression between *Pink1 RNAi* and w^{1118} flies with age.** With the exception of Week 2, there is no observable difference in the expression of *Parkin* between genotypes.

Pink1 RNAi and w^{1118} Transmission Electron Microscopy

Testing of Fixative and Resin:

The microscopic analysis of *Pink1 RNAi* and w^{1118} muscle ultrastructure was intended to provide a comparative analysis of the morphological differences between the two genotypes. It was hypothesized that the loss of *Pink1* expression would present myocytes with severely compromised mitochondria and degrades myofibrils. A comparative cross-sectional study of indirect flight muscle (IFM) and tergotrochanter muscle (TTM) was conducted.

Data from Shuang Shao, a previous student in the laboratory, identified the freeze-fracture preparation as the best method for the preservation of *Drosophila* muscle tissue. She discovered that vacuolization of tissue and mitochondrial abnormalities existed as artifact of the dissection procedure (Shao 2010, MHC honors thesis). These abnormalities can be attributed to necrosis of the tissue in the interim between extraction of thorax tissue and fixation. From her data, I decided to test two different fixatives and resins with the freeze-fracture preparation in order to further optimize this process of *Drosophila* muscle fixation.

One-week old w^{1118} flies were used during this optimization procedure. The use of wild-type served to assure that any abnormalities viewed were a result of the fixation procedure, rather than the presence of the transgene. Mitochondrial abnormalities present in flies fixed with 2.5% glutaraldehyde in 0.1 M $NaPO_4$ buffer ($NaPO_4$ buffer) and infiltrated with either Spurrs/Quetol extra-low

viscosity resin (Spurr's) or Embed 812 medium-hardness resin were not present in flies fixed with 2.5% glutaraldehyde in 0.1 M sodium cacodylate buffer, pH 7.4 (Na cacodylate buffer) and infiltrated with either resin. The negative effects of $NaPO_4$ buffer are discontinuous mitochondrial membrane and disintegration of cristae. Sections fixed in $NaPO_4$ buffer also appear highly vacuolated and less cytoplasmic material can be viewed. No differences were observed between samples fixed in the same buffer, but different resins. Embed 812 resin proved easier to section and was employed in the *Pink1 RNAi* and w^{1118} study.

Figure 15. **Section of a one-week old *w*^{1118} *Drosophila* IFM thorax myocyte.** This section was taken from a sample of Drosophila thorax tissue fixed with 2.5% glutaraldehyde in a .1M $NaPO_4$ buffer and infiltrated with Embed 812 medium-hardness resin. The orientation of the myofibrils (My) and Z-bands indicates that this is a transverse section of the myocyte. Both intact (M) and abnormal mitochondria (aM) are present in this section. Mitochondrial 'blow-outs' are apparent. The residual cristae (C) of these mitochondria are visible within the remaining outer membrane (OM). These mitochondrial defects are atypical in young wild-type flies; such an anomaly may be attributable to the fixation method used or fixation problems specific to this particular specimen. A section of tracheae (T), a portion of the extensive network of epithelial tubes that form the respiratory system of the fly, is present. Glycogen granules (Gly), the source of the metabolic fuel produced by the mitochondria, pepper the cyoplasm. Lead citrate precipitates (St), artifacts of the staining process, are also present.

Figure 16. **Section of a one-week old *w*^{1118} *Drosophila* IFM thorax myocyte.** This section was taken from a sample of *Drosophila* thorax tissue fixed with 2.5 % glutaraldehyde in a .1M Na cacadylate buffer and infiltrated with Embed 812 medium-hardness resin. Myofibrils (My) that provides the basic contractile capability of muscle run parallel and are closely surrounded by multiple mitochondria (M). The mitochondria are intact here, both the outer mitochondrial membrane and the internal the cristae (C) remain continuous.

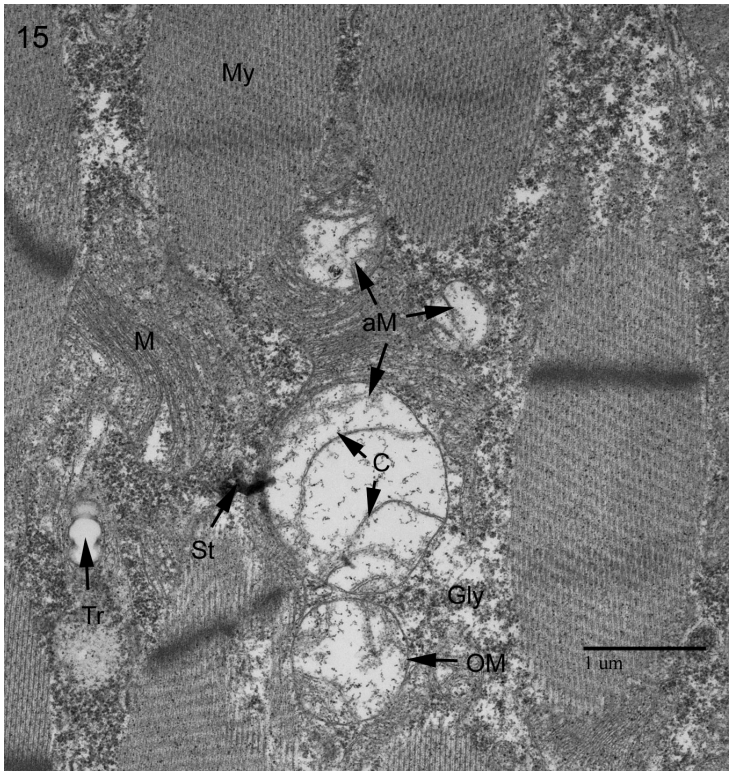
15
My
aM
M
C
St
Tr
Gly
OM
1 um

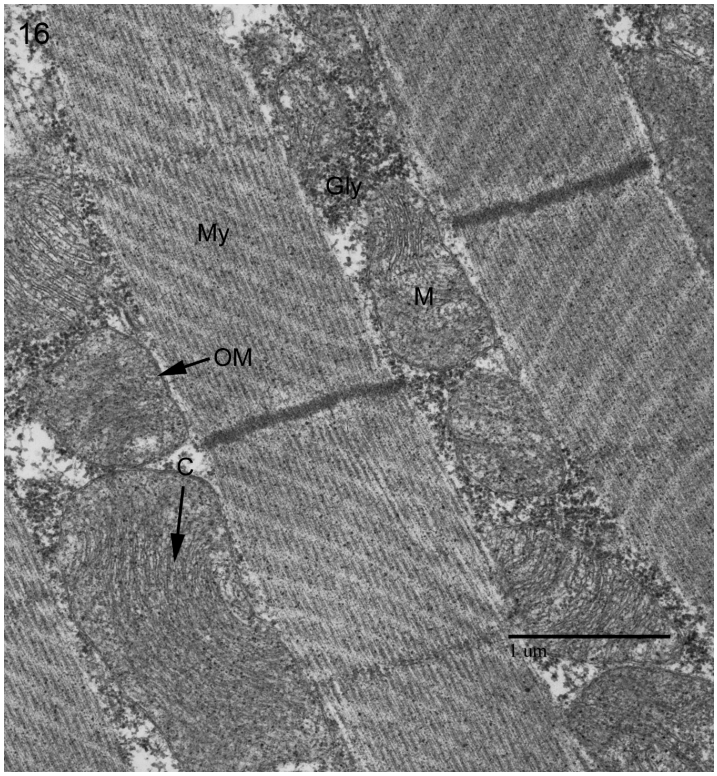
16
Gly
My
M
OM
C
1 um

***Pink1 RNAi* and w^{1118} analysis:**

The freeze-fracture dissection technique, employing the Na cacodylate buffer and the Embed 812 resin, was used for the cross-sectional analysis of *Pink1 RNAi* and w^{1118} flies aged 1, 2, 3, and 4 weeks.

Drosophila myocyte ultrastructure is very similar to the myocyte ultrastructure found in most mammals, making *Drosophila* muscle tissue an excellent biological platform for research (Wantanabe and Williams 1953). *Drosophila* thorax flight musculature consists of four main muscle groups: dorsal longitudinal, tergosternal, oblique dorsal, and tergocoxal. Muscle fibers consist predominantly of long myofibrils ensconced in neighboring globular mitochondria. Granules of glycogen (a glucose polymer broken down to be used to fuel glycolysis) and areas of the sarcoplasmic reticulum (a membranous Ca^{++} storing network used in excitation-contraction coupling) are visible within myocyte preparations. As in mammals, longitudinal myofibrils are composed of banded myofilaments composed of actin and myosin. *Drosophila* myofiber structure reveals the presence of A, Z, I, M and H bands (Shafiq 1963). Z-bands (Z-discs), electron dense areas of striated muscle, bracket neighboring sarcomeres. In *Drosophila*, α-actinin is the main protein component of Z-bands, giving them their electron-dense appearance during TEM (Saide 1989).

Indirect flight muscle and tergotrochanter muscle were viewed for each genotype for each week. Indirect flight muscles are fibrillar muscles attached to

the outer wall of the thorax that control the propelling force in flight (Demerec 1994). Tergotrochanter muscles, the second major group of indirect flight muscles, are also found in the thorax (Hartenstein 2006). These muscles, characterized by narrower myofibrils, few mitochondria, and extensive sarcoplasmic reticulum are connected to and help to direct the movement of the trochanter muscles of the leg (Demerec 1994). For each week, four *Pink1 RNAi* animals and at least two w^{1118} animals were observed. The hypothesized abnormalities in the *Pink1 RNAi* flies were strikingly absent or diminished in all samples except for one three-week old animal. Mitochondrial abnormalities and myofibrillar disintegration within the *Pink1 RNAi* animals are absent in most samples. There is some evidence of myofibril tearing in some samples, but consistent degeneration is not present. In other *Pink1 RNAi* samples, mitochondria appear swollen. This swelling is discernable by the presence of enlarged and morphologically variable cristae, and in some samples, the apparent presence of cytosolic materials (such as glycogen) within the mitochondria. The seemingly intra-mitochondrial cytosolic materials are unaccompanied by disintegration of mitochondrial outer membrane and, may therefore be, a vestige of sample sectioning. There is inconsistency in the appearance of these findings, not only between flies of the same genotype and ages, but within samples themselves.

Consistently, cytosolic gaps between indirect flight muscle myofibrils are found in *Pink1 RNAi* flies. Cytosolic gaps are present in w^{1118} flies as well, but there, gaps are concentrated predominantly towards the edges of tissue samples.

These peripheral gaps can result from mechanical stress on the edges of samples. There was no consistency in location of these gaps in *Pink1 RNAi* flies. Additionally, equal areas of little to no cytosol visibility exist within the *Pink1 RNAi* samples. These areas appear akin to the ^{w1118} samples in which parallel myofibrils are ensconced by normal mitochondria. This points to an intracellular inconsistency in the *Pink1 RNAi* flies.

One three-week old fly of the *Pink1 RNAi* group demonstrated severe mitochondrial abnormalities and myofibril degradation. This degradation is extensive and pervasive throughout the tissue sample. Mitochondria appear either swollen or lysed. The outer membranes are ruptured and the residual cristae lack any normal morphological organization. These findings are substantially different from all other flies observed, in which the mitochondria and myofibrils are intact and undeteriorated.

The following figures present the observed muscle morphology in each genotype for each week at different magnifications.

Figure 17. **One-week old w^{1118} indirect flight muscle**
The orientation of the Z-bands (Z) and I-bands (I) reveals that this is an oblique cut of the tissue. Few gaps between mitochondria and myofibrils are visible, indicating the density of each organelle within the tissue. Scale bar 1µm.

Figure 18. **Normal one-week old *Pink1 RNAi* indirect flight muscle.**
The myofibrils (My) in this longitudinal section of muscle run parallel. Mitochondria (M) with intact outer membranes (OM) and densely packed cristae (C) fill in the areas between the myofibrils. Individual myofilaments are distinguishable (Mf) in each sarcomeric subunit. These subunits are bracketed by Z-bands (Z) and I-bands (I). Scale bar 1µm.

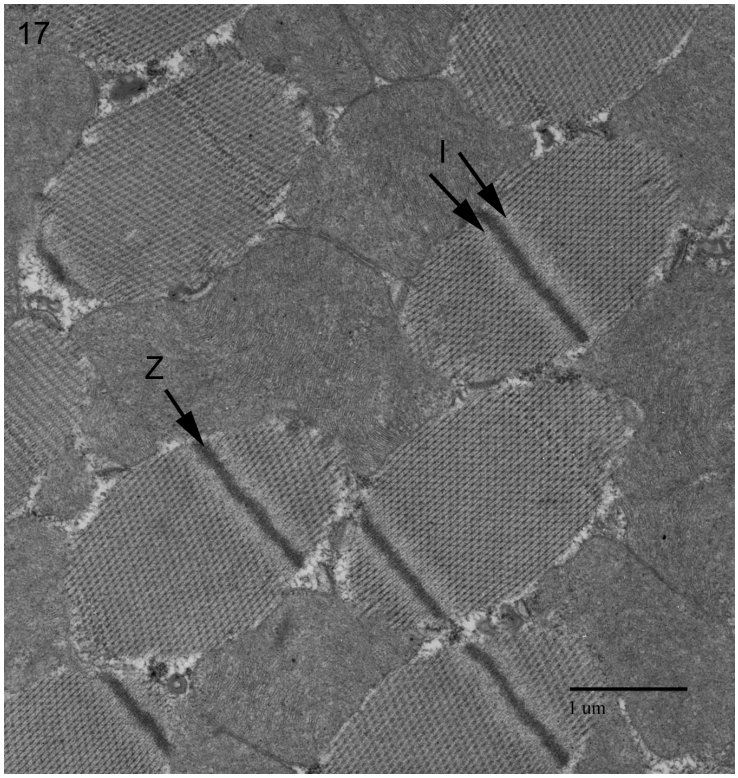
17
I
Z
1 um

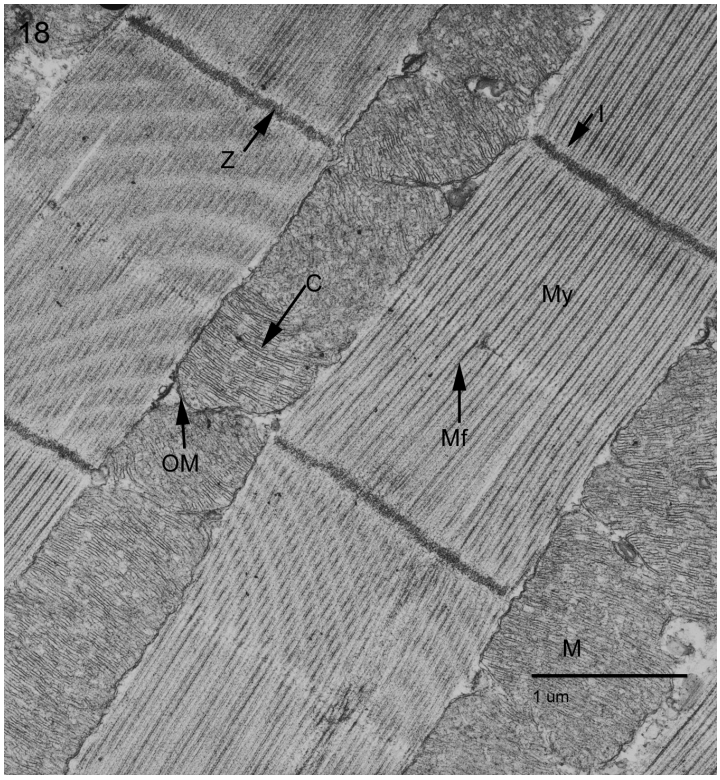
18
Z
I
C
My
OM
Mf
M
1 um

Figure 19. **One-week old w^{1118} indirect flight muscle at the edge of a section shows larger cytosolic gaps.**
While the myofibers and mitochondria still appear normal, the increased appearance of cytoplasm near the peripheries of sections indicates that they are artifact resultant of mechanical or chemical stress during the fixation process, and not any deficiency of the tissue. Scale bar is 1µm.

Figure 20. **One-week old *Pink1 RNAi* indirect flight muscle presenting normal muscle morphology.**
Once again, the I-band (I) and Z-disc borders of sarcomeres are distinguishable and indicate a longitudinal orientation of the specimen in which a glancing section of myofibril has been taken. There is no vacuolization, and glycogen granules (Gly) are visible in the cytosol at the borders of the exposed myofibrils. H-bands, bisecting A-bands, are also distinguishable here, indicating that the muscle is relaxed. Scale bar is 1µm.

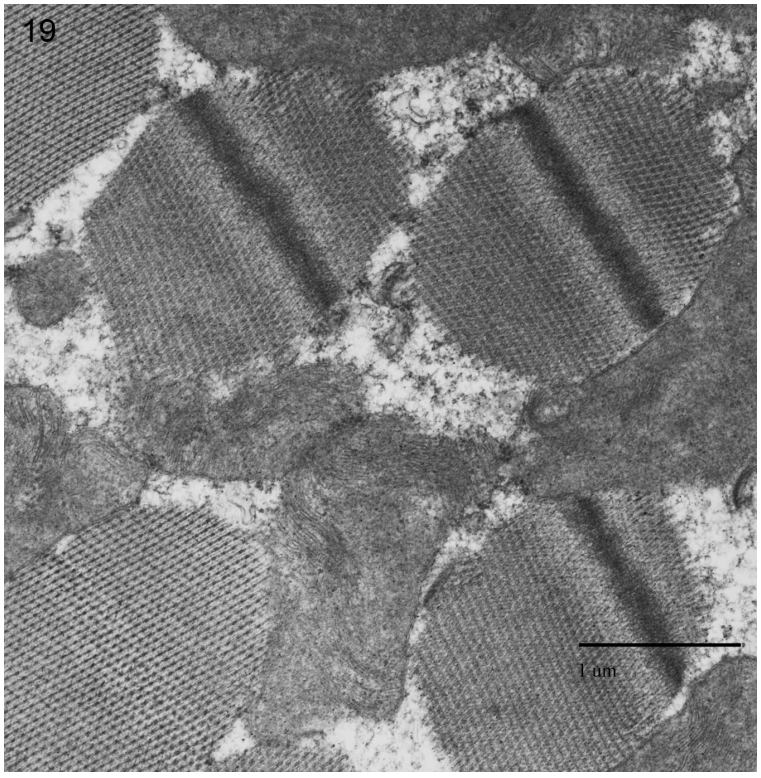
19
1 um

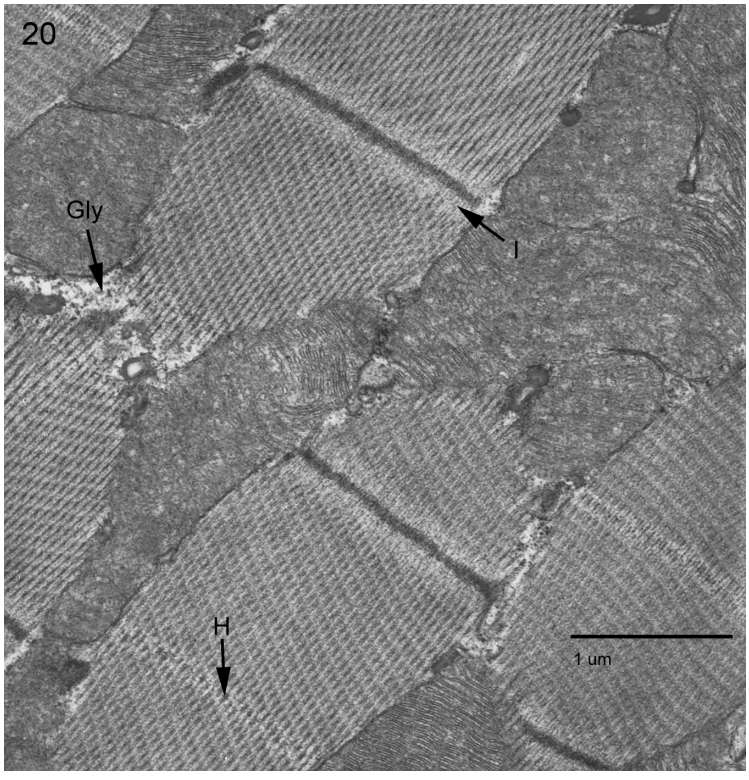
20
Gly
I
H
1 um

Figure 21. **One week old *w*^{1118} indirect flight muscle with visible cytosol at myofibril periphery.**
This section, another area of the same tissue in Figure 19, shows increased cytosol visibility. Mitochondria remain densely packed around the myofibrils. The cytosolic visibility may be indicative of yet another glancing cut of the myofibrils. Scale bar is 2μm.

Figure 22. **Tergotrochanter muscle of a one-week old *Pink1 RNAi* fly with normal mitochondria.**
Membrane of the sarcoplasmic reticulum (SR) is interspersed between the parallel myofibers (My). The orientation of the myofilaments (Mf) within each myofiber and the aligned bisection of the myofilaments by Z-bands indicate that this is a longitudinal section of tergotrochanter muscle tissue. Mitochondria (M) are visible and present no unusual morphology. Scale bar is 1μm.

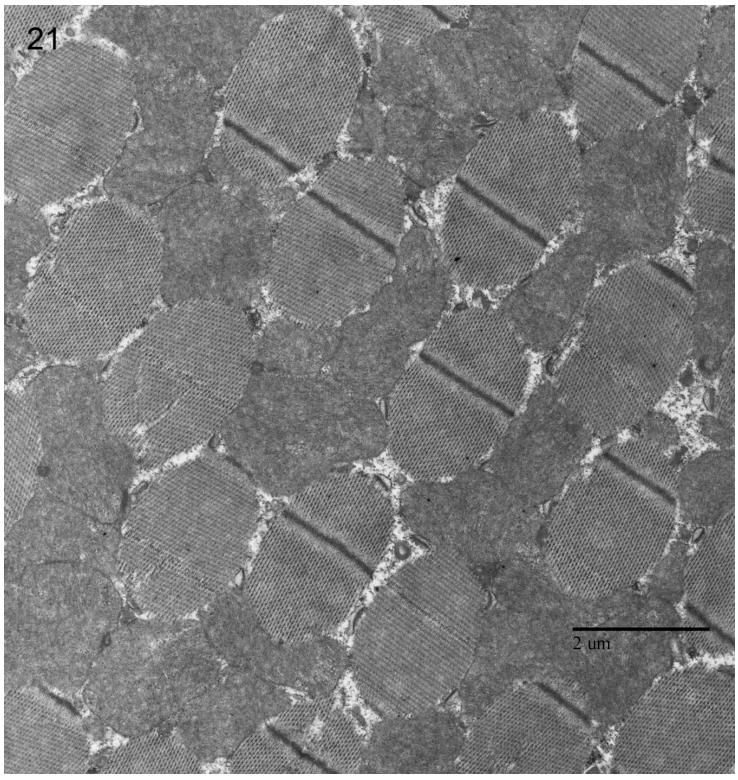
21
2 um

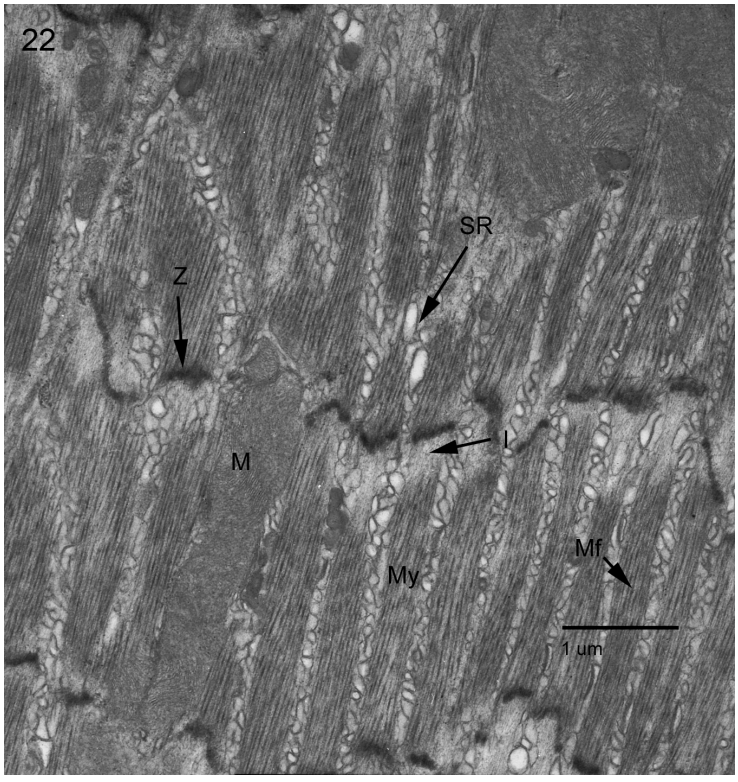
22
SR
Z
I
M
Mf
My
1 um

Figure 23. **Two-week old *Pink1 RNAi* indirect flight muscle has normal mitochondria.**
A longitudinal cut through the myocyte reveals parallel myofibrils. Entire A-bands (A), bracketed by I-bands (I) and Z-bands (Z) have visible M-bands (Mb). There are intact mitochondria (M) with highly organized electron dense cristae (C). These mitochondria are densely packed, but sarcoplasmic reticulum and glycogen (Gly) rich cytoplasm are visible. Scale bar is 1μm.

Figure 24. **Two-week old *Pink1 RNAi* indirect flight muscle with visible cytoplasm localized at the edges of bisected myofibrils.**
Parallel myofibrils wit visible H-bands (H) and M-bands (Mb) are ensconced by intact mitochondria. Glycogen (Gly) rich cytoplasm (Cy) is visible, but its appearance seems to be localized at the edges of myofibrils that have been bisected by sectioning. These types of cytosolic gaps can be assumed to be artifact and not vacuolization. Scale bar is 1μm.

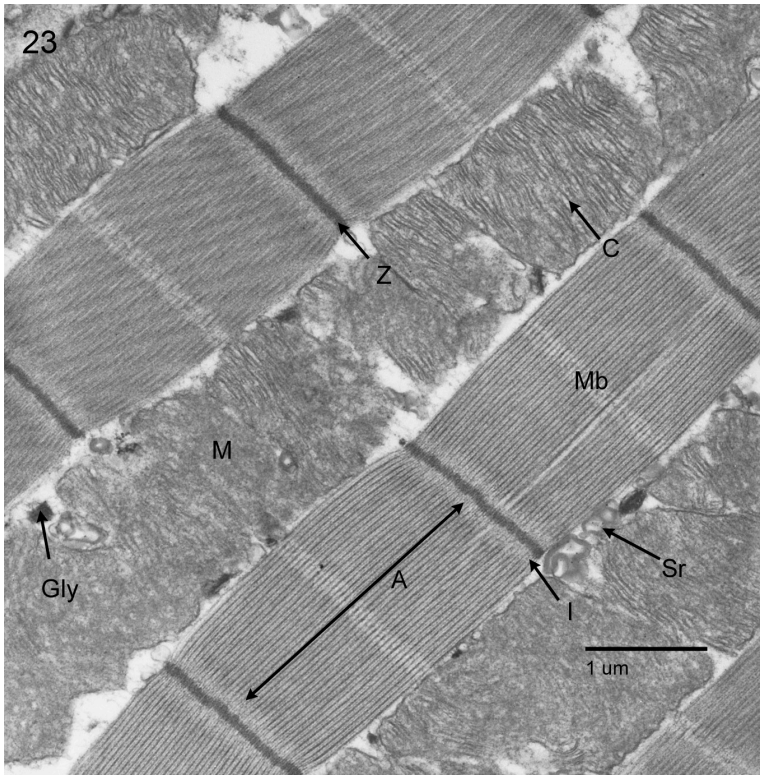
23
Z
C
Mb
M
Gly
A
I
Sr
1 um

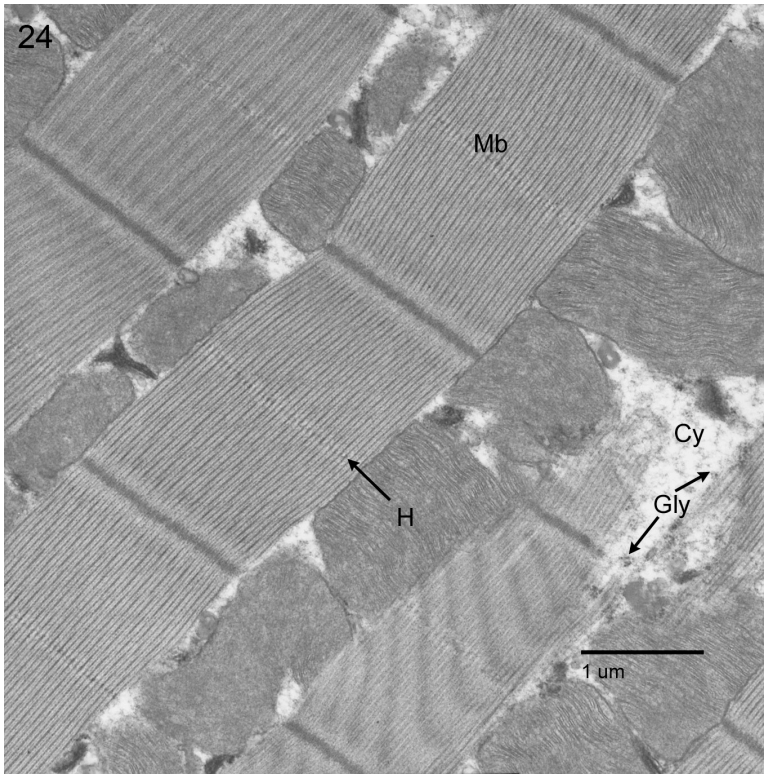
24
Mb
Cy
H
Gly
1 um

Figure 25. **Two-week old *Pink1 RNAi* indirect flight muscle with torn myofibrils.**
As seen in Figure N (4285), cytosolic gaps are found at the ends of myofibrils that have been bisected by sectioning. These myofibrils also appear torn (Tr). The localization of the tears at the edges of the bisected myofibrils is suggestive of their origination through some form of mechanical stress during sectioning. Scale bar is 1μm.

Figure 26. **Two-week old w^{1118} indirect flight muscle has normal morphology.** Here, mitochondria are densely packed around myofibrils. No degradation of any kind is witnessed. There is some visible cytosol, its appearance is minimal and inconsistent. Scale bar is 1μm.

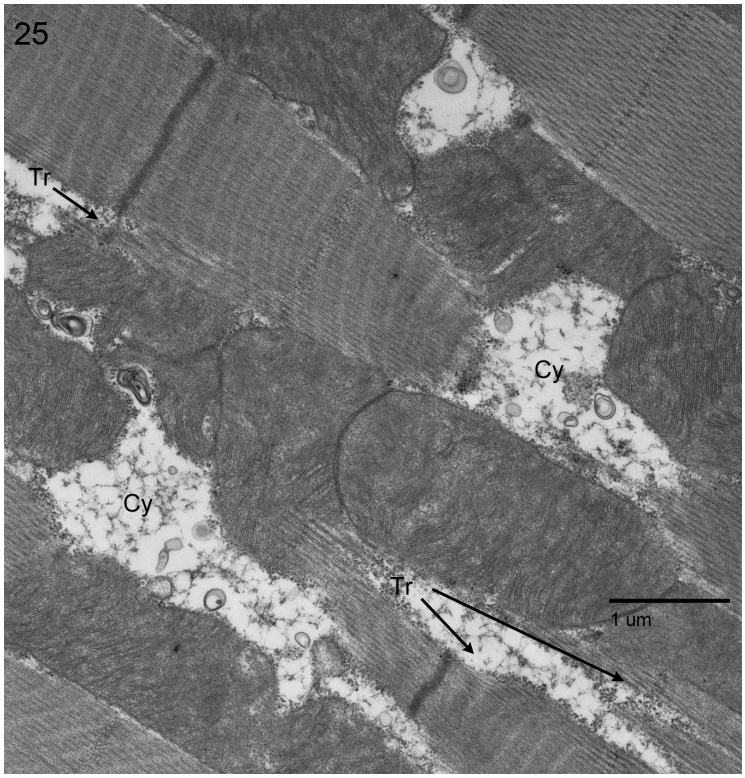
25
Tr
Cy
Cy
Tr
1 um

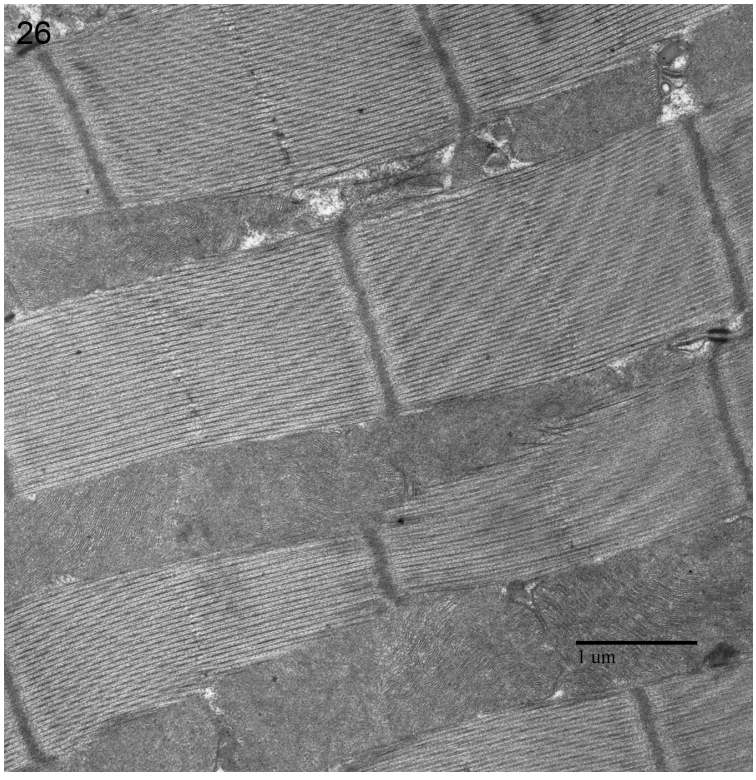
26
1 um

Figure 27. **Two-week old *Pink1 RNAi* indirect flight muscle appears normal.** At this magnification, the densly packed cristae (C) and outer mitochondria membranes (OM) are observable. Some sarcosplasmic reticulum (SR) is identifiable, as is cytosolic glycogen (Gly). Myofibril structure is unblemished; this longitudinal sample reveals the characteristic Z-band (Z), I-band (I), M-band (M) pattern. Scale bar is 1μm.

Figure 28. **Two-week old w^{1118} indirect flight muscle.**
There is little outwards difference between the indirect flight muscle here and that seen in Figure 4300. Once again mitochondria (M) have intact outer membranes (OM) and densely packed cristae (C). Myofibers are intact and unblemished. Some extraneous lead citrate precipitate is visible (St). Scale bar is 1μm.

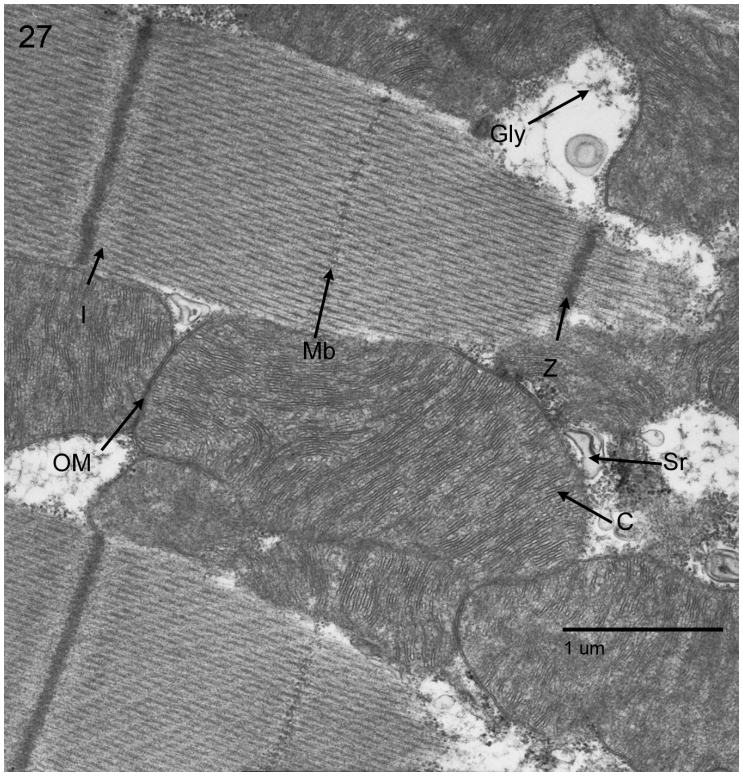
27
Gly
I
Mb
Z
OM
Sr
C
1 um

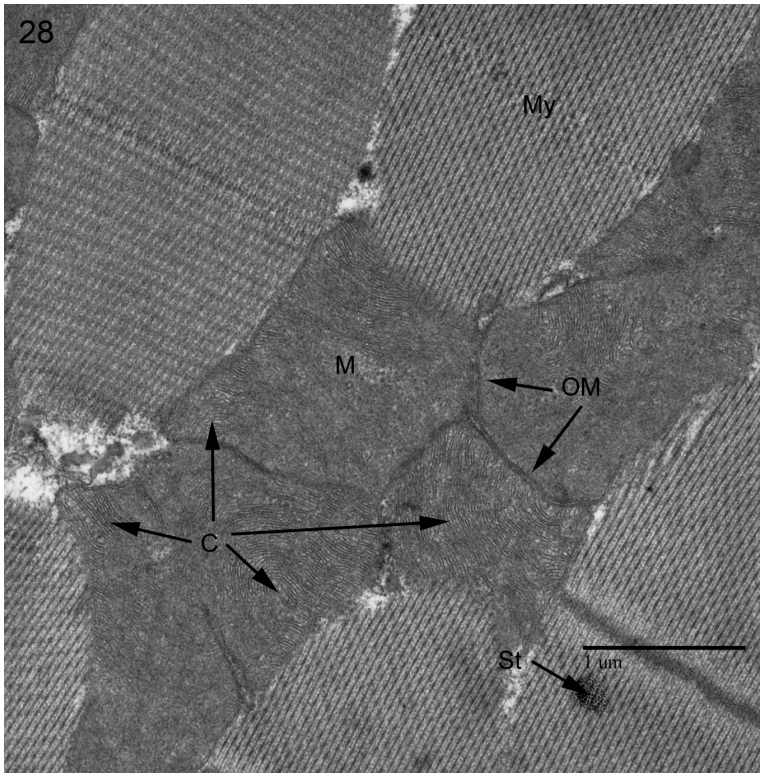
28
My
M
OM
C
St
1 um

Figure 29. **Indirect flight muscle of a two-week old *Pink1 RNAi* animal.**
The muscle ultrastructure here reveals normal myofibrils (My) surrounded by intact mitochondria (M). Glycogen (Gly) rich cytosol (Cy) is visible, but these gaps between mitochondria and myofibrils are not pervasive enough to be described as vacuolization. Tracheae (T) are visible. Scale bar is 2μm.

Figure 30. **Two-week old w^{1118} indirect flight muscle.**
An expansive oblique section of muscle exhibiting densely packed mitochondria (M) between intact myofibrils (My). The lateral cut can be determined via Z-band and I-band orientation. Glancing cross-sections of tracheae (T) are observable. Scale bar is 1μm.

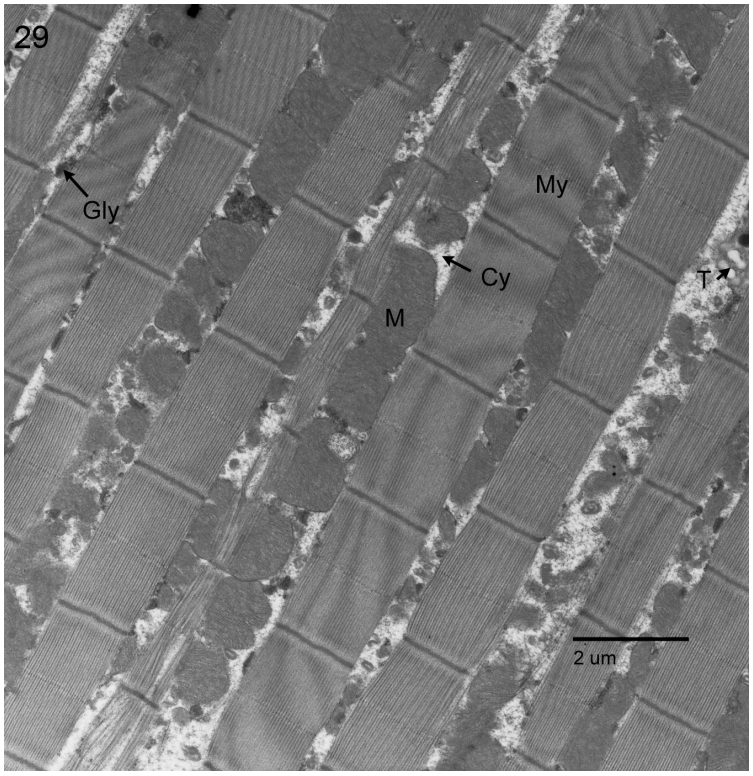
29
Gly
My
Cy
T
M
2 um

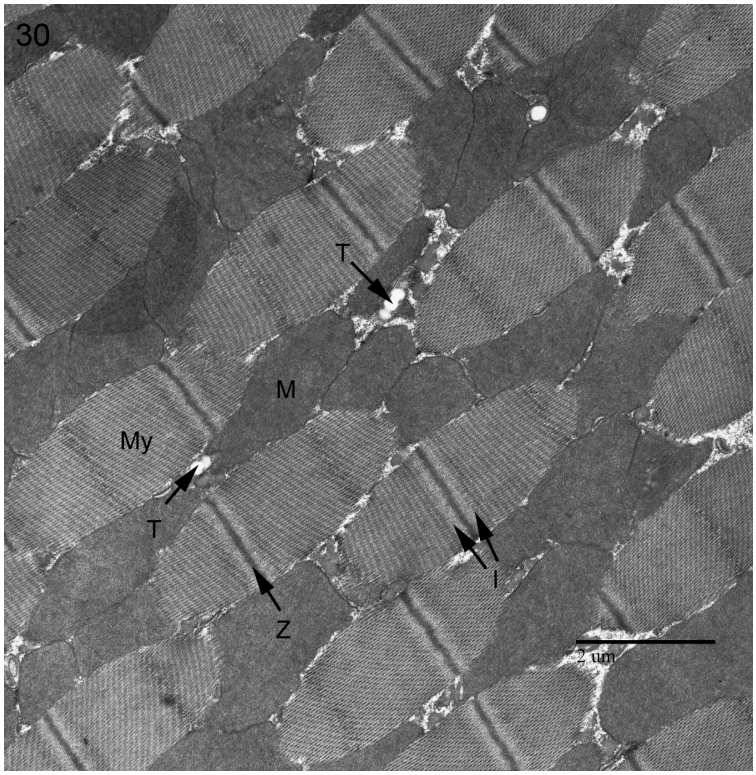
30
T
M
My
T
I
Z
2 um

Figure 31. **Two-week old *Pink1 RNAi* tergotrochanter muscle.**
A lateral section of tissue revealing thin myofibrils (My). The myofibrils run parallel and have aligned Z-bands (Z). Sarcoplasmic reticulum (SR) appears between adjacent myofibrils and electron dense mitochondria (M) with intact and organized cristae (C) can be seen. Scale bar is 1μm.

Figure 32. **Two-week old w^{1118} tergotrochanter muscle.**
As in the *Pink1 RNAi* sample of corresponding age, myofibrils (M) are intact and aligned at their Z-bands (Z). Once again, considerable amounts of sarcoplasmic material (SR) are visible and bands of intact mitochondria (M) run alongside the myofibrils. The disorientation of the myofibrils is due to the plane of section. Scale bar is 1μm.

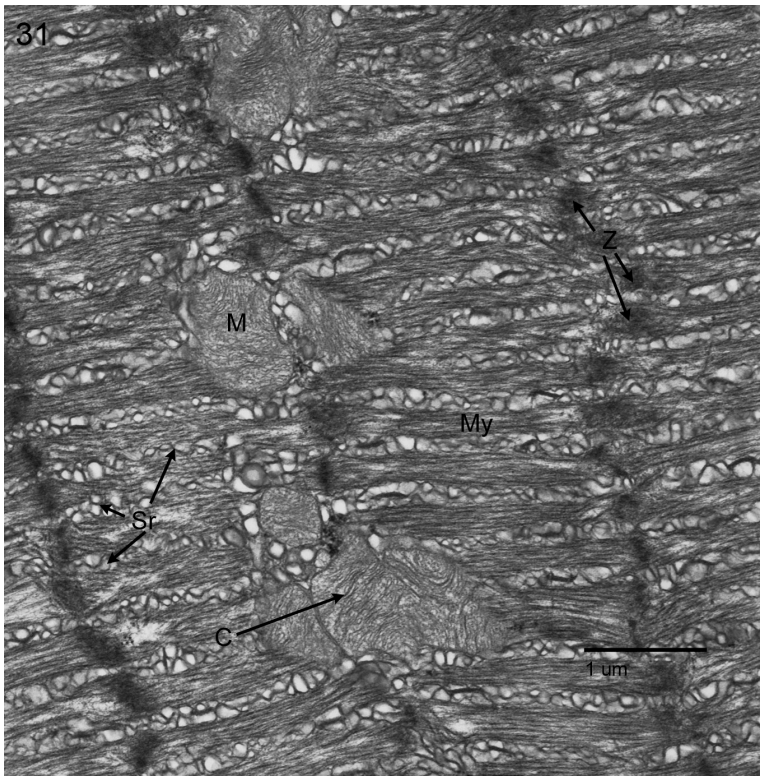
31
Z
M
My
Sr
C
1 um

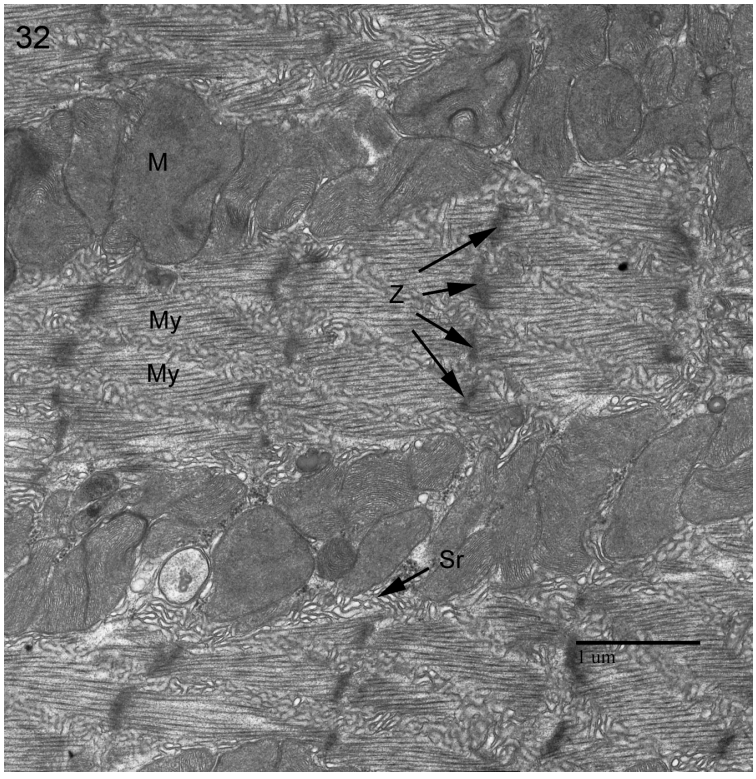
32
M
Z
My
My
Sr
1 um

Figure 33. **Three-week old *Pink1 RNAi* indirect flight muscle with unevenly distributed mitochondria**
A longitudinal section of tissue reveals parallel myofibrils (My) separated by normal, electron dense mitochondria (M) and areas of open cytoplasm (Cy) containing free glycogen (Gly) granules. The differences in mitochondrial density between myofibrils continues throughout the animal. Scale bar is 1µm. (4325)

Figure 34. **Three-week old *Pink1 RNAi* indirect flight muscle.**
In this section, taken from the edges of a sample, a lateral cut of the myofibril arrangement reveals swollen mitochondria (sM). This swelling is denoted by visible gaps between cristae. Additionally, cristae (C) uncircumscribed by outer mitochondrial membrane are visible. A glancing cut of the trachea (T) is also discernable within the glycogen rich cytosol. Scale bar is 1µm.

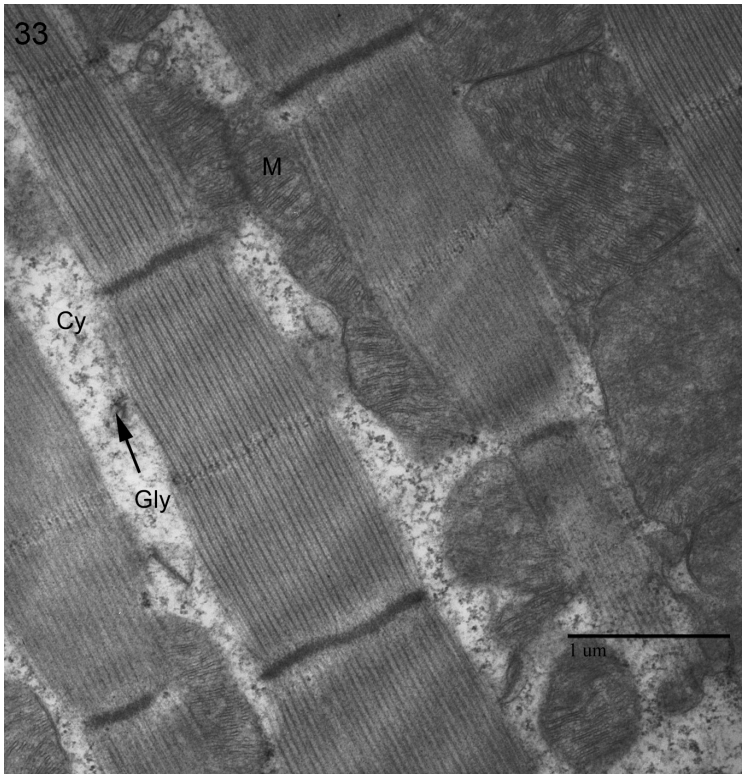
33
M
Cy
Gly
1 um

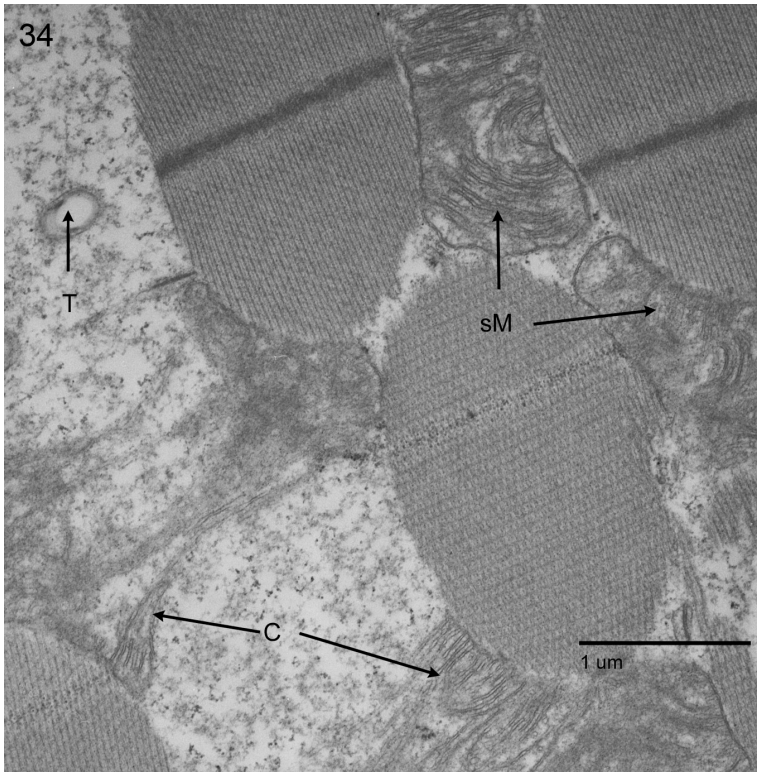
34
T
sM
C
1 um

Figure 35. **Indirect flight muscle of three-week old *w*^{1118} *Drosophila.***
A longitudinal section of thick, intact, parallel myofibrils ensconced by morphologically normal mitochondria. Scale bar is 1μm.

Figure 36. **Three-week old *Pink1 RNAi* indirect flight muscle has visible cytosol where myofibrils are bisected.**
A longitudinal cut of the musculature bisects the parallel myofibrils (My). Once again, at the areas of bisection, glycogen (Gly) rich cytosol (Cy) is present. The localization of these gaps can once again be attributable to orientation of the tissue during sectioning. Mitochondria appear healthy within intact outer membranes (OM). Scale bar is 1μm.

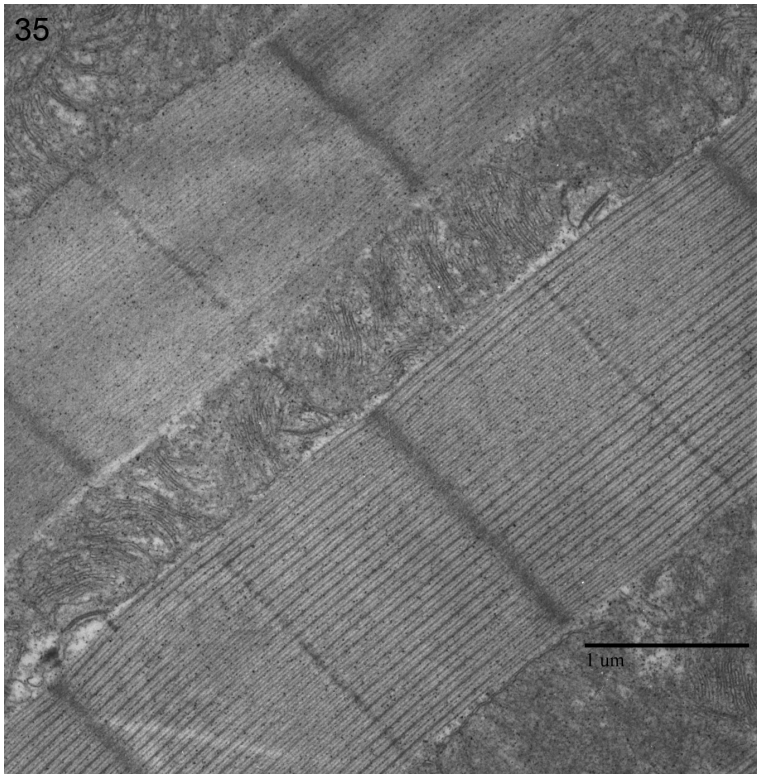
35
1 um

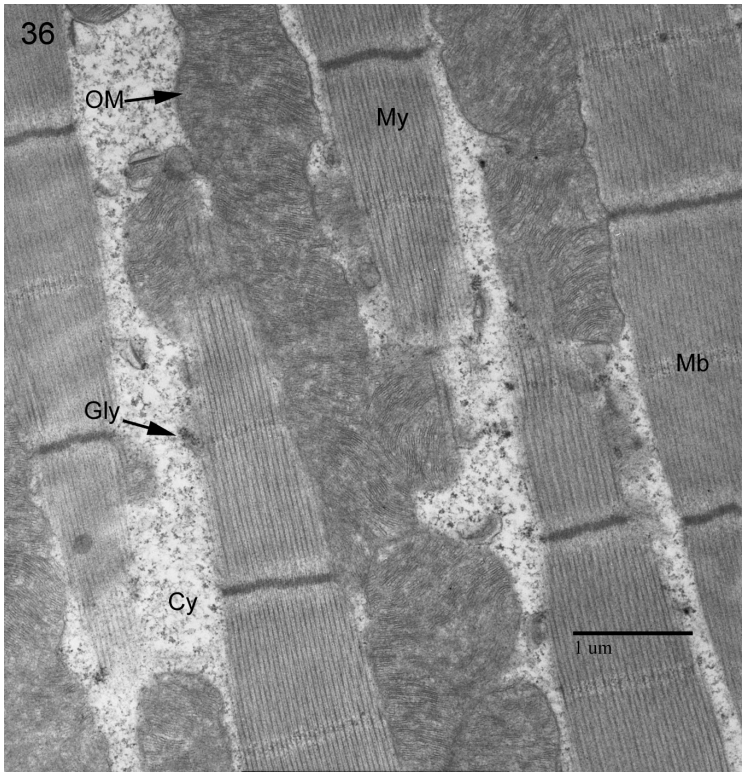
36
OM
My
Mb
Gly
Cy
1 um

Figure 37. **Three-week old *Pink1 RNAi* indirect flight muscle shows some myofibril damage.**
In this lateral section of tissue, myofibrils appear torn (Tr). The tears are seen only in the myofibrils and no damage is apparent in the surrounding mitochondria. Scale bar is 1μm.

Figure 38. **Three-week old w^{1118} indirect flight muscle with a glancing cut of a myofibril reveals no localization of visible cytosol.**
Intact myofibrils are surrounded by mitochondria with densely packed cristae (C). There is a glancing cut taken of one myofibril (bMy), but no cytosolic gaps appear where it is bisected. Scale bar is 1μm.

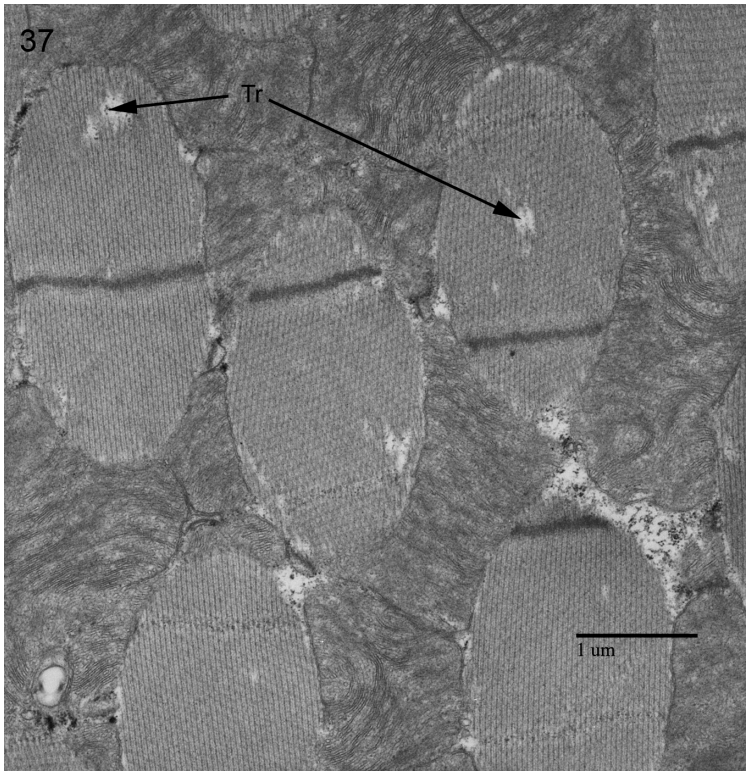
37
Tr
1 um

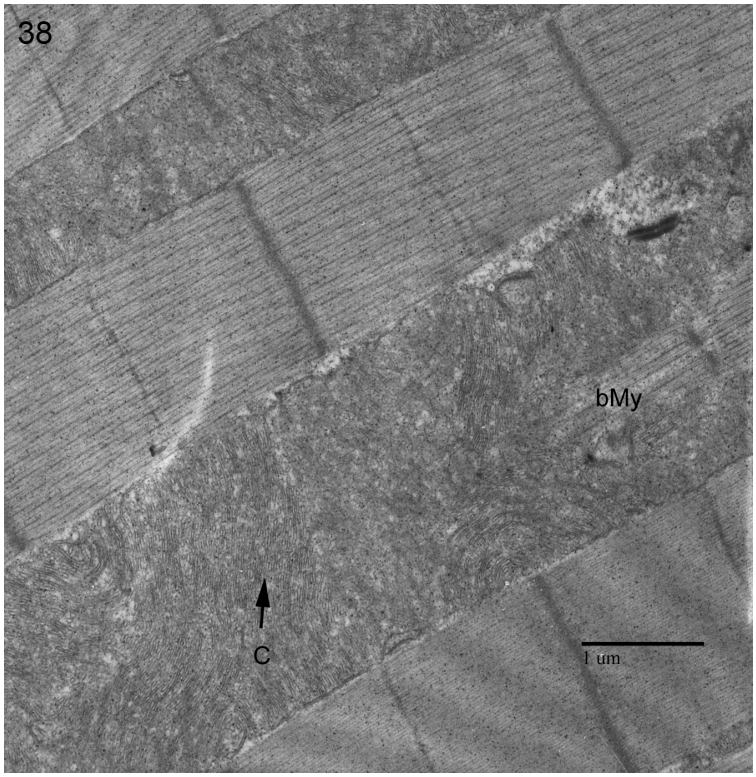
38
bMy
C
1 um

Figure 39. **Three-week old *Pink1 RNAi* indirect flight muscle reveals possible mitochondrial swelling.**
This micrograph, taken at the edge of a section, reveals tears (Tr) in the myofibrils and swelling of mitochondria (sM). Some mitochondria appear to have discontinuous outer membrane (dOM), but the associated cristae do not appear severely distorted. Large areas of open cytosol (Cy) are also present in this lateral section of tissue. Scale bar is 1µm.

Figure 40. **Three-week old w^{1118} indirect flight muscle has normal tissue integrity.**
In this longitudinal cut, mitochondria are electron dense, morphologically normal, and are tightly packed around parallel myofibrils. Residual lead carbonate precipitate is present (St). Scale bar is 1µm.

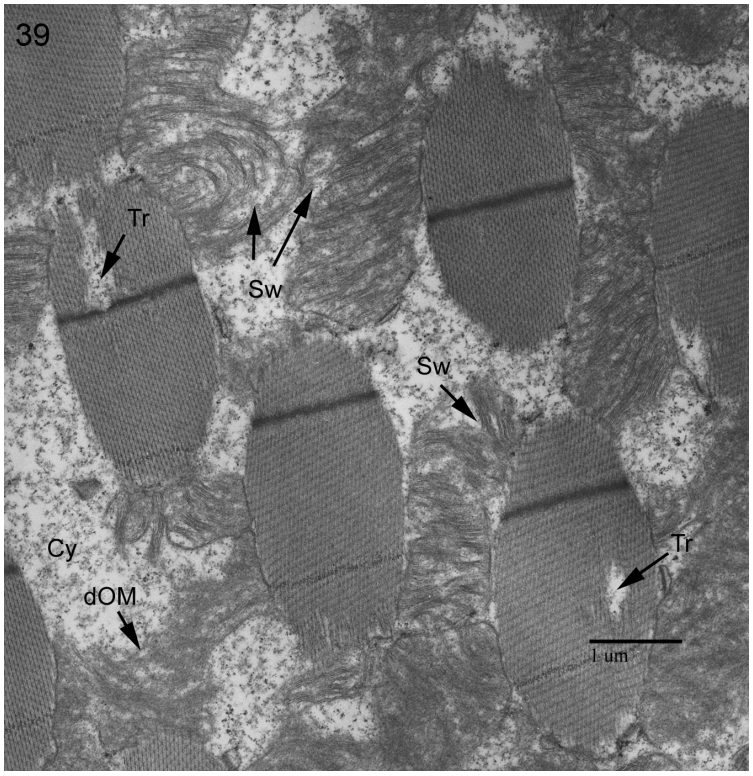
39
Tr
Sw
Sw
Cy
dOM
Tr
1 um

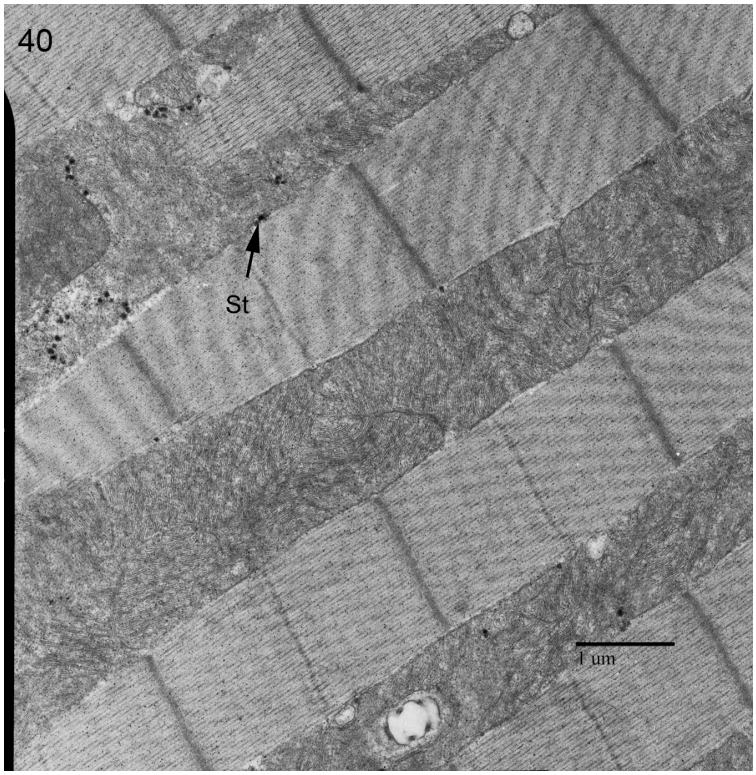
40
St
1 um

Figure 41. **Three-week old w^{1118} indirect flight muscle from the edge of a tissue sample reveals extensive visible cytosol and enlarged mitochondrial cristae.**
The edges of this section of tissue, mitochondria are intact, yet their cristae appear enlarged (eC). Glycogen rich cystol is seen around the myofibrils. Tracheae (T) also appear here. This pattern was not prevalent through the rest of the sample and is expected to be a product of fixation, infiltration, and sectioning. Scale bar is 1μm.

Figure 42. **Tergotrochanter muscle of a three-week old w^{1118} fly appears normal.**
Once again, parallel myofibrils (My) with aligned Z-bands (Z) are surrounded by intact mitochondria (M) and sarcoplasmic reticulum (SR). The straight line that diagonally bisects the micrograph, is most likely a knife mark (Kn), a product of sectioning. Scale bar is 1μm.

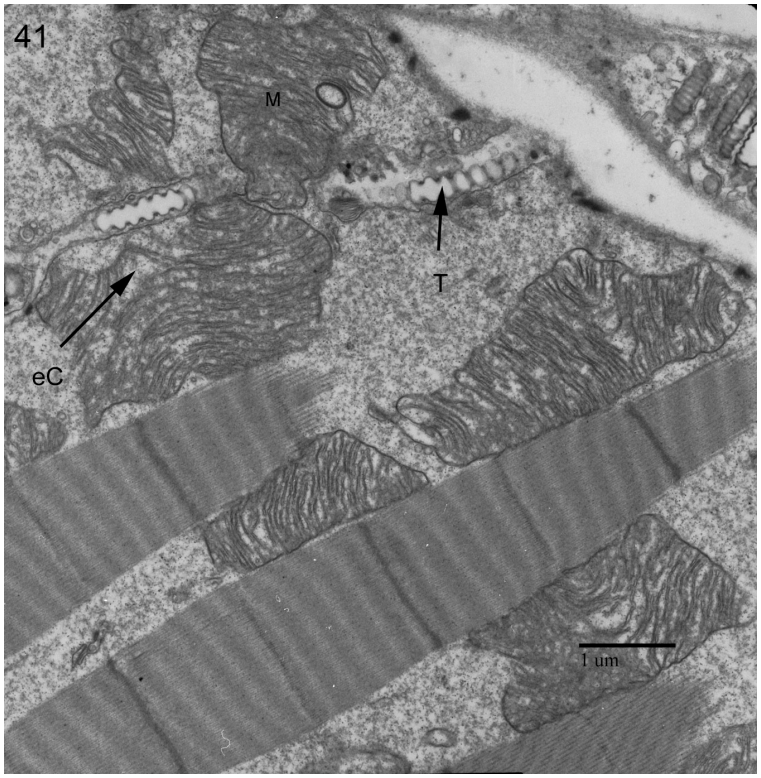
41
M
T
eC
1 um

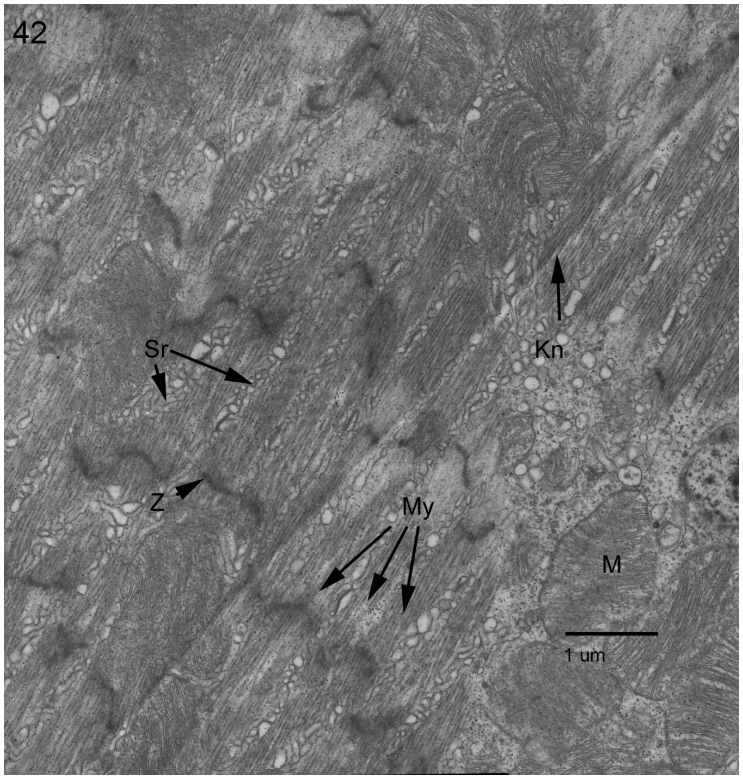
42
Sr
Kn
Z
My
M
1 um

Figure 43. **A three-week *Pink1 RNAi* animal presents hypothesized mitochondrial and myofibrillary degradation.**
A longitudinal section of indirect flight muscle reveals severe abnormalities. Mitochondrial membranes are interrupted; cristae (C) are enlarged and unorganized and the outer mitochondrial membrane is discontinuous. Myofibrils appear to be degraded. This degradation appears as decreased electron density of the myofilaments, in the areas of the Z-band in particular. Scale bar is 1µm.

Figure 44. **Indirect flight muscle of a three-week old *Pink1 RNAi* fly shows severe degradation.**
Myofibril degradation (dMf) is appears to be most concentrated around the Z-disc. Abnormal, enlarged mitochondria (aM) are present. Outer membranes appear ballooned and cristae (C) are irregular and discontinuous. Scale bar is 1µm.

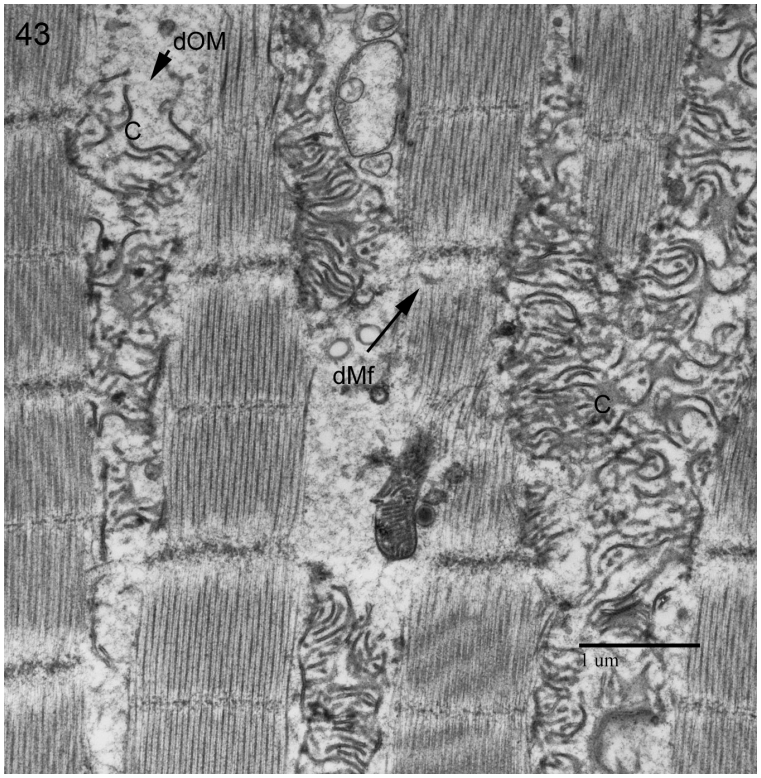
43
dOM
C
dMf
C
1 um

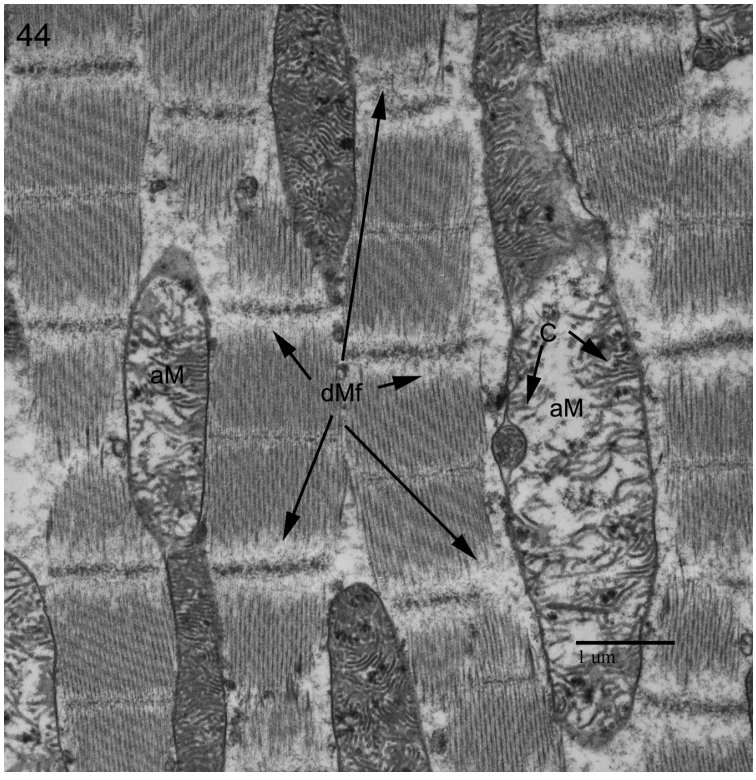
44
aM
dMf
C
aM
1 um

Figure 45. **Severe degradation of myofibrils in a three-week old *Pink1 RNAi* fly appears to have cytosolic elements invading the areas of compromised myofibrils.**
Once again, myofibril degradation (dMf) is most apparent at the Z-bands. In this section, a granularization appears at the residual Z-bands implying a cytosolic invasion of the degenerated organelle. This granularization is can also be attributable to overlying cytosol. Enlarged, swollen mitochondria (sM) with enlarged cristae (eC) also continue to be the norm in this animal. Scale bar is 1μm.

Figure 46. **Degradation of muscle ultrastructure in a three-week old *Pink1 RNAi* fly continues to be pervasive.**
Abnormal mitochondria (aM) with deteriorated cristae (C) but intact outer membrane (OM) are present. Myofibrillary degradation (dMF) continues to be present, but is not only localized to Z-discs in this section. Tracheae (T) appear normal. Scale bar is 1μm.

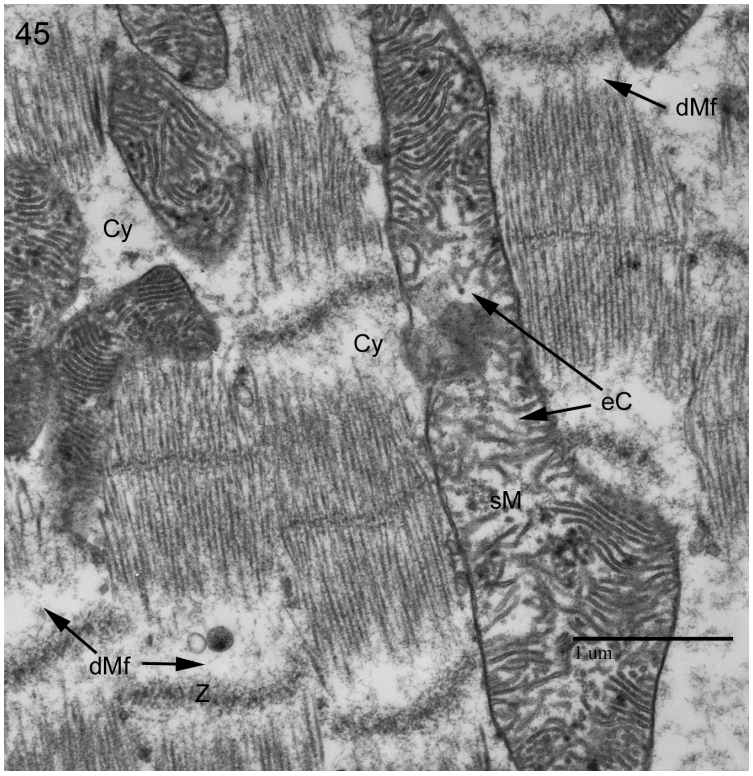
45
dMf
Cy
Cy
eC
sM
dMf
Z
1 um

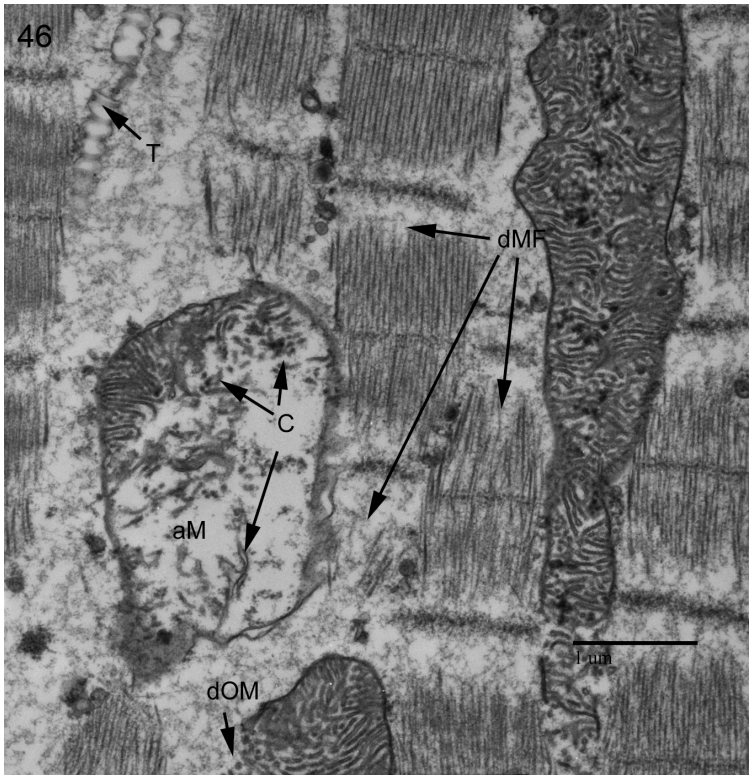
46
T
dMF
C
aM
1 um
dOM

Figure 47. **Degraded three-week old *Pink1 RNAi* myocyte organelles.** Here, swollen mitochondria (sM) with disorganized cristae, but intact outer membranes are found with additional abnormal mitochondria (aM) with discontinuous outer membranes (dOM) and degraded cristae. Once again, myofiber degradation (dMf) is most present in Z-band zones. M-bands (Mb) are highly visible here as well, another possible product of degradation. Scale bar is 1μm.

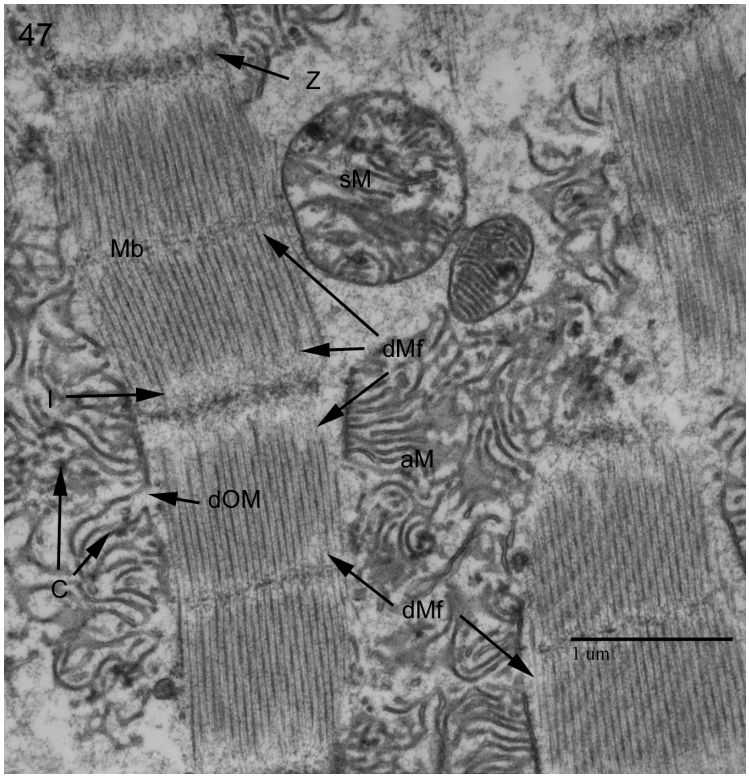
47
Z
sM
Mb
dMf
I
aM
dOM
C
dMf
1 um

Figure 48. **Indirect flight muscle of a four-week old *Pink1 RNAi* fly.** Organized, electron dense cristae (C) are apparent. The longitudinal section of mysfribls shows characteristic Z (Z), I (I), and M (Mb) bands. The open areas between myofibrils are once again present in this section of tissue. Here, these gaps do not show the normal granulations normally visible in sections of cytosol. The cytosolic elements may have been displaced by resin during the embedding process (Cy/R). Scale bar is 1µm.

Figure 49. **Longitudinal section of four-week old w^{1118} indirect flight muscle.** Normal myofibril and mitochondrial morphology is observed. Mitochondria, with intact outer membrane (OM) and highly organized cristae (C), are tightly packed around fibrils. There is little cytosol seen in this sample, though it must be noted, that it was apparent in the periphery of the same section of tissue. Scale bar is 1µm.

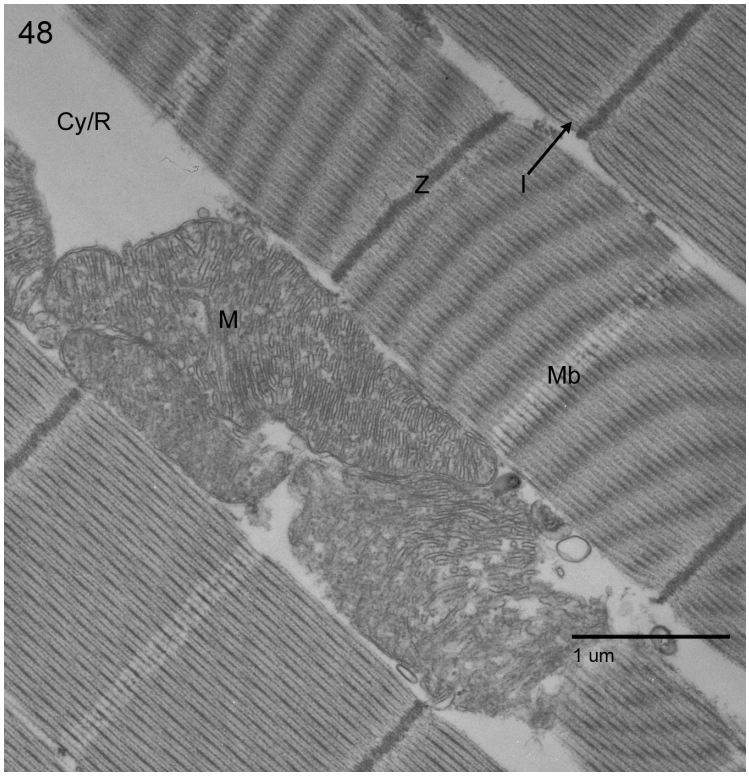
48
Cy/R
Z
I
M
Mb
1 um

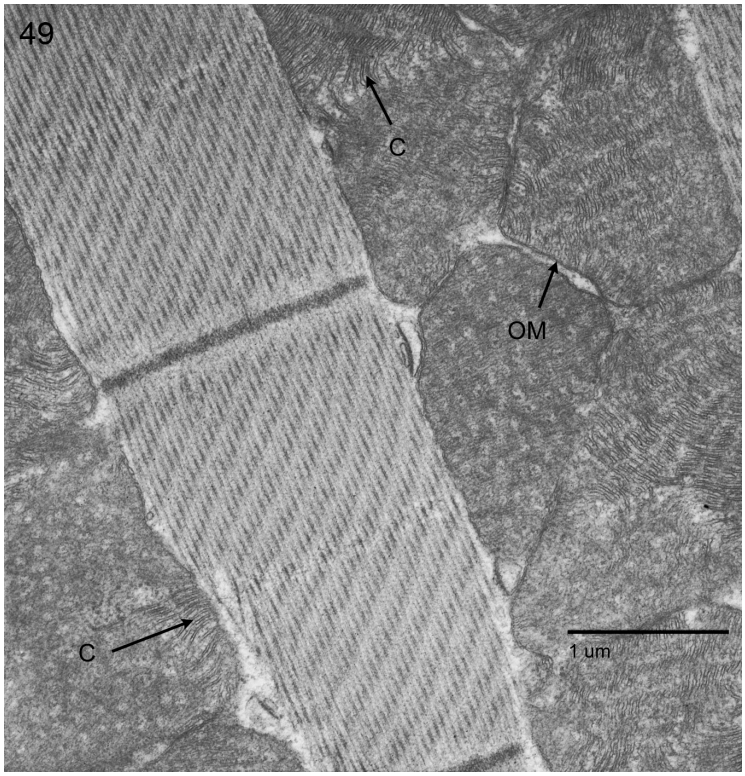
49
C
OM
C
1 um

Figure 50. **Indirect flight muscles of a four-week old *Pink1 RNAi* animal.** Cytosol (Cy) is once again apparent and most prevalent at the edges of myofibrils. As with other samples, mechanical tearing of the tissue is observed (Tr). Despite mechanical damage, mitochondria (M) with organized cristae (C) and electron dense myofibrils with defined M-bands (Mb) remain intact. Scale bar is 1µm.

Figure 51. **Four-week old indirect flight muscle of a w^{1118} fly.** Normal arrangement and structure of visible organelles (M, OM, Z, My all are labeled). A cross-section of trachea (T) is closely surrounded by mitochondria. Scale bar is 1µm.

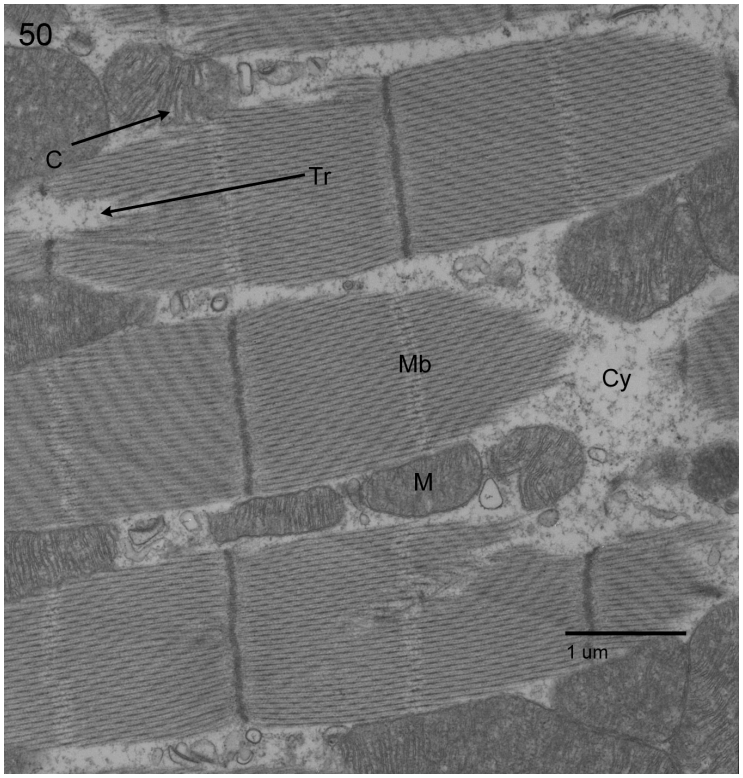
50
C
Tr
Mb
Cy
M
1 um

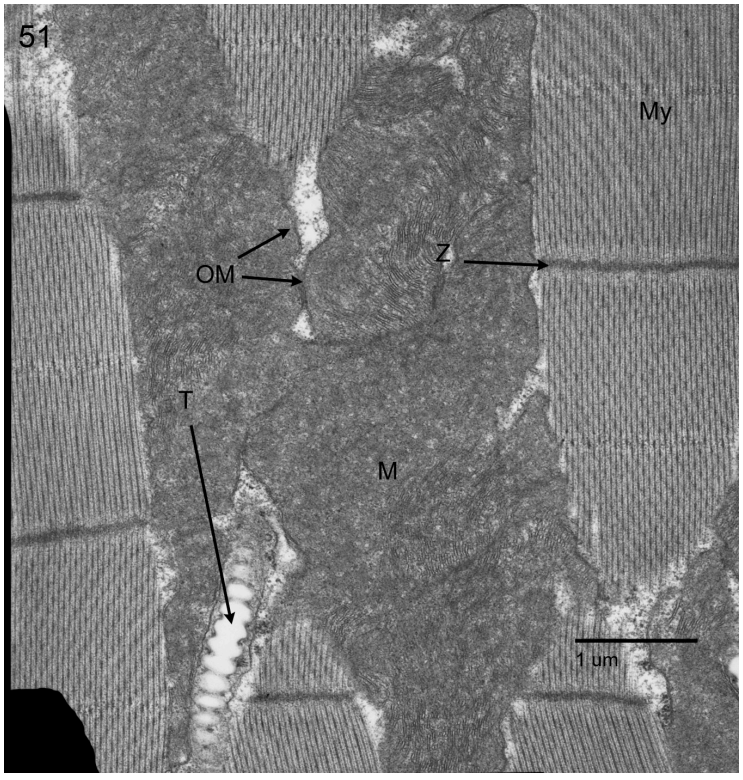
51
My
OM
Z
T
M
1 um

Figure 52. **Tergotrochanter muscle of a four week-old *Pink1 RNAi Drosophila*.** Sarcoplasmic reticulum (SR) is seen in this glancing section of myofibril (My). Mitochondira are intact. Due to the orientation of the tissue, Z-bands (Z) and I-bands (I) appear much wider than usual. Scale bar is 1µm.

Figure 53. **Tergotrochanter muscle of a four week-old w^{1118} animal.** Once again, myofibrils (My) and mitochondria (M) are not deteriorated in any way. Sarcoplasmic reticulum (SR) is sandwiched between parallel myofibrils. Scale bar is 1µm.

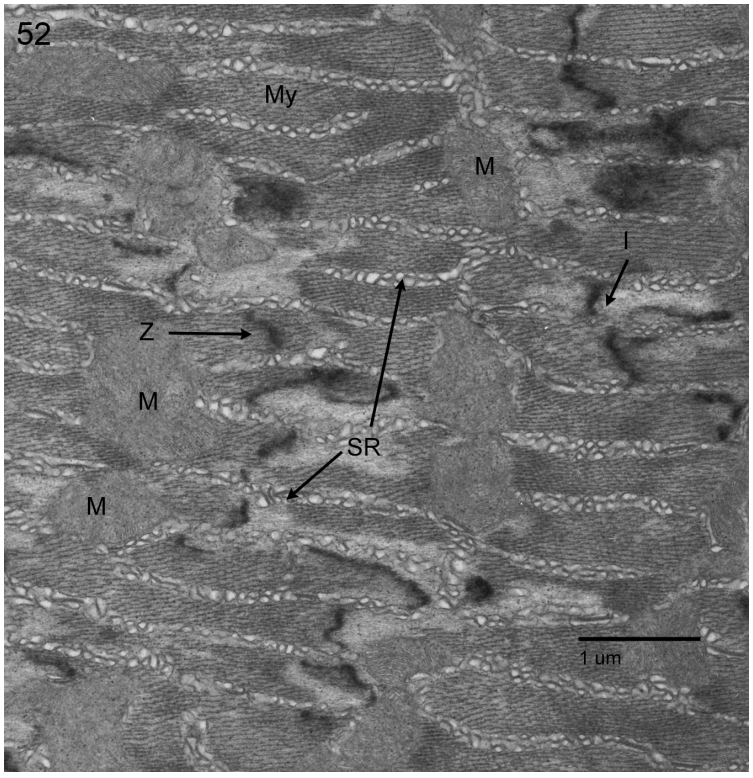
52
My
M
I
Z
M
SR
M
1 um

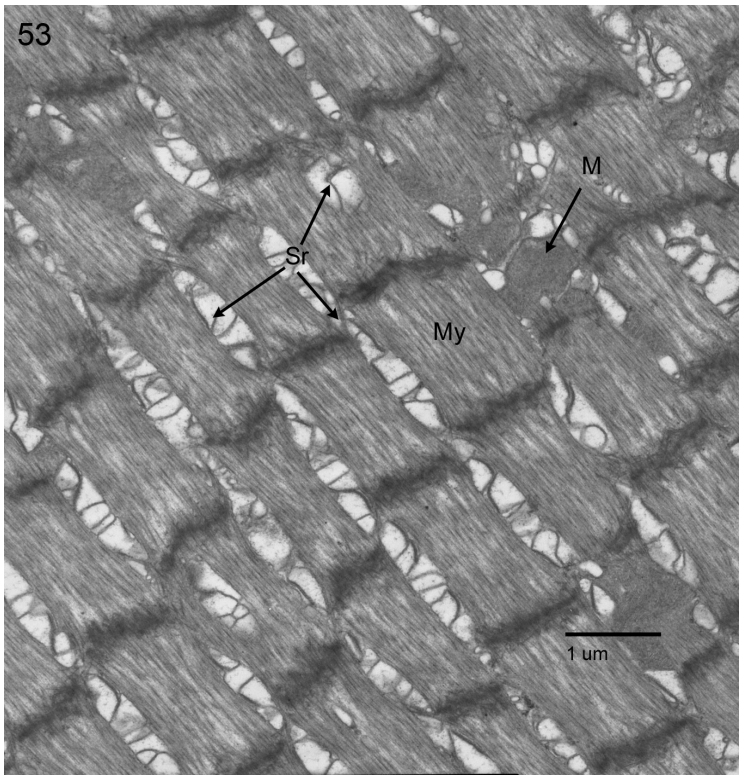
53
M
Sr
My
1 um

w^{1118} and *Pink1 RNAi* Climbing Assays:

The climbing ability of both w^{1118} and *Pink1 RNAi* flies remained relatively uncompromised over the four-week period. Once again, there is an age-dependent decrease of muscle capability across genotypes. The w^{1118} flies begin with a lower climbing capacity than the single transgenic flies. The initial climbing success rate of 84.91% in the wild-type flies is comparable to their final climbing success average of 80.30%. The *Pink1 RNAi* animals outperfom the w^{1118} flies in weeks one and two. In weeks three and four, the *Pink1 RNAi* climbing ability averages of 77.19% and 77.45% are eclipsed by the wild-type, even if only by a margin of 3 to 5%.

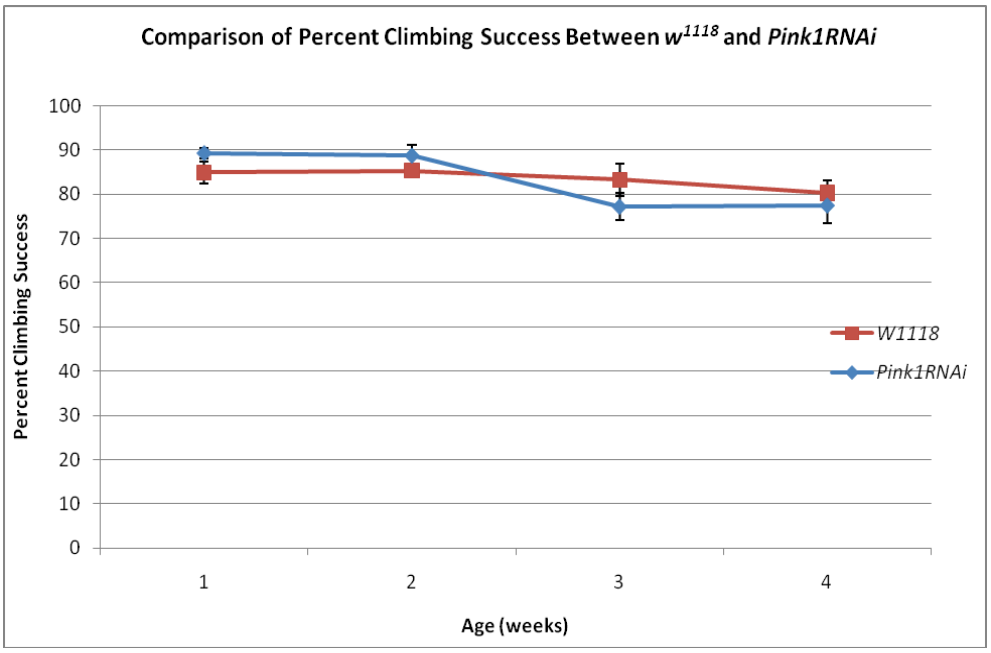

Figure 54. **A comparative analysis of the climbing success of w^{1118} and *Pink1 RNAi* genotypes over the four-week period.** Inconsistent with the hypothesis of this investigation, *Pink1 RNAi* flies do not experience a dramatic decrease in climbing ability as compared to the w^{1118} flies.

DISCUSSION

In the present study, it has been demonstrated that *hParkin* expression can ameliorate the detrimental effects of *hAPP* expression in *Drosophila* skeletal muscle, presumably via UPS upregulation. Additionally, this study presents results that are contrary to much research done on the effects *Pink1 RNAi*. In spite of the findings of other researchers, little detrimental effects to the musculature or climbing ability of *Pink1 RNAi* flies is seen in this study. Additionally, no significant difference is found in the expression of endogenous *Parkin* in the presence of *Pink1 RNAi* knock-out.

hAPP and hParkin Climbing Analysis:

The behavioral data confirms that *hParkin* can act as an ameliorative agent to *hAPP* expression. The re-verification of the continued decline in climbing ability seen in *hAPP* flies, despite the lack of endogenous Aβ processing machinery, suggests one of two things: 1. an unidentified enzymatic reaction is

responsible for the initiation of the Aβ cascade in the presence of hAPP; or 2. that the presence of hAPP, even without processing, induces toxicity.

Protein aggregation is one of the primary origins of oxidative stress seen in both s-IBM and PD pathologies. Here, the decreased behavior of the *hAPP* genotype, and the subsequent rescue by *hParkin* expression, contribute to the hypothesis that the main cause of behavioral decline is due to protein accumulation. *hParkin* acts as the E3 ligase of the UPS system; there, it targets proteins for proteasomal degradation. Parkin's cytoprotective role against Aβ accumulation may be what is occurring here (Rosen et al., 2010). There is no β-secretase homologue found in *Drosophila* muscle, nor does endogenous amyloidgenic processing of APPL occur (Fortini et al., 1999). Because this impediment to the generation of toxic Aβ species exists within the skeletal muscle, the beneficial effects of UPS upregulation via *hParkin* expression seen in this experiment, still leave questions unanswered (Fossgreen et al., 1998). It is possible that the insertion of *hAPP*, which possesses the Aβ cleavage site, activates the present endogenous α-secretase? An investigation into the reactivity of α-secretase with *hAPP* expression should be considered. It is possible the human transgene offers *Drosophila* α-secretase a different target of proteolysis, a target which is capable of producing the C99 fragment (Nunan & Small, 2000). Immunohistochemistry techniques are presently being used in our lab in order to assay for the presence of Aβ in the skeletal muscles of these single transgenics.

While *Parkin* overexpression is seen to decrease intracellular Aβ accumulation in neuronal cell culture, it is important to recall that *hAPP* is expressed here without a mechanism to cleave it. The inclusion bodies of s-IBM patients do have whole hAPP (Askanas, 1998; 2011). Although Parkin's effects have been tested specifically with Aβ deposition, it is possible that that UPS may degrade accumulation of whole hAPP, if any exists within this model (Askanas & Engel, 1998; Fratta et al., 2005).

If Aβ deposition, or deleterious hAPP accumulation, does occur from the expression of the *hAPP* transgene, then the effects on climbing ability are easily explainable; mitochondrial deficiencies due to oxidative stress inhibit muscle function (Askanas et al. 2009). It is logical to reason that *hParkin*'s protective role against oxidative stress would serve to rescue the fly (Pesah, 2005). However, TEM experiments performed by a lab-mate, Anisha Singh, do not confirm the presence of mitochondrial disturbances in *hAPP* flies (Singh, unpublished).

Although there is no definitive answer as to why, transgenic *hAPP* expression does impede muscle activity and *hParkin* ameliorates this impediment.

PCR Analysis on *Pink1RNAi* and w^{1118}animals:

The qPCR analysis of endogenous *Drosophila Parkin* between *Pink1 RNAi* and w^{1118} animals demonstrates no significant difference in expression. This is contrary to our hypothesis, that *Pink1* expression is necessary for proper *Parkin* expression, due to the presumable downstream nature of *Parkin* activity.

Although the rescuing effect of *hParkin* overexpression to *Pink1* knock-out (or mutation) has been demonstrated in multiple studies, it does not necessarily indicate that the position of *Parkin* in the *Pink1/Parkin* biochemical pathway is downstream (Yang et al., 2006; Clark et al., 2006). It is possible that the interaction of *Pink1/Parkin* may occur at the level of protein interaction. Pink1 may act as an indirect or direct transcription factor for *Parkin* expression, or it may just be that the actions of the two proteins, together in the cell, induce a biochemical cascade of mitochondrial maintenance. Considering the phosphorylative ability of Pink1, I would suggest using Western blotting techniques to compare levels of phosphorylated *Parkin* between *Pink1 RNAi* and w^{1118} flies.

Due to continuous sample contamination and time constraints, the sample size for each condition of this analysis was very low (n=2). This is too low to yield statistically significant results. I would recommend testing more samples before a definitive conclusion is reached.

The hypotheses and future plans stated in the previous paragraphs should only be considered if all evidence produced in this study was verifiably linked to a confirmed source of material. The TEM analysis and behavioral data collected as part of this experiment indicate that the RNA interference of *Pink1* was either non-functional, or possessed very low penetrance.

Transmission Electron Microscopy:

The low levels of hypothesized mitochondrial abnormalities in *Pink1 RNAi* found during TEM analysis, suggest that an unsuccessful attempt at RNA interference occurred. Although the fixatives and resins had been optimized to control for any false positive artifact, it is not enough to account for complete absence of mitochondrial abnormalities in *Pink1 RNAi* samples. Additionally, if *Pink1 RNAi* had been constant, it can be presumed that the anomalous results for the three week-old *Pink RNAi* animal would not be present.

The occasional swelling of mitochondria in the morphologically normal *Pink1 RNAi* flies is attributable to artifact. The swelling occurred in a small portion of samples, and was dispersed unevenly throughout the tissue. This uneven distribution concentrated abnormalities along the peripheries of the tissue, areas most vulnerable to thawing during the transfer from liquid nitrogen to fixative. If this transfer did not occur in a timely manner, destabilization and necrosis of the tissue could occur due to the formation of ice crystals. This could present as a swelling of the mitochondria.

The cytoplasmic gaps seen in the *Pink1 RNAi* flies that were not present in the w^{1118} still remain somewhat befuddling. Though these gaps appeared with increased prevalence in the *Pink1 RNAi* tissue, once again, their distribution was concentrated at the tissue periphery. Moreover, TEM remains a variable technique; tissue orientation during sectioning can account for the production of the gaps between myofibrils. The combination of intact mitochondria and

cytoplasmic gaps in the same tissue sample suggest that the gaps are conceivably sectioning artifact, and not a product of a transgene. There remains no way to entirely control for sectioning artifact.

Although no statistical analysis was done to account for the frequency/size of these gaps, the persistence of cytoplasmic material, such as glycogen, remains a reminder of a still-functioning and well-preserved myocyte. Additionally, the constant presence of electron dense mitochondria and myofibrils within these large areas of open cytosol indicate that little damage had occurred. The effects of *Pink1 RNAi* knock-out observed in previous studies, such as discontinuous mitochondrial membranes and myofilament degradation were simply not there (Yang et al. 2008).

The TEM results were consistent, with the exception of one three-week old *Pink1 RNAi* animal. In this animal, the *Pink1 RNAi* phenotype was present; discontinuous mitochondrial outer membranes, enlarged and disorganized cristae, intense vacuolization, and myofibril degradation were all present within the sample. These observations, contiguous with the effects of *Pink1 RNAi* observed in other research laboratories, indicate that this animal is an example of effective *Pink1* knock-out (Yang et al., 2006; Clark et al., 2006). Despite the interpretation of this result as a product of proper transgene function, this result can be an artifact of fixation. Should the sample have experienced a rise in temperature between freeze-fracture and primary fixation, any and all of these effects may have been witnessed.

The possible occurrence of low penetrance of the transgene is a very real possibility. This could be due to failed transcription of the double stranded transcript by the *Dmef* driver, a low and insufficient degree of RNAi (leaving sustainable amounts of Pink1 behind), or the possible misalignment of the introduced *dsPink1* and the endogenous *Drosophila* transcript (Viney & Thompson, 2008).

The efficiency of transgene expression was not something tested in this experiment; we had hoped that TEM would serve as a morphological verification of the effects of *Pink1 RNAi.* Whole animals were used in RNA isolation in order to increase the yield of preserved nucleic acids and to decrease any detrimental effect to RNA integrity. qPCR with *Pink1* primers would show up positive because the RNA interference only occurs in the skeletal muscles. I would suggest the creation and implementation of a skeletal muscle dissection procedure in order to procure samples for a qPCR control.

Behavioral Analysis:

The results of the *Pink1 RNAi* and w^{1118} climbing data correlate to the negative results of the TEM and qPCR data. As with the other forms of experimentation, should low penetrance of the RNAi have occurred, then a larger sample size would have needed to be taken to produce any significant difference between control and transgenic animals. Additionally, it should be noted that some *Pink1 RNAi* flies did possess the abnormal wing posture observed in

previous studies (Yang, 2006). Although the penetrance of this phenotype was not recorded, the expressivity of this trait was variable. In a much larger population, a higher degree of climbing inability may have been viewed, but random sampling may or may not produce significant and analyzable differences.

CONCLUSIONS

The detrimental effects of *hAPP* expression continue to elude the Woodard Laboratory. I suggest the continuation of immunohistochemistry techniques in order to assay for the presence of Aβ and confirm whether or not there is initiation of the Aβ cascade in the presence of the *hAPP* transgene. Additionally, I would suggest possible transgenic manipulation of *Drosophila α-*secretase; if differences in the behavioral effects of *hAPP* expression are apparent in instances of *Drosophila* α-*secretase* knock-out or upregulation, it may foretell a novel biochemical interaction.

There existed no qPCR control to assay whether or not *Pink1* was truly knocked out of *Drosophila* skeletal muscle. I would suggest developing a dissection technique to excise thorax musculature from flies for RNA isolation. This would allow for qPCR samples to contain only muscle tissue—the tissue in which *Pink1* has been silenced. Without such a control, non-muscle tissues contaminate qPCR samples.

For all future research in the Woodard Laboratory that employs TEM techniques, I suggest using the fixation and embedding methods that have been optimized here. The freeze-fracture dissection method, combined with Na cacodylate fixation, and embedment in Embed 812 resin, reduces the appearance of artifact. It is important that the artifact is reduced, as mitochondrial abnormalities resulting from fixation procedure and genetic manipulation are indistinguishable. Due to the imprecision of TEM techniques, I suggest that a more precise molecular biology technique, with an analyzable control, is always used in conjunction with microscopy.

REFERENCES

Abdo, Wilson F., Tom van Mierlo, Gerald J. Hengstman, H. J. Schelhaas, Baziel G. van Engelen, and Marcel M. Verbeek. 2009. Increased plasma amyloid-β_{42} protein in sporadic inclusion body myositis. *Acta Neuropathologica* 118 (3) (09): 429-31.

Allikian, Michael J., Gira Bhabha, Patrick Dospoy, Ahlke Heydemann, Pearl Ryder, Judy U. Earley, Matthew J. Wolf, Howard A. Rockman, and Elizabeth M. McNally. 2007. Reduced life span with heart and muscle dysfunction in drosophila sarcoglycan mutants. *Human Molecular Genetics* 16 (23) (December 01): 2933-43.

Amemiya, K., R. P. Granger, and M. C. Dalakas. 2000. Clonal restriction of T-cell receptor expression by infiltrating lymphocytes in inclusion body myositis persists over time. *Brain* 123 (10): 2030.

Amo, Taku, Shigeto Sato, Shinji Saiki, Alexander M. Wolf, Masaaki Toyomizu, Clement A. Gautier, Jie Shen, Shigeo Ohta, and Nobutaka Hattori. 2011. Mitochondrial membrane potential decrease caused by loss of PINK1 is not due to proton leak, but to respiratory chain defects. *Neurobiology of Disease* 41 (1) (01): 111-8.

Askanas, V., and W. Engel. 2001. Inclusion-body myositis: Newest concepts of pathogenesis and relation to aging and alzheimer disease. *Journal of Neuropathology & Experimental Neurology* 60 (1): 1.

Askanas, V., W. Engel, R. B. Alvarez, J. McFerrin, and A. Broccolini. 2000. Novel immunolocalization of [alpha]-synuclein in human muscle of inclusion-body myositis, regenerating and necrotic muscle fibers, and at

neuromuscular junctions. *Journal of Neuropathology & Experimental Neurology* 59 (7): 592.

Askanas, V., and W. K. Engel. 2008. Inclusion-body myositis: Muscle-fiber molecular pathology and possible pathogenic significance of its similarity to Alzheimer's and Parkinson's disease brains. *Acta Neuropathologica* 116 (6): 583-95.

Askanas, V., and W. K. Engel. 2003. Proposed pathogenetic cascade of inclusion-body myositis: Importance of amyloid-[beta], misfolded proteins, predisposing genes, and aging. *Current Opinion in Rheumatology* 15 (6): 737.

Askanas, V., J. McFerrin, S. Baque, RB Alvarez, E. Sarkozi, and WK Engel. 1996. Transfer of beta-amyloid precursor protein gene using adenovirus vector causes mitochondrial abnormalities in cultured normal human muscle. *Proceedings of the National Academy of Sciences of the United States of America* 93 (3): 1314.

Askanas, V., W. K. Engel, and R. B. Alvarez. 1992. Light and electron microscopic localization of beta-amyloid protein in muscle biopsies of patients with inclusion-body myositis. *The American Journal of Pathology* 141 (1) (Jul): 31-6.

Askanas, V., W. K. Engel, C. C. Yang, R. B. Alvarez, V. M. Lee, and T. Wisniewski. 1998. Light and electron microscopic immunolocalization of presenilin 1 in abnormal muscle fibers of patients with sporadic inclusion-body myositis and autosomal-recessive inclusion-body myopathy. *The American Journal of Pathology* 152 (4) (Apr): 889-95.

Askanas, Valerie, and King Engel. 1998. Sporadic inclusion-body myositis and its similarities to alzheimer disease brain. *Scandinavian Journal of Rheumatology* 27 (6) (11/23): 389-405.

Askanas, Valerie, and W. King Engel. 2011. Sporadic inclusion-body myositis: Conformational multifactorial ageing-related degenerative muscle disease associated with proteasomal and lysosomal inhibition, endoplasmic reticulum stress, and accumulation of amyloid-β42 oligomers and phosphorylated tau. *La Presse Médicale* 40 (4, Part 2) (4): e219-35.

Askanas, Valerie, and W. King Engel.. 2007. Inclusion-body myositis, a multifactorial muscle disease associated with aging: Current concepts of pathogenesis. *Current Opinion in Rheumatology* 19 (6) (November): 550-9.

Askanas, Valerie, W. King Engel, and Anna Nogalska. 2009. Inclusion body myositis: A degenerative muscle disease associated with intra-muscle fiber multi-protein aggregates, proteasome inhibition, endoplasmic reticulum stress and decreased lysosomal degradation. *Brain Pathology* 19 (3): 493-506.

Bennett, Eric J., Neil F. Bence, Rajadas Jayakumar, and Ron R. Kopito. 2005. Global impairment of the ubiquitin-proteasome system by nuclear or cytoplasmic protein aggregates precedes inclusion body formation. *Molecular Cell* 17 (3) (02/04): 351-65.

Bennet, Eric J., N. F. Bence, R. Jayakumar, and R. R. Kopito. 2005. Global impairment of the ubiquitin-proteasome system by nuclear or cytoplasmic protein aggregates precedes inclusion body formation. *Molecular Cell* 17 (3) (2/4): 351-65.

Bennett, M. C. 2005. The role of α-synuclein in neurodegenerative diseases. *Pharmacology & Therapeutics* 105 (3) (03): 311-31.

Bilen, Julide, and Nancy M. Bonini. 2005. Drosophila as a model for human neurodegenerative disease. *Annual Review of Genetics* 39 (1) (12): 153-71.

Braak, H., K. D. Tredici, U. Rüb, R. A. I. de Vos, E. N. H. Jansen Steur, and E. Braak. 2003. Staging of brain pathology related to sporadic parkinson's disease. *Neurobiology of Aging* 24 (2): 197-211.

Cai, Huaibin, Yanshu Wang, Diane McCarthy, Hongjin Wen, David R. Borchelt, Donald L. Price, and Philip C. Wong. 2001. BACE1 is the major β-secretase for generation of Aβ peptides by neurons. *Nature Neuroscience* 4 (3) (03): 233.

Chan, H. Y. E., and N. M. Bonini. 2000. Drosophila models of human neurodegenerative disease. *Cell Death & Differentiation* 7 (11) (11): 1075.

Chiveri, Luca, Monica Sciacco, Gigliola Fagiolari, Massimo Serafini, Parizia Ciscato, Chiara Zecca, Sefano Messina, et al. 2006. An adult case of mitochondrial DNA depletion with associated IBM features. *Basic Appl Myol* 16 (1): 5-8.

Chomczynski, Piotr, and Nicoletta Sacchi. 2006. *The single-step method of RNA isolation by acid guanidinium thiocyanate-phenol-chloroform extraction: Twenty-something years on.(ribonucleic acid)*. Vol. 1.

Clark, Ira E., Mark W. Dodson, Changan Jiang, Joseph H. Cao, Jun R. Huh, Hong Seol Jae, Soon Ji Yoo, Bruce A. Hay, and Ming Guo. 2006. Drosophila pink1 is required for mitochondrial function and interacts genetically with parkin. *Nature* 441 (7097) (06/29): 1162-6.

Dalakas, M. C., K. Y. Park, C. Semino-Mora, H. S. Lee, K. Sivakumar, and L. G. Goldfarb. 2000. Desmin myopathy, a skeletal myopathy with cardiomyopathy caused by mutations in the desmin gene. *New England Journal of Medicine* 342 (11): 770-80.

Dalakas, M. C. 2004. Inflammatory disorders of muscle: Progress in polymyositis, dermatomyositis and inclusion body myositis. *Current Opinion in Neurology* 17 (5) (Oct): 561-7.

Darios, F., O. Corti, C. B. Lucking, C. Hampe, M. P. Muriel, N. Abbas, W. J. Gu, et al. 2003. Parkin prevents mitochondrial swelling and cytochrome c release in mitochondria-dependent cell death. *Human Molecular Genetics* 12 (5) (Mar 1): 517-26.

Deas, Emma, Nicholas W. Wood, and H. Plun-Favreau. 2011. Mitophagy and parkinson's disease: The PINK1–parkin link. *BBA - Molecular Cell Research* 1813 (4) (04): 623-33.

Demerec, M. 1994. Biology of drosophila. *Cold Spring Harbor Laboratory Pr*.

Dries, D. R., and G. Yu. 2008. Assembly, maturation, and trafficking of the γ-secretase complex in Alzherumer's. *Current Alzheimer Research* 5 (2): 132.

Driscoll, Monica, and Beate Gerstbrein. 2003. Dying for a cause: Invertebrate genetics takes on human neurodegeneration. *Nature Reviews Genetics* 4 (3) (03): 181.

Duffy, Joseph B. 2002. GAL4 system in drosophila: A fly geneticist's swiss army knife. *Genesis* 34 (1-2): 1-15.

Farzan, Michael, Christine E. Schnitzler, and Natalya Vasilieva. 2000. BACE2, a b-secretase homolog, cleaves at the b site and within the amyloid-b region of the amyloid-b precursor protein. *Proceedings of the National Academy of Sciences of the United States of America* 97 (17) (08/15): 9712-7.

Feany, M. B., and W. W. Bender. 2000. A drosophila model of parkinson's disease. *Nature* 404 (6776) (Mar 23): 394-8.

Fortini, Mark E., and Marian P. Skupski. 2000. A survey of human disease gene counterparts in the drosophila genome. *Journal of Cell Biology* 150 (2) (07/24): F23.

Fossgreen, Anke, Bodo Bruckner, and Christian Czech. 1998. Transgenic drosophila expressing human amyloid precursor protein show g-secretase activity and a blistered-wing phenotype. *Proceedings of the National Academy of Sciences of the United States of America* 95 (23) (11/10): 13703-8.

Fratta, P., W. K. Engel, J. McFerrin, K. J. A. Davies, S. W. Lin, and V. Askanas. 2005. Proteasome inhibition and aggresome formation in sporadic inclusion-body myositis and in amyloid-{beta} precursor protein-overexpressing cultured human muscle fibers. *American Journal of Pathology* 167 (2): 517.

Gargano, J. W., I. Martin, P. Bhandari, and M. S. Grotewiel. 2005. Rapid iterative negative geotaxis (RING): A new method for assessing age-related locomotor decline in drosophila. *Experimental Gerontology* 40 (5): 386-95.

Goate, A., and M. Chartier-Harlin. 1991. Segregation of a missense mutation in the amyloid precursor protein gene with familial. *Nature* 349 (6311) (02/21): 704.

Goebels, N., D. Michaelis, M. Engelhardt, S. Huber, A. Bender, D. Pongratz, M. A. Johnson, et al. 1996. Differential expression of perforin in muscle-infiltrating T cells in polymyositis and dermatomyositis. *The Journal of Clinical Investigation* 97 (12) (Jun 15): 2905-10.

Greene, J. C., A. J. Whitworth, I. Kuo, L. A. Andrews, M. B. Feany, and L. J. Pallanck. 2003. Mitochondrial pathology and apoptotic muscle degeneration in drosophila parkin mutants. *Proceedings of the National Academy of Sciences of the United States of America* 100 (7): 4078.

Greene, J. C., A. J. Whitworth, L. A. Andrews, T. J. Parker, and L. J. Pallanck. 2005. Genetic and genomic studies of drosophila parkin mutants implicate oxidative stress and innate immune responses in pathogenesis. *Human Molecular Genetics* 14 (6) (Mar 15): 799-811.

Groth, Amy C., Matthew Fish, Roel Nusse, and Michele P. Calos. 2004. Construction of transgenic drosophila by using the site-specific integrase from phage ΦC31. *Genetics* 166 (4) (04): 1775-82.

Haass, Christian, and Michael G. Schlossmacher. 1992. Amyloid beta-peptide is produced by cultured cells during normal metabolism. *Nature* 359 (6393) (09/24): 322.

Haass, Christian, and Dennis J. Selkoe. 2007. Soluble protein oligomers in neurodegeneration: Lessons from the alzheimer's amyloid β-peptide. *Nature Reviews Molecular Cell Biology* 8 (2) (02): 101-12.

Haass, Christian, and Harald Steiner. 2002. Alzheimer disease γ-secretase: A complex story of GxGD-type presenilin proteases. *Trends in Cell Biology* 12 (12) (12): 556.

Hannon, Gregory J. 2002. RNA interference. *Nature* 418 (6894) (07/11): 244.

Hardy, John. 1997. Amyloid, the presenilins and alzheimer's disease. *Trends in Neurosciences* 20 (4) (5/13): 154-9.

Hare, James. 2010. Trafficking of amyloid β-precursor protein products C83 and C99 on the endocytic pathway. *Biochemical & Biophysical Research Communications* 401 (2) (10/15): 219-24.

Hartenstein, V. Sink, H. 2006. Chapter 2:The muscle pattern of drosophila. In , 8-27Springer Verlag.

Hughes, A. J., S. E. Daniel, L. Kilford, and A. J. Lees. 1992. Accuracy of clinical diagnosis of idiopathic parkinson's disease: A clinico-pathological study of 100 cases. *Journal of Neurology, Neurosurgery & Psychiatry* 55 (3): 181.

Hussain, I., D. J. Powell, D. R. Howlett, G. A. Chapman, L. Gilmour, P. R. Murdock, D. G. Tew, et al. 2000. ASP1 (BACE2) cleaves the amyloid precursor protein at the β-secretase site. *Molecular and Cellular Neuroscience* 16 (5) (11): 609-19.

Imai, Y., M. Soda, and R. Takahashi. 2000. Parkin suppresses unfolded protein stress-induced cell death through its E3 ubiquitin-protein ligase activity. *The Journal of Biological Chemistry* 275 (46) (Nov 17): 35661-4.

Jankovic, J. 2008. Parkinson's disease: Clinical features and diagnosis. *Journal of Neurology, Neurosurgery & Psychiatry* 79 (4) (04): 368-76.

Jin, L. W., M. G. Hearn, C. E. Ogburn, N. Dang, D. Nochlin, W. C. Ladiges, and G. M. Martin. 1998. Transgenic mice over-expressing the C-99 fragment of betaPP with an alpha-secretase site mutation develop a myopathy similar to

human inclusion body myositis. *The American Journal of Pathology* 153 (6) (Dec): 1679-86.

Junn, Eunsung, and M. Maral Mouradian. 2002. Human α-synuclein over-expression increases intracellular reactive oxygen species levels and susceptibility to dopamine. *Neuroscience Letters* 320 (3) (3/8): 146-50.

Kamp, Frits, Nicole Exner, Anne Kathrin Lutz, Nora Wender, Jan Hegermann, Bettina Brunner, Brigitte Nuscher, et al. 2010. Inhibition of mitochondrial fusion by α-synuclein is rescued by PINK1, parkin and DJ-1. *EMBO Journal* 29 (20) (10/20): 3571-89.

Kitada, T., S. Asakawa, N. Hattori, H. Matsumine, Y. Yamamura, S. Minoshima, M. Yokochi, Y. Mizuno, and N. Shimizu. 1998. Mutations in the parkin gene cause autosomal recessive juvenile parkinsonism. *Nature* 392 (6676): 605.

Klein, C., A. Djarmati, K. Hedrich, N. Schafer, C. Scaglione, R. Marchese, N. Kock, et al. 2005. PINK1, parkin, and DJ-1 mutations in italian patients with early-onset parkinsonism. *European Journal of Human Genetics : EJHG* 13 (9) (Sep): 1086-93.

Kruger, R., W. Kuhn, T. Muller, D. Woitalla, M. Graeber, S. Kosel, H. Przuntek, J. T. Epplen, L. Schols, and O. Riess. 1998. Ala30Pro mutation in the gene encoding alpha-synuclein in parkinson's disease. *Nature Genetics* 18 (2) (Feb): 106-8.

Kumamoto, Toshihide, Hidetsugu Ueyama, Hiroshi Tsumura, Itaru Toyoshima, and Tomiyasu Tsuda. 2004. Expression of lysosome-related proteins and genes in the skeletal muscles of inclusion body myositis. *Acta Neuropathologica* 107 (1) (01): 59-65.

Lim, Kah-Leong, and Jeanne Tan. 2007. Role of the ubiquitin proteasome system in parkinson's disease. *BMC Biochemistry* 8 : S13.

Ling-Yang Hao, Benoit I. Giasson, and Nancy M. Bonini. 2010. DJ-1 is critical for mitochondrial function and rescues PINK1 loss of function. *Proceedings of the National Academy of Sciences of the United States of America* 107 (21) (05/25): 9747-52.

Lippa, C. F., H. Fujiwara, D. M. Mann, B. Giasson, M. Baba, M. L. Schmidt, L. E. Nee, et al. 1998. Lewy bodies contain altered alpha-synuclein in brains of many familial alzheimer's disease patients with mutations in presenilin and amyloid precursor protein genes. *The American Journal of Pathology* 153 (5) (Nov): 1365-70.

Liu, Qinghua, Tim A. Rand, Savitha Kalidas, Fenghe Du, Hyun-Eui Kim, Dean P. Smith, and Xiaodong Wang. 2003. R2D2, a bridge between the initiation and effector stepsof the drosophila RNAi pathway. *Science* 301 (5641) (09/26): 1921-5.

Lovato, TyAnna L., Adrian R. Benjamin, and Richard M. Cripps. 2005. Transcription of myocyte enhancer factor-2 in adult drosophila myoblasts is induced by the steroid hormone ecdysone. *Developmental Biology* 288 (2) (12/15): 612-21.

Lundberg, I. E. 2000. The role of cytokines, chemokines, and adhesion molecules in the pathogenesis of idiopathic inflammatory myopathies. *Current Rheumatology Reports* 2 (3) (Jun): 216-24.

Lünemann, J. D., J. Schmidt, D. Schmid, K. Barthel, A. Wrede, M. C. Dalakas, and C. Münz. 2007. β - Amyloid is a substrate of autophagy in sporadic inclusion body myositis. *Annals of Neurology* 61 (5): 476-83.

Luo, L. Q., L. E. Martin-Morris, and K. White. 1990. Identification, secretion, and neural expression of APPL, a drosophila protein similar to human amyloid protein precursor. *The Journal of Neuroscience : The Official Journal of the Society for Neuroscience* 10 (12) (Dec): 3849-61.

Luo, Yi, Brad Bolon, Steve Kahn, Brian D. Bennett, Safura Babu-Khan, Paul Denis, Wei Fan, et al. 2001. Mice deficient in BACE1, the alzheimer's β-secretase, have normal phenotype and abolished β-amyloid generation. *Nature Neuroscience* 4 (3) (03): 231.

Mello, Craig C., and Darryl Conte Jr. 2004. Revealing the world of RNA interference. *Nature* 431 (7006) (09/16): 338-42.

Moslemi, A. R., C. Lindberg, and A. Oldfors. 1997. Analysis of multiple mitochondrial DNA deletions in inclusion body myositis. *Human Mutation* 10 (5): 381-6.

Murata, K., and M. C. Dalakas. 1999. Expression of the costimulatory molecule BB-1, the ligands CTLA-4 and CD28, and their mRNA in inflammatory myopathies. *The American Journal of Pathology* 155 (2) (Aug): 453-60.

Needham, Merrilee, and Frank L. Mastaglia. 2007. Inclusion body myositis: Current pathogenetic concepts and diagnostic and therapeutic approaches. *Lancet Neurology* 6 (7) (07): 620-31.

Nitsch, R. M., B. E. Slack, R. J. Wurtman, and J. H. Growdon. 1992. Release of alzheimer amyloid precursor derivatives stimulated by activation of muscarinic acetylcholine receptors. *Science* 258 (5080): 304.

Nunan, Janelle, and David H. Small. 2000. Regulation of APP cleavage by α-, β- and γ-secretases. *FEBS Letters* 483 (1) (10/13): 6-10.

Olanow, C. W. 2007. The pathogenesis of cell death in parkinson's disease–2007. *Movement Disorders* 22 (S17): S335-42.

Oldfors, A., and C. Lindberg. 2005. Diagnosis, pathogenesis and treatment of inclusion body myositis. *Current Opinion in Neurology* 18 (5) (Oct): 497-503.

Park, J., S. B. Lee, S. Lee, Y. Kim, S. Song, S. Kim, E. Bae, et al. 2006. Mitochondrial dysfunction in drosophila PINK1 mutants is complemented by parkin. *Nature* 441 (7097) (Jun 29): 1157-61.

Park, Jeehye, Gina Lee, and Jongkyeong Chung. 2009. The PINK1–Parkin pathway is involved in the regulation of mitochondrial remodeling process. *Biochemical & Biophysical Research Communications* 378 (3) (01/16): 518-23.

Pesah, Y., T. Pham, H. Burgess, B. Middlebrooks, P. Verstreken, Y. Zhou, M. Harding, H. Bellen, and G. Mardon. 2004. Drosophila parkin mutants have decreased mass and cell size and increased sensitivity to oxygen radical stress. *Development (Cambridge, England)* 131 (9) (May): 2183-94.

Pesah, Yakov, Tuan Pham, Heather Burgess, Brooke Middlebrooks, Patrik Verstreken, Yi Zhou, Mark Harding, Hugo Bellen, and Graeme Mardon. 2004. Drosophila parkin mutants have decreased mass and cell size and increased sensitivity to oxygen radical stress. *Development (09501991)* 131 (9) (05): 2183-94.

Pesce, V., A. Cormio, F. Fracasso, J. Vecchiet, G. Felzani, A. Lezza, P. Cantatore, and M. N. Gadaleta. 2001. Age-related mitochondrial genotypic and phenotypic alterations in human skeletal muscle. *Free Radical Biology and Medicine* 30 (11): 1223-33.

Pfaffl, M. W. 2001. A new mathematical model for relative quantification in real-time RT–PCR. *Nucleic Acids Research* 29 (9): e45.

Polymeropoulos, M. H., C. Lavedan, E. Leroy, S. E. Ide, A. Dehejia, A. Dutra, B. Pike, H. Root, J. Rubenstein, and R. Boyer. 1997. Mutation in the α-

synuclein gene identified in families with parkinson's disease. *Science* 276 (5321): 2045.

Poole, Angela C., Ruth E. Thomas, Laurie A. Andrews, Heidi M. McBride, Alexander J. Whitworth, and Leo J. Pallanck. 2008. The PINK1/Parkin pathway regulates mitochondrial morphology. *Proceedings of the National Academy of Sciences of the United States of America* 105 (5) (02/05): 1638-43.

Price, P., L. Santoso, F. Mastaglia, M. Garlepp, C. C. Kok, R. Allcock, and N. Laing. 2004. Two major histocompatibility complex haplotypes influence susceptibility to sporadic inclusion body myositis: Critical evaluation of an association withHLA-DR3. *Tissue Antigens* 64 (5) (11): 575-80.

Raju, R., and M. C. Dalakas. 2005. Gene expression profile in the muscles of patients with inflammatory myopathies: Effect of therapy with IVIg and biological validation of clinically relevant genes. *Brain* 128 (8): 1887.

Raju, Raghavanpillai, Olavo Vasconcelos, Rebekah Granger, and Marinos C. Dalakas. 2003. Expression of IFN-γ-inducible chemokines in inclusion body myositis. *Journal of Neuroimmunology* 141 (1) (08): 125.

Riparbelli, Maria Giovanna, and Giuliano Callaini. 2007. The drosophila parkin homologue is required for normal mitochondrial dynamics during spermiogenesis. *Developmental Biology* 303 (1) (03): 108-20.

Rosen, D. R., L. Martin-Morris, L. Q. Luo, and K. White. 1989. A drosophila gene encoding a protein resembling the human beta-amyloid protein precursor. *Proceedings of the National Academy of Sciences of the United States of America* 86 (7) (Apr): 2478-82.

Rosen, K. M., C. E. H. Moussa, H. K. Lee, P. Kumar, T. Kitada, G. Qin, Q. Fu, and H. W. Querfurth. 2010. Parkin reverses intracellular ??amyloid accumulation and its negative effects on proteasome function. Journal of Neuroscience Research 88 (1): 167-78.

Rosen, Kenneth M., Vimal Veereshwarayya, Charbel E. -H Moussa, Qinghao Fu, Matthew S. Goldberg, Michael G. Schlossmacher, Jie Shen, and Henry W. Querfurth. 2006. Parkin protects against mitochondrial toxins and β-amyloid accumulation in skeletal muscle cells. *Journal of Biological Chemistry* 281 (18) (05/05): 12809-16.

Saide, J. D., S. Chin-Bow, J. Hogan-Sheldon, L. Busquets-Turner, J. O. Vigoreaux, K. Valgeirsdottir, and M. L. Pardue. 1989. Characterization of

components of Z-bands in the fibrillar flight muscle of drosophila melanogaster. *The Journal of Cell Biology* 109 (5) (Nov): 2157-67.

Samaranch, Lluís, Oswaldo Lorenzo-Betancor, José M. Arbelo, Isidre Ferrer, Elena Lorenzo, Jaione Irigoyen, Maria A. Pastor, et al. 2010. PINK1-linked parkinsonism is associated with lewy body pathology. *Brain: A Journal of Neurology* 133 (4) (04): 1128-42.

Schmidt, Jens, Goran Rakocevic, Raghavanpillai Raju, and Marinos C. Dalakas. 2004. Upregulated inducible co - stimulator (ICOS) and ICOS - ligand in inclusion body myositis muscle: Significance for CD8+ T cell cytotoxicity. *Brain* 127 (5) (May 01): 1182-90.

Schneider, David. 2000. Using drosophila as a model insect. *Nature Reviews Genetics* 1 (3) (12): 218.

Shafiq, S. A. 1963. Electron microscopic studies on the indirect flight muscles of drosophila melanogaster. I. structure of the myofibrils. *The Journal of Cell Biology* 17 (May): 351-62.

Silvestri, L., V. Caputo, E. Bellacchio, L. Atorino, B. Dallapiccola, E. M. Valente, and G. Casari. 2005. Mitochondrial import and enzymatic activity of PINK1 mutants associated to recessive parkinsonism. *Human Molecular Genetics* 14 (22) (Nov 15): 3477-92.

Singh, A. 2011. *hAPP* and *hParkin*. Unpublished data.

Sisodia, Sangram S., and Peter H. St George-Hyslop. 2002. γ-Secretase, notch, Aβ and alzheimer's disease: Where do the presenilins fit in? *Nature Reviews Neuroscience* 3 (4) (04): 281-90.

Small, David H., and Catriona A. McLean. 1999. Alzheimer's disease and the amyloid ? protein. *Journal of Neurochemistry* 73 (2): 443-9.

Spillantini, M. G., M. L. Schmidt, V. M. Lee, J. Q. Trojanowski, R. Jakes, and M. Goedert. 1997. Alpha-synuclein in lewy bodies. *Nature* 388 (6645) (Aug 28): 839-40.

Spillantini, Maria Grazia, R. A. Crowther, and Ross Jakes. 1998. a-synuclein in filamentous inclusions of lewy bodies from parkinson's disease and dementia with lewy bodies. *Proceedings of the National Academy of Sciences of the United States of America* 95 (11) (05/26): 6469-73.

Sugarman, M. C., T. R. Yamasaki, S. Oddo, J. C. Echegoyen, M. P. Murphy, T. E. Golde, M. Jannatipour, M. A. Leissring, and F. M. LaFerla. 2002. Inclusion body myositis-like phenotype induced by transgenic overexpression of APP in skeletal muscle. *Proceedings of the National Academy of Sciences of the United States of America* 99 (9): 6334.

Takeuchi, Y., H. Iwami, F. Inoue, S. Iino, H. Yoshioka, T. Kusunoki, and K. Saida. 1985. Rimmed vacuoles in biopsied muscle of nemaline myopathy. *Acta Neuropathologica* 68 (3): 253-5.

Teixeira, Antonio, Patrick Cherin, Alexandre Demoule, Mich Levy-Soussan, Christian Straus, Eric Verin, Marc Zelter, Jean-Philippe Derenne, Serge Herson, and Thomas Similowski. 2005. Diaphragmatic dysfunction in patients with idiopathic inflammatory myopathies. *Neuromuscular Disorders* 15 (1) (01): 32-9.

Tiegs, O. W. 1955. The flight muscles of insects-their anatomy and histology; with some observations on the structure of striated muscle in general. *Philosophical Transactions of the Royal Society of London.Series B, Biological Sciences* 238 (656) (February 10): 221-348.

Valente, E. M., P. M. Abou-Sleiman, V. Caputo, M. M. Muqit, K. Harvey, S. Gispert, Z. Ali, et al. 2004. Hereditary early-onset parkinson's disease caused by mutations in PINK1. *Science (New York, N.Y.)* 304 (5674) (May 21): 1158-60.

Vassar, Robert, Brian D. Bennett, and Safura Babu-Khan. 1999. b-secretase cleavage of alzheimer's amyloid precursor protein by the transmembrane aspartic protease BACE. *Science* 286 (5440) (10/22): 735-41.

Vassar, Robert, Dora M. Kovacs, Riqiang Yan, and Philip C. Wong. 2009. The β-secretase enzyme BACE in health and alzheimer's disease: Regulation, cell biology, function, and therapeutic potential. *The Journal of Neuroscience* 29 (41) (14): 12787-94.

Vattemi, Gaetano, W. K. Engel, Janis McFerrin, Joseph D. Buxbaum, Lucia Pastorino, and Valerie Askanas. 2001. Presence of BACE1 and BACE2 in muscle fibres of patients with sporadic inclusion-body myositis. *Lancet* 358 (9297) (12/08): 1962.

Vattemi, Gaetano, Anna Nogalska, W. K. Engel, Carla D'Agostino, Frederic Checler, and Valerie Askanas. 2009. Amyloid-β42 is preferentially

accumulated in muscle fibers of patients with sporadic inclusion-body myositis. *Acta Neuropathologica* 117 (5) (05): 569-74.

Viney, M. E., and F. J. Thompson. 2008. Two hypotheses to explain why RNA interference does not work in animal parasitic nematodes. *International Journal for Parasitology* 38 (1) (01): 43-7.

Wantanabe, M. I., and C. M. WILLIAMS. 1953. Mitochondria in the flight muscles of insects. II. effects of the medium on the size form, and organization of isolated sarcosomes. *The Journal of General Physiology* 37 (1) (Sep): 71-90.

Whitworth, Alexander J., Dorothy A. Theodore, and Jessica C. Greene. 2005. Increased glutathione S-transferase activity rescues dopaminergic neuron loss in a drosophila model of parkinson's disease. *Proceedings of the National Academy of Sciences of the United States of America* 102 (22) (05/31): 8024-9.

Wojcik, Slawomir, W. K. Engel, Riqiang Yan, Janis McFerrin, and Valerie Askanas. 2007. NOGO is increased and binds to BACE1 in sporadic inclusion-body myositis and in AβPP-overexpressing cultured human muscle fibers. *Acta Neuropathologica* 114 (5) (11): 517-26.

Wolfe, Michael S., Weiming Xia, and Beth L. Ostaszewski. 1999. Two transmembrane aspartates in presenilin-1 required for presenilin endoproteolysis and g-secretase activity. *Nature* 398 (6727) (04/08): 513-7.

Yamamoto, Ayako, Arno Friedlein, Yuzuru Imai, Ryosuke Takahashi, Philipp J. Kahle, and Christian Haass. 2005. Parkin phosphorylation and modulation of its E3 ubiquitin ligase activity. *Journal of Biological Chemistry* 280 (5) (02/04): 3390-9.

Yang, Yufeng, Stephan Gehrke, Yuzuru Imai, Zhinong Huang, Yingshi Ouyang, Ji-Wu Wang, Lichuan Yang, M. F. Beal, Hannes Vogel, and Bingwei Lu. 2006. Mitochondrial pathology and muscle and dopaminergic neuron degeneration caused by inactivation of drosophila pinki is rescued by parkin. *Proceedings of the National Academy of Sciences of the United States of America* 103 (28) (07/11): 10793-8.

Yang, Yufeng, Yingshi Ouyang, Lichuan Yang, M. F. Beal, Angus McQuibban, Hannes Vogel, and Bingwei Lu. 2008. Pinki regulates mitochondrial dynamics through interaction with the fission/fusion machinery. *Proceedings of the National Academy of Sciences of the United States of America* 105 (19) (05/13): 7070-5.

Ye, Yihong, Nina Lukinova, and Mark E. Fortini. 1999. Neurogenic phenotypes and altered notch processing in drosophila presenilin mutants. *Nature* 398 (6727) (04/08): 525-9.

Yuan, Joshua, Ann Reed, Feng Chen, and C. N. Stewart. 2006. Statistical analysis of real-time PCR data. *BMC Bioinformatics* 7 (1): 85.